Camila Pereira Ramos

Relic Abundances from the Boltzmann Equation

Natal - RN

2021

Camila Pereira Ramos

Relic Abundances from the Boltzmann Equation

Dissertação de Mestrado apresentada ao Programa de Pós-Graduação em Física da Universidade Federal do Rio Grande do Norte como requerimento parcial para a obtenção do grau de Mestre em Física.

Universidade Federal do Rio Grande do Norte

Centro de Ciências Exatas e da Terra

Departamento de Física

Programa de Pós-Graduação em Física

Orientador: Farinaldo da Silva Queiroz

Coorientadora: Clarissa Martins Siqueira

Natal - RN

2021

Universidade Federal do Rio Grande do Norte - UFRN
Sistema de Bibliotecas - SISBI
Catalogação de Publicação na Fonte. UFRN - Biblioteca Setorial Prof. Ronaldo Xavier de Arruda - CCET

Ramos, Camila Pereira.
Relic abundances from the Boltzmann equation / Camila Pereira Ramos. - 2021.
91f.: il.

Dissertação (Mestrado em Física) - Universidade Federal do Rio Grande do Norte, Centro de Ciências Exatas e da Terra, Programa de Pós-Graduação em Física. Natal, 2021.
Orientador: Farinaldo da Silva Queiroz.
Coorientadora: Clarissa Martins Siqueira.

1. Física - Dissertação. 2. Matéria escura - Dissertação. 3. WIMPs - Dissertação. 4. Equação de Boltzmann - Dissertação. 5. Abundância de relíquias - Dissertação. I. Queiroz, Farinaldo da Silva. II. Siqueira, Clarissa Martins. III. Título.

RN/UF/CCET CDU 53

Elaborado por Joseneide Ferreira Dantas - CRB-15/324

Acknowledgements

I would like to thank my family, for raising and giving me the freedom to choose Physics, specially my mother, who always encouraged me to pursue my dreams, and my eldest brother, for all of the support.

I thank my supervisor, Farinaldo, who introduced me to particle physics. A great reference as a professor and researcher. My co-supervisor, Clarissa, for motivating and inspiring me, and also for the guidance.

I thank my dear boyfriend, Efraim, for all of the patience and kindness, throughout difficult and joyful times. Additionally, I thank my dearest friends, my kindred spirits, Victoria, Paola, Renivânia, Alice, Gustavo, Jacinto, Giovanni, and Rubens. Everyone contributed to this work, simply by being by my side, once this journey without my friends would be dull.

I thank the Particles & Astroparticles Group, from the International Insitute of Physics, for the great discussions during the Journal Clubs.

I would also like to express my gratitude towards CNPq, UFRN, and the Physics Department.

Finally, I thank the professors Aion Viana, Alex Dias and Rodrigo Holanda, for their constructive criticisms and important corrections that helped me to improve this work.

Resumo

Dados observacionais que suportam a existência de matéria escura (ME) têm sido amplamente documentados, apontando para a presença de uma matéria não barionica, responsável por cerca de 25% da quantidade de energia do Universo. Contudo, tal tipo de matéria não foi detectada até o momento e o modelo padrão de física de partículas (MP) não possui uma explicação para ME. Neste trabalho, as partículas massivas fracamente interagentes (WIMPs) são apresentadas. É, então, o objetivo principal mostrar que estes candidatos à ME geram a abundância necessária para obter a quantidade estimada de ME no Universo. Esse resultado é obtido através da solução da equação de Boltzmann no cenário do Universo primordial.

Palavras-Chave: Matéria Escura, WIMPs, Equação de Boltzmann, Abundância de Relíquias.

Abstract

Observational data that support the existence of dark matter (DM) has been largely documented, pointing to the presence of a non-baryonic matter that is responsible for around 25% of the energy budget of the Universe. However, such type of matter has not been detected so far, and the standard model of particle physics (SM) does not have an explanation for DM. In this work, the weakly interacting massive particles (WIMPs), the main candidates for DM, are presented. It is then the main goal to show that this DM candidate generates the abundance required to obtain the estimated amount of DM in the Universe. This result is obtained by solving the Boltzmann equation, in the early Universe scenario.

Keywords: Dark Matter, WIMPs, Boltzmann Equation, Relic Abundaces.

List of Figures

List of Tables

Contents

1 Introduction

Considering the past decades, the effort of physicists around the globe to describe all observed phenomena is very well documented and condensed in two powerful theories, the Standard Model of particle physics (SM), that describes the Universe in small scales, predicting with extraordinary precision high-energy events, and the General Relativity (GR), with its description of the same Universe, but in large, astronomical scales. For instance, the SM anticipated the existence of the Higgs boson, recently discovered by ATLAS (ATLAS, 2012) and CMS (CMS, 2012). While GR details the existence of black holes (Akiyama et al., 2019) and the gravitational waves (Abbott et al., 2016), also recently observed.

Despite all the fantastic accomplishments made by these theories, different aspects of the Universe remain unexplained, such as matter-antimatter asymmetry, the neutrino oscillations, or the origin and nature of the dark matter (DM), the latter being the main topic of this dissertation.

Independent observations point to this unknown kind of matter that accounts for roughly 25% of the energy budget of the Universe. The DM is found to be neither luminous nor baryonic[1], and its only form of interaction observed so far is gravitational. Multiple evidences, on scales of galaxies, galaxy clusters, or even larger, suggest the existence of DM, and such evidences even show that DM populated the Universe since its inception. Although this intriguing mystery seems far from a solution, there is nowadays a plethora of models, experiments, and candidates to explain the DM nature.

This dissertation focuses on exploring one candidate: the weakly interaction massive particle (WIMP), and on exploring how could these particles explain the amount of DM observed today.

The starting line is the SM, more precisely the electroweak sector of the SM, for it successfully describes the electromagnetic and weak forces, and also addresses its particle content. Next, in Chapter 3, with properties from GR, the standard cosmological model is discussed, in order to explore the early Universe scenario. In this sense, all the necessary tools to understand the DM evidences are shown. A tool called the Boltzmann equation is also introduced to detail the evolution of the particles composing the early Universe, as they start to fall out of equilibrium with the cosmic plasma. During Chapter 4, some of the main evidences for DM are presented. In the same chapter, the Boltzmann equation will be solved for WIMP particles, in order to obtain the observed relic abundance. Finally, the last part of Chapter 4 is devoted to an overview of experiments that search for WIMPs.

[1] Here, baryonic matter refers to all types of known matter, such as electrons, positrons, etc.

This work uses the natural system of units, therefore $\hbar = c = k_B = 1$. Additionally, some prior knowledge in quantum field theory, as well as classical mechanics, classic electrodynamics and quantum mechanics are necessary in order to better understand the topics explored throughout this work.

2 Standard Model: Electroweak Sector

The main purpose of this chapter is to review some aspects of the electroweak sector of the standard model (SM), or the Electroweak Theory, The SM is a very successful and precise theory, with one of its main accomplishes being the prediction of the Higgs boson. The understanding of the SM can provide an insight about how to extend it, since this theory cannot explain some unsolved problems.

The most fundamental question that elementary particle physics attempts to answer regards what is matter made of. For instance, if matter is made of atoms - which were once thought to be indivisible - and such atoms are made of elementary particles, how such particles interact with each other? With the work of many scientists around the world and throughout many generations, the SM was built, motivated by these questions. The SM then describes three of the four interactions observed so far in nature, and also categorizes all elementary particles detected at the moment.

It is worth mentioning that the beginning of the SM is in 1930, when Pauli proposed the existence of the neutrino (Pauli, 1930). At that time, the only elementary particles detected were the electron (Thomson, 1897) and the proton (Rutherford, 1919). The process for the hypothesis of this third particle was the beta decay, where the neutron decays into a proton, an electron, and an anti-neutrino. Fermi, in 1934, tried to describe the beta decay based on an interaction of four fermions (Fermi, 1934). With the $(V-A)$ structure[1] being used to describe weak interactions (Feynman; Gell-Mann, 1958; Sudarshan; Marshak, 1958; Sakurai, 1958), some physicists tackled the problem of explaining such interactions with symmetry groups[2] (Bludman, 1958; Lopes, 1958; Lee; Yang, 1960), until Glashow used the gauge group $SU(2)_L \otimes U(1)_Y$ to portray the weak and electromagnetic interactions amongst elementary particles (Glashow, 1961). Shortly after, Weinberg and Salam, independently, used the Higgs mechanism to generate mass to elementary particles without explicitly breaking the gauge symmetry of the model (Weinberg, 1967; Salam, 1968), the process is made through a spontaneous symmetry breaking, detailed in the next pages. The model assembled by Glashow, Weinberg and Salam composes the electroweak sector of the SM. In addition, the SM also requires the existence of gauge bosons, particles responsible for mediating the forces of nature.

The Higgs mechanism is presumed to take place in the Universe fractions of seconds after the Big Bang, when the Universe reached the temperature of electroweak scales, around 246 GeV in energy scales, giving mass to particles (Kolb; Turner, 1990). This is the first point that shall be reviewed. From there, all the sectors of the SM will arise. This first

[1] This structure can be described by the Lagrangian: $\mathcal{L}_{V-A} \supset \bar{\psi}\gamma^{\mu}(1-\gamma^{5})\psi$.
[2] For a more detailed narrative of the SM history, see (Weinberg, 2004).

part ends then with the achievements that the SM accomplishes, and also its limitations.

2.1 The Higgs mechanism

Since the SM is built using the non-abelian symmetry group $SU(3)_c \otimes SU(2)_L \otimes SU(1)_Y$, Lorentz invariance and renormalizability, it is required that all gauge bosons and fermions be massless in order to explicitly preserve the gauge symmetry. However, the Universe is composed by massive particles. In order to provide mass to these particles without explicitly breaking any gauge symmetry of the SM, the Higgs mechanism, a tool to provide the spontaneous symmetry breaking, is introduced.

To illustrate the Higgs mechanism, suppose the Lagrangian for a complex scalar field ($\phi(x) = \phi_1(x) + i\phi_2(x)$)

$$\mathcal{L} = \tfrac{1}{4}F_{\mu\nu}F^{\mu\nu} + \tfrac{1}{2}(\partial_\mu\phi)^*(\partial^\mu\phi) - V(\phi^*\phi), \tag{2.1}$$

where $F_{\mu\nu} = \partial_\nu A_\mu - \partial_\mu A_\nu$ is the kinetic term for the electromagnetic field $A_\mu = (V, -\boldsymbol{A})$, and $V(\phi^*\phi) = \frac{\mu^2}{2}(\phi^*\phi) + \frac{\lambda}{4}(\phi^*\phi)^2$ is the potential for the so-called ϕ^4 theory[3]. This Lagrangian is invariant under global gauge symmetry ($\phi \to e^{iq\alpha}\phi$, being q and α constants) as verified below

$$\begin{aligned} \mathcal{L} &\to \tfrac{1}{4}F_{\mu\nu}F^{\mu\nu} + \tfrac{1}{2}e^{-iq\alpha}e^{iq\alpha}(\partial_\mu\phi)^*(\partial^\mu\phi) - e^{-iq\alpha}e^{iq\alpha}\tfrac{\mu^2}{2}(\phi^*\phi) - (e^{-iq\alpha}e^{iq\alpha})^2\frac{\lambda}{4}(\phi^*\phi)^2 \\ &= \tfrac{1}{4}F_{\mu\nu}F^{\mu\nu} + (\partial_\mu\phi)^*(\partial^\mu\phi) - \tfrac{\mu^2}{2}(\phi^*\phi) - \frac{\lambda}{4}(\phi^*\phi)^2 = \mathcal{L}. \end{aligned} \tag{2.2}$$

For a local gauge transformation, e.g. $\phi \to e^{iq\alpha(x)}\phi$, on the other hand, some changes are needed to achieve the gauge invariance. Making the following substitution

$$\partial_\mu \to \mathscr{D}_\mu \equiv \partial_\mu + iqA_\mu, \tag{2.3}$$

with A_μ transforming as

$$A_\mu \to A'_\mu = A_\mu - \partial_\mu\alpha(x) \tag{2.4}$$

the Lagrangian

$$\mathcal{L} = \tfrac{1}{4}F_{\mu\nu}F^{\mu\nu} + \tfrac{1}{2}\mathscr{D}_\mu\phi^*\mathscr{D}^\mu\phi - \tfrac{\mu^2}{2}(\phi^*\phi) - \tfrac{\lambda}{4}(\phi^*\phi)^2 \tag{2.5}$$

[3] This potential is chosen because it corresponds to the most general potential that can fulfill two requirements: dimensionality and gauge invariance.

is now invariant under a local gauge symmetry and also includes an interaction term between the A_μ field and the complex scalar field, ϕ. The same analogy can be applied for the Dirac Lagrangian, resulting on the interaction between a photon and matter, or fermions.

In order to understand the description of the scalar field, it is necessary to analyze the potential $V(\phi^*\phi)$. Firstly, λ must be positive, otherwise the potential would not be bounded from below, therefore it will not have a finite, stable minimum. Secondly, μ^2 can be: (a) positive or (b) negative.

The Figure 1(a) represents the potential for the first case, where $\mu^2 > 0$. In this case, the potential has a minimum at $\phi = 0$. If μ^2 is chosen to be negative, the lowest energy state does not occur at $\phi = 0$, but is degenerate. The vacuum states are obtained by deriving the potential with respect to the field, and then setting this value to zero, as follows:

$$\left[\frac{dV(|\phi|)}{d|\phi|}\right]_{\phi_0} = \mu^2|\phi|_0 + \lambda|\phi|_0^3 = 0 \tag{2.6}$$

$$\mu^2 + \lambda|\phi|_0^2 = 0 \tag{2.7}$$

$$|\phi|_0^2 = -\frac{\mu^2}{\lambda} \tag{2.8}$$

$$|\phi|_0 = \pm\sqrt{\frac{-\mu^2}{\lambda}} \equiv \pm v, \tag{2.9}$$

as shown in the Figure 1(b). The choice of the vacuum state then breaks the symmetry of the Lagrangian. Choosing between $|\phi|_0 = +v$ or $|\phi|_0 = -v$ will not make any difference, since the Lagrangian holds global symmetry, remembering that the point were $\phi = 0$ for $\mu^2 < 0$ represents a point of unstable equilibrium. The vacuum state is then chosen to be at $\phi = v$ and the symmetry is spontaneously broken. Examining the perturbations of the field around the chosen vacuum state, by writing $\phi(x)_1 = v + \eta(x)$, and $\phi_2(x) = \xi(x)$, the descriptions of the particle state (excitations of the field) can be obtained.

Consider, then, the kinetic part of the Lagrangian

$$\mathscr{L}_K = -\tfrac{1}{4}F_{\mu\nu}F^{\mu\nu} + \tfrac{1}{2}(\partial_\mu\eta)(\partial^\mu\eta) + \tfrac{1}{2}(\partial_\mu\xi)(\partial^\mu\xi) + \tfrac{1}{2}q^2v^2A_\mu A^\mu + qv(\partial_\mu\xi)A^\mu. \tag{2.10}$$

It is visible that the symmetry is now broken, leaving kinetic terms for A_μ, $\eta(x)$ and $\xi(x)$, the mass term for A_μ and the mixing term of ξ and A_μ. Looking at the potential now,

$$V = \tfrac{1}{2}\mu^2\eta^2 + \tfrac{1}{2}\mu^2v^2 + \mu^2v\eta + \tfrac{\mu^2}{4v^2}[(\eta + v)^4 + \xi^4 + 2\eta^2\xi^2] + \tfrac{4\mu^2}{v}\eta\xi^2, \tag{2.11}$$

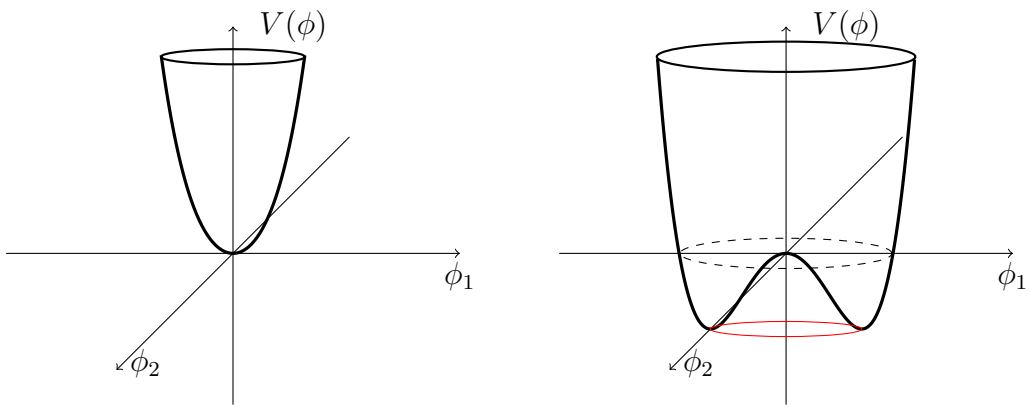

(a) For $\mu^2 > 0$, there is only one vacuum state at $\phi = 0$, maintaining the $U(1)$ symmetry of the Lagrangian.

(b) For $\mu^2 < 0$, the vacuum is degenerate. Any choice will break the $U(1)$ symmetry of the Lagrangian.

Figure 1 – Potential $V(\phi) = \frac{1}{2}\mu^2(\phi^*\phi) + \frac{1}{4}\lambda(\phi^*\phi)^2$ as function of ϕ_1 e ϕ_2 for two different values of μ^2.

the first term on the right hand side (RHS) of the equation above is the mass term for the η field, where $m_\eta = -2\mu^2$. The ξ field is massless and the remaining of the RHS of (2.11) is composed of mixing terms. The total Lagrangian can then be written as

$$\mathscr{L} = \mathscr{L}_{kin} - V_{int}, \tag{2.12}$$

where

$$\mathscr{L}_{kin} = \underbrace{\tfrac{1}{2}(\partial_\mu\eta)(\partial^\mu\eta) + \tfrac{1}{2}\mu^2\eta^2}_{\text{massive } \eta \text{ field}} + \underbrace{\tfrac{1}{2}(\partial_\mu\xi)(\partial^\mu\xi)}_{\text{massless } \xi \text{ field}} + \underbrace{\tfrac{1}{2}q^2v^2A_\mu A^\mu - \tfrac{1}{4}F_{\mu\nu}F^{\mu\nu}}_{\text{massive boson}} + qv(\partial_\mu\xi)A^\mu \tag{2.13}$$

is the kinetic term and V_{int} takes into account all the interaction terms between η, ξ, and A_μ, and self-interaction terms. It is possible to take a step further and simplify $\mathscr{L}_{kin}$ by replacing

$$A_\mu \to A'_\mu = A_\mu + \tfrac{1}{qv}\partial_\mu\xi \tag{2.14}$$

the gauge boson then transforms as $\partial_\mu\alpha \to -\partial_\mu\xi/qv$.

Since the scalar field, after the spontaneous symmetry breaking, was expanded around the vacuum by writing $\phi(x) = \eta(x) + v + i\xi(x)$, in first order the same field can be expressed as

$$\phi \cong (\eta + v)e^{i\frac{\xi}{v}}, \tag{2.15}$$

applying the local gauge transformation, considering $\alpha(x) = -\eta(x)$,

$$\phi \rightarrow \phi' \cong e^{-i\frac{\xi}{v}}(\eta + v)e^{i\frac{\xi}{v}} = \eta + v, \tag{2.16}$$

resulting in a real scalar field. This gauge fixing is called *unitary gauge*. The Lagrangian below is then finally derived

$$\mathscr{L} = \tfrac{1}{2}(\partial_\mu \eta)(\partial^\mu \eta) + \tfrac{1}{2}\mu^2\eta^2 + \tfrac{1}{2}q^2v^2A'_\mu A'^\mu - \tfrac{1}{4}F_{\mu\nu}F^{\mu\nu} - V_{int}. \tag{2.17}$$

Therefore, by choosing the vacuum of the potential, the symmetry of the inital Lagrangian was broken. The consequences result in a massive scalar field, η, a massive gauge boson field, A_μ, and a massless scalar field, ξ. The latter was absorbed into the transformation of A_μ, becoming one of its degrees of freedom and dissapearing from the Lagrangian obtained above. The ξ field is then recognized as the Goldstone boson. It is valid to mention that the number of degrees of freedom is conserved during the process.

After presenting an illustrated process of the Higgs mechanism, the same process can be applied for the SM of particle physics. The complex scalar field ϕ is now represented by the $SU(2) \times U(1)$ doublet

$$\phi = \begin{pmatrix} \phi^+ \\ \phi^0 \end{pmatrix} = \begin{pmatrix} \phi_1 + i\phi_2 \\ \phi_3 + i\phi_4 \end{pmatrix}, \tag{2.18}$$

where ϕ_1, ϕ_2, ϕ_3, and ϕ_4 are four real scalar fields. The Higgs mechanism, in this context, should generate mass to the bosons $W^\pm$ and Z^0. Therefore, one of its scalar field should be neutral, ϕ^0, and the other charged, ϕ^+. The charged field will account for the additional degrees of freedom for the charged gauge bosons, W^+ and W^-, whereas the field ϕ_4 becomes the degree of freedom for the neutral gauge boson, Z^0.

2.2 The scalar sector

Considering again the Lagrangian for the scalar field,

$$\mathscr{L}_s = \tfrac{1}{2}(\mathscr{D}_\mu\phi)^\dagger(\mathscr{D}^\mu\phi) - \tfrac{\mu^2}{2}\phi^\dagger\phi - \tfrac{\lambda}{4}(\phi^\dagger\phi)^2. \tag{2.19}$$

Since ϕ is now a $SU(2) \otimes U(1)$ doublet, the covariant derivative is given by

$$\mathscr{D}_\mu = \partial_\mu + ig\frac{\sigma^a}{2}W^a_\mu + ig'\frac{Y}{2}B_\mu, \tag{2.20}$$

where g and g' are the coupling constants of the $SU(2)$ and $U(1)$ groups, respectively, and σ^a the Pauli matrices, or generators of the $SU(2)$ group. Y is the $U(1)$ group generator, described further. The bosonic fields W^a_μ and B_μ transform as

$$W_\mu \to W_\mu^{'} = W_\mu - \frac{1}{g}\partial_\mu \alpha - \boldsymbol{\alpha} \times \boldsymbol{W}_\mu \text{ and} \tag{2.21}$$

$$B_\mu \to B_\mu^{'} = B_\mu - \partial_\mu \chi. \tag{2.22}$$

The Lagrangian is then invariant under $SU(2)_L \otimes U(1)_Y$ gauge transformations. Once again, taking a closer look at the potential, there are two scenarios:

- $\mu^2 > 0$: The potential has a well-defined vacuum at $\phi_1 = \phi_2 = \phi_3 = \phi_4 = 0$. The Lagrangian then describes four real scalar fields with mass μ interacting with W_μ^a and Z_μ, two massles fields;
- $\mu^2 < 0$: Here, the potetial is minimum at

$$\left[\frac{dV}{d|\phi|}\right]_{\phi_0} = 0, \tag{2.23}$$

where

$$|\phi|^2 = \phi_1^2 + \phi_2^2 + \phi_3^2 + \phi_4^2. \tag{2.24}$$

Therefore the vacuum expectation value is given by Eq.(2.9),

$$|\phi|_0^2 = -\frac{\mu^2}{\lambda}.$$

As mentioned before, the vacuum is degenerate and any choice for the minimum will break the symmetry of the Lagrangian. After the spontaneous breaking symmetry, there will be left three Goldstone bosons, which become degrees of freedom for the massive gauge bosons, and also a massive scalar field. Considering the unitary gauge,

$$\begin{aligned} |\phi_i|_0 = 0, \qquad & i = 1, 2, 4; \\ |\phi_3|_0 = v. & \end{aligned} \tag{2.25}$$

The field at the minimum of the potential is then

$$\phi_0 = \begin{pmatrix} 0 \\ v \end{pmatrix}, \tag{2.26}$$

and now expanding the field around the minimum yields

$$\phi = \begin{pmatrix} 0 \\ h+v \end{pmatrix}, \tag{2.27}$$

where $h = h(x)$ is a real scalar field.

Rewriting the potential, the Lagrangian is now

$$\mathscr{L}_s = \tfrac{1}{2}(\mathscr{D}_\mu\phi)^\dagger(\mathscr{D}_\mu\phi) + \mu^2h^2 - v\lambda h^3 - \tfrac{1}{4}\lambda h^4 - \tfrac{1}{4}\mu^2v^2, \tag{2.28}$$

where the mass term for the h field can be identified as $m_h = -\sqrt{2}\mu^2$.

Expliciting the kinetic term,

$$\mathscr{D}_\mu\phi = \begin{pmatrix} \partial_\mu + \frac{ig}{2}W_\mu^3 + \frac{ig'Y}{2}B_\mu & \frac{ig}{2}(W_\mu^1 - iW_\mu^2) \\ \frac{ig}{2}(W_\mu^1 + iW_\mu^2) & \partial_\mu - \frac{ig}{2}W_\mu^3 + \frac{ig'Y}{2}B_\mu \end{pmatrix} \begin{pmatrix} 0 \\ h+v \end{pmatrix}, \tag{2.29}$$

where Y can be obtained by the definition of the charge operator Q,

$$Q = T_3 + \frac{Y}{2}, \tag{2.30}$$

with T_3 being the third component of the weak isospin, equal to $-\frac{1}{2}$ for ϕ_0. Since the field is neutral, $Q = 0$ and then $Y = 1$. It is convenient to define

$$W_\mu^\pm = W_\mu^1 \mp iW_\mu^2, \tag{2.31}$$

to achieve

$$\mathscr{D}_\mu\phi = \frac{1}{2}\begin{pmatrix} 2\partial_\mu + igW_\mu^3 + ig'B_\mu & igW_\mu^+ \\ igW_\mu^- & 2\partial_\mu - igW_\mu^3 + ig'B_\mu \end{pmatrix} \begin{pmatrix} 0 \\ h+v \end{pmatrix} \tag{2.32}$$

$$\mathscr{D}_\mu\phi = \frac{1}{2}\begin{bmatrix} igW_\mu^+(h+v) \\ 2\partial_\mu hi(g'B_\mu - gW_\mu^3W_\mu^3)(h+v) \end{bmatrix}. \tag{2.33}$$

Now, the remaining step is to multiply the term above by its conjugated to obtain the explicit kinetic term for the Lagrangian,

$$\begin{aligned}\tfrac{1}{2}(\mathscr{D}_\mu\phi)^\dagger(\mathscr{D}^\mu\phi) =&\tfrac{1}{2}\partial_\mu h\partial^\mu h + \tfrac{1}{8}g^2W_\mu^-W^{+\mu}(h+v)^2+\\ &\tfrac{1}{8}(h+v)^2[g^2W_\mu^3W^{3\mu}+g'^2B_\mu B^\mu - gg'(W_\mu^3B_\mu+B_\mu W^{3\mu})].\end{aligned} \tag{2.34}$$

The term in squared brackets can be written in the matrix form

$$v^2\begin{pmatrix}W_\mu^3 & B_\mu\end{pmatrix}\begin{pmatrix}g^2 & -gg'\\ -gg' & g'^2\end{pmatrix}\begin{pmatrix}W^{3\mu}\\ B^\mu\end{pmatrix} = \begin{pmatrix}W_\mu^3 & B_\mu\end{pmatrix}\mathbf{M}\begin{pmatrix}W^{3\mu}\\ B^\mu\end{pmatrix}, \tag{2.35}$$

where $\mathbf{M}$ is dubbed mass matrix. Since this is a non-diagonal matrix, its mass terms mix with each other, hence it is impossible to identify the mass of each gauge boson separately. With a diagonal mass matrix, the gauge bosons are said to be *physical*. Therefore, with a unitary transformation the diagonal representation can be obtained

$$\begin{pmatrix}A_\mu & Z_\mu\end{pmatrix}\begin{pmatrix}0 & 0\\ 0 & g^2+g'^2\end{pmatrix}\begin{pmatrix}A^\mu\\ Z^\mu\end{pmatrix}, \tag{2.36}$$

with

$$A_\mu = \frac{g'W_\mu^3+gB_\mu}{\sqrt{g^2+g'^2}}, \tag{2.37}$$

$$Z_\mu = \frac{gW_\mu^3-g'B_\mu}{\sqrt{g^2+g'^2}}. \tag{2.38}$$

Now going back to the Lagrangian for the gauge bosons, Eq. (2.19), with the modifications

$$\begin{aligned}\mathscr{L}_s =&\tfrac{1}{2}(\partial_\mu h)(\partial^\mu h) + v^2\lambda h^2 + \tfrac{1}{8}v^2g^2W_\mu^-W^{+\mu} + \tfrac{1}{8}v^2(g^2+g^{'2})Z_\mu Z^\mu+\\ &\tfrac{1}{4}vg^2W_\mu^-W^{+\mu}h + \tfrac{1}{4}v(g^2+g^{'2})Z_\mu Z^\mu h + \tfrac{1}{8}(g^2+g^{'2})Z_\mu Z^\mu h^2+\\ &\tfrac{1}{8}g^2W_\mu^-W^{+\mu}h^2 - v\lambda h^3 - \tfrac{1}{4}\lambda h^4 + \tfrac{1}{4}\lambda v^4,\end{aligned} \tag{2.39}$$

there is the kinetic and mass terms for the higgs bosons, the mass terms for the $W^\pm$ and Z^0 bosons, and interaction terms between $W^\pm$, Z^0 and the h field. There is no mass term for the A boson, identified as the photon, nor an interaction term between the photon and the Higgs boson[4]. The masses of all bosons in the SM are

[4] This is due the massless nature of the photon, and the fact that the Higgs boson is chargeless.

$$m_h = \sqrt{2\lambda}v, \quad m_W = \tfrac{1}{2}gv, \quad m_Z = \tfrac{1}{2}v\sqrt{g^2 + g'^2} \quad e \quad m_A = 0. \tag{2.40}$$

The SM sets, through the Higgs mechanism, a relation between the masses of $W^{\pm}$ and Z^0. This can be done by writing g and g' as

$$\frac{g'}{g} = tan\theta_W, \tag{2.41}$$

with θ_W being the Weinberg angle. Hence,

$$m_W = m_Z \cos\theta_W. \tag{2.42}$$

The relation between W^3_μ, B_μ, A_μ, and Z_μ is written in terms of the Weinberg angle, as a rotation matrix

$$\begin{pmatrix} W^3_\mu & B_\mu \end{pmatrix} = \begin{pmatrix} \sin\theta_W & \cos\theta_W \\ \cos\theta_W & -\sin\theta_W \end{pmatrix} \begin{pmatrix} A_\mu \\ Z_\mu \end{pmatrix}. \tag{2.43}$$

The experimental value of the Weinberg angle is given by $\sin^2\theta_W \cong 0.231$ (Sirunyan et al., 2018). The numerical value for the masses of the gauge bosons can be achieved by evaluating the decay width of the processes $Z^0 \to \bar{\nu}\nu$, and $W^- \to e\bar{\nu_e}$ (Quigg, 1983), currently corresponding to $m_W = 80.379 \pm 0.012$ GeV, and $m_Z = 91.1876 \pm 0.0021$ GeV (Zyla et al., 2020).

The Higgs mechanism was proposed by Peter Higgs in 1964, and independently by Robert Brout and François Englert (Englert; Brout, 1964), and Gerald Guralnik, Carl Richard Hagen, and Tom Kibble (Guralnik; Hagen; Kibble, 1964). In 2012, the ATLAS ans CMS experiments announced the discovery of the Higgs boson (ATLAS, 2012; CMS, 2012), with mass 125.25 ± 0.17 GeV (Zyla et al., 2020).

2.3 Fermion sector

Here the description of the weak interactions for leptons and quarks is made, as well as the mass generations for said particles. The dynamic representation of the fermions, i.e., half-integer spin particles, is specified by the Dirac Lagrangian

$$\mathscr{L}_{Dirac} = \bar{\Psi}(i\gamma^\mu\partial_\mu - m)\Psi. \tag{2.44}$$

However, due the different transformation properties of the left- and right-handed chiral states, the mass term in the Lagrangian,

$$-\bar{\Psi}\Psi = -m(\bar{\Psi}_R\Psi_L + \bar{\Psi}_L\Psi_R), \tag{2.45}$$

does break the $SU(2)_L \otimes U(1)_Y$ gauge symmetry, thus it is not a good representation to be part of the Lagrangian of the SM. On that account, the Higgs mechanism can be used again, this time to generate mass to these fermions.

2.3.1 Leptons

The Lagrangian that describes the dynamics of leptons and its interactions between gauge bosons and involves the Dirac Lagrangian, except for the mass term, and with the substitution $\partial_\mu \to \mathscr{D}_\mu$ to maintain the gauge invariance,

$$\mathscr{L}_l = \bar{\Psi}_l i\gamma^\mu \mathscr{D}_\mu \Psi_l = \bar{e}_{jR} i\gamma^\mu(\partial_\mu + i\tfrac{g'}{2}Y_{e_{jR}}B_\mu)e_{jR} + \bar{L}_j i\gamma^\mu(\partial_\mu + i\tfrac{g'}{2}Y_{L_j}B_\mu + i\tfrac{g}{2}\tau^a \cdot W^a_\mu)L_j, \tag{2.46}$$

where

$$e_{jR} = e_R, \mu_R, \tau_R, \quad \text{and} \quad L_j = \begin{pmatrix}\nu_e \\ e\end{pmatrix}_L, \begin{pmatrix}\nu_\mu \\ \mu\end{pmatrix}_L, \begin{pmatrix}\nu_\tau \\ \tau\end{pmatrix}_L, \tag{2.47}$$

are the right-handed leptons, represented as singlets, and the left-handed lepton doublets, respectively.

Starting with the interactions between leptons and charged gauge bosons[5],

$$\mathscr{L}^l_{cc} = -\tfrac{g}{\sqrt{2}}(\bar{\nu}_{e_j L}\gamma^\mu e_{jL}W^+_\mu + \bar{e}_{jL}\gamma^\mu \nu_{e_j L}W^-_\mu), \tag{2.48}$$

which, using definitions of the chiral operators, can be written as

$$\mathscr{L}^l_{cc} = \tfrac{g}{2\sqrt{2}}[\bar{\nu}_{e_j}\gamma_\mu(1-\gamma_5)e_j W^+ + \bar{e}_j\gamma^\mu(1-\gamma_5)\nu_{e_j}W^-]. \tag{2.49}$$

The expression above has the $V-A$ structure of the weak currents. The constant g can be related to the Fermi constant, G_F, associated with the weak interactions, that give

[5] In matrix representation, this description corresponds to non-diagonal terms.

rise to the beta decay, introduced by Fermi. The value of G_F is well known experimentally, and found in the Appendix A. The relation between g and G_F is given by the equation

$$\frac{G_F}{\sqrt{2}} = \frac{g^2}{8m_W^2}. \tag{2.50}$$

That being said, the vacuum expected value can be found,

$$v = 246 \text{ GeV}. \tag{2.51}$$

Looking more closely now to the terms responsible for the interactions with the Z-boson and the photon[6],

$$\begin{aligned}\mathscr{L}_{nc}^{l} = \frac{gg'}{\sqrt{g^2+g'^2}}\bar{e}_j\gamma^\mu e_j A_\mu - \frac{\sqrt{g^2+g'^2}}{2}\bar{\nu}_{e_jL}\gamma^\mu Z_\mu + \frac{g-g'^2}{2\sqrt{g^2+g'^2}}\bar{e}_{jL}\gamma^\mu e_{jL}Z_\mu \\ - \frac{g'^2}{\sqrt{g^2+g'^2}}\bar{e}_{jR}\gamma^\mu e_{jR}Z_\mu,\end{aligned} \tag{2.52}$$

some known constants can be used to simplify the equation above. Since there is a symmetry corresponding to the Quantum Electrodynamics, the electric charge can be identified by

$$e = \frac{gg'}{\sqrt{g^2+g'^2}}, \tag{2.53}$$

resulting in

$$g\sin\theta_W = e = g'\cos\theta_W. \tag{2.54}$$

Now the Lagrangian for the leptonic neutral current is rewritten as

$$\begin{aligned}\mathscr{L}_{nc}^{l} = &-\frac{1}{\sqrt{2}}\left(\frac{G_F m_Z^2}{\sqrt{2}}\right)^{1/2}\{\bar{e}_j[(2\sin^2\theta_W - 1)\gamma^\mu(1-\gamma_5) \\ &+ 2\sin^2\theta_W\gamma^\mu(1+\gamma_5)]e_j Z_\mu \bar{\nu}_{e_j}\gamma^\mu(1-\gamma_5)\nu_{e_j}Z_\mu\} + e\bar{e}_j\gamma^\mu e_j A_\mu,\end{aligned} \tag{2.55}$$

which provides the interactions between leptons and the neutral bosons. With these Lagrangians at hand, the hadronic sector can be discussed.

2.3.2 Quarks

In analogy to the leptons, the hadronic Lagrangian provides the interactions between quarks and gauge bosons. Still, there are some differences to discuss.

[6] Now, there are the diagonal terms, in matrix representation.

Similarly as before, the neutral and charged currents will be obtained from the Lagrangian

$$\mathscr{L}_q = \bar{Q}_{jR} i\gamma^\mu \mathscr{D}_\mu Q_{jR} + \bar{Q}_{jL} i\gamma^\mu \mathscr{D}_\mu Q_{jL}, \tag{2.56}$$

where

$$Q_{jR} = u_R, d_R, c_R, s_R, t_R, b_R, \tag{2.57}$$

and

$$Q_{jL} = \begin{pmatrix} u \\ d \end{pmatrix}_L, \begin{pmatrix} c \\ s \end{pmatrix}_L, \begin{pmatrix} t \\ b \end{pmatrix}_L. \tag{2.58}$$

Starting with the neutral current, i.e., the diagonal terms of the above equation, for the first family of quarks is

$$\begin{aligned} \mathscr{L}^q_{nc} = &- \frac{1}{\sqrt{2}} \left(\frac{G_F m_Z^2}{\sqrt{2}} \right)^{1/2} \{ \bar{u}\gamma^\mu [(1-\gamma_5)T_3 \\ &- 4\sin^2\theta Q_u] u Z_\mu \bar{d}_\theta \gamma^\mu [(1-\gamma_5)T_3 - 4\sin^2\theta Q_d] d_\theta Z_\mu \} \\ &- Q_u \bar{u}\gamma^\mu u A_\mu - Q_d \bar{d}_\theta \gamma^\mu d_\theta A_\mu, \end{aligned} \tag{2.59}$$

where $d \to d_\theta = d\cos\theta_c + s\sin\theta_c$. The d quark has a dependence on θ_c, or the Cabbibo angle, and the s quarks.

In 1963, Cabbibo (Cabibbo, 1963) observed that the universality of weak interactions at low energies is not maintained for hadronic decays. However, this universality can be restored, by writing the d quark as d_θ, and if the s quark is an orthogonal state given by the transformation $s \to s_\theta = -d\sin\theta_c + s\cos\theta_c$. With these transformations, there is a change of flavor in the neutral current, a consequence not observed experimentally. Thus, in 1970, Glashow, Iliopoulos, and Maiani (Glashow; Iliopoulos; Maiani, 1970) proposed the existence of another quark, the *charm* quark, composing a doublet with the s quark. The terms involving flavor change are then canceled and the problem is solved. This scenario can be generalized for all three families, using a matrix called the Cabbibo-Kobayashi-Maskawa (CKM) matrix (Kobayashi; Maskawa, 1973), which involves the Cabbibo angle.

The transformation for s and d quarks, in the matricial form, is

$$\begin{pmatrix} d' \\ s' \end{pmatrix} = \begin{pmatrix} \cos\theta_c & \sin\theta_c \\ -\sin\theta_c & \cos\theta_c \end{pmatrix} \begin{pmatrix} d \\ s \end{pmatrix}. \tag{2.60}$$

This is somewhat similar to the case of the Z boson and the photon, since the transformation shows that the s and d quarks are superpositions of the mass eigenstates, being the mixture suppressed by the value of θ_c.

As for the charged current, it is analogous to the leptons. For the first family, the relation is given by

$$\mathscr{L}_{cc}^{q} = -\left(\frac{G_F m_W^2}{\sqrt{2}}\right)^{1/2} [\bar{u}\gamma_\mu(1-\gamma_5)d_\theta W^+ + \bar{d}_\theta\gamma^\mu(1-\gamma_5)uW^-]. \tag{2.61}$$

2.3.3 Yukawa Lagrangian

After the interactions of the fermions with the gauge bosons, in this section the main goal is to obtain the fermions mass terms. As explained earlier, a simple mass term such as the one from the Dirac Lagrangian does not preserve the gauge invariance required for the SM. Therefore, the Higgs doublet can be used once again to generate such terms. The process occurs through the Yukawa Lagrangian, where its components are

$$\mathscr{L}_Y = \mathscr{L}_Y^l + \mathscr{L}_Y^q. \tag{2.62}$$

The first term, the Yukawa Lagrangian for leptons, is simple due the fact that, in the SM, the neutrinos are massless, hence there is no mixture terms and the Lagrangian can be written as

$$\mathscr{L}_Y^l = -G_{e_j}(\bar{e}_{jR}\phi^\dagger L + \bar{L}\phi e_{jR}), \tag{2.63}$$

and after the spontaneous symmetry breaking, the result is

$$\mathscr{L}_Y^l = -G_{e_j}\left[\bar{e}_{jR}\begin{pmatrix}0 & \frac{v+h}{\sqrt{2}}\end{pmatrix}\begin{pmatrix}\nu_{e_j}\\ e_j\end{pmatrix}_L + \begin{pmatrix}\bar{\nu}_{e_j} & \bar{e}_j\end{pmatrix}_L\begin{pmatrix}0\\ \frac{v+h}{\sqrt{2}}\end{pmatrix}e_{jR}\right]. \tag{2.64}$$

Thus, the mass terms for leptons, as well as its interaction with the Higgs boson, is

$$\mathscr{L}_Y^l = -\frac{G_{e_j}v}{\sqrt{2}}\bar{e}_j e_j - \frac{G_{e_j}}{\sqrt{2}}\bar{e}_j e_j h, \tag{2.65}$$

where $m_{e_j} = G_{e_j}v/\sqrt{2}$. As mentioned before, in the SM, the neutrinos are massless. Currently, the observation of neutrino oscillations imply that neutrinos are massive (Gonzalez-Garcia; Maltoni, 2008). Nevertheless, when the SM was built, such evidences did not exist, nor the detection of a right-handed neutrino, even until now[7].

[7] So far, the right-handed neutrinos have not been detected. One of the most commons ways to provide mass to neutrinos is via seesaw mechanism, which is beyond the scope of this dissertation.

It is also important to point out that the Higgs interacts with the leptons proportionally to the masses of these leptons.

In order to generate mass to all quarks, the following doublet must be used

$$\tilde{\phi} = \begin{pmatrix} \phi^{0*} \\ -\phi^{-} \end{pmatrix}, \tag{2.66}$$

that can be obtained by the relation

$$\tilde{\phi} = i\sigma^2\phi^*. \tag{2.67}$$

Therefore, this is not a new scalar, only a $SU(2)$ transformation of ϕ. The difference now is that the hypercharge Y is equal to -1 and the third component of the weak isospin, T_3 is equal to $+1/2$, meaning that the use of $\tilde{\phi}$ will guarantee that the u, c, and t quarks are massive. The Yukawa Lagrangian for quarks is shown in the equation below

$$\mathscr{L}_Y^q = -\sum_{i,j=1}^{3} \left[G_{ij}^U \bar{R}_{U_i} (\tilde{\phi}^\dagger Q_{jL}) + G_{ij}^D \bar{R}_{D_i} (\phi^\dagger Q_{jL}) \right] + h.c., \tag{2.68}$$

where

$$R_{U_i} = u_R, c_R, t_R, \quad \text{and } R_{D_i} = d_R, s_R, b_R. \tag{2.69}$$

After the spontaneous symmetry breaking process, it can be represented in the matricial form

$$\mathscr{L}_Y^q = -\left[\overline{\begin{pmatrix} u', & c', & t' \end{pmatrix}}_R M^U \begin{pmatrix} u' \\ c' \\ t' \end{pmatrix}_L + \overline{\begin{pmatrix} d', & s', & b' \end{pmatrix}}_R M^D \begin{pmatrix} d' \\ s' \\ b' \end{pmatrix}_L \right] + h.c., \tag{2.70}$$

where M^U and M^D are non-diagonal matrices related to G^U and G^D, respectively, by

$$M_{ij}^U = \frac{v}{\sqrt{2}} G_{ij}^U, \quad \text{and } M_{ij}^D = \frac{v}{\sqrt{2}} G_{ij}^D. \tag{2.71}$$

With the use of unitary transformations the diagonal matrices can be found[8]. If $U_{L,R}$ and $D_{L,R}$ are matrices that diagonalize M^U and M^D, respectively,

[8] A square matrix A' is diagonalizable if there exists an invertible matrix U and a diagonal matrix A such that $A = U^{-1}A'U$.

$$U_R^{-1} M^U U_L = \begin{pmatrix} m_u & 0 & 0 \\ 0 & m_c & 0 \\ 0 & 0 & m_t \end{pmatrix}, \tag{2.72}$$

$$D_R^{-1} M^D D_L = \begin{pmatrix} m_d & 0 & 0 \\ 0 & m_s & 0 \\ 0 & 0 & m_b \end{pmatrix}. \tag{2.73}$$

Therefore, the Lagrangian can be written in the diagonal basis, where the states q' are superpositions of the eigenstates q, specified by the unitary transformations,

$$\begin{pmatrix} u' \\ c' \\ t' \end{pmatrix}_{L,R} = U_{L,R} \begin{pmatrix} u \\ c \\ t \end{pmatrix}_{L,R}, \tag{2.74}$$

$$\begin{pmatrix} d' \\ s' \\ b' \end{pmatrix}_{L,R} = D_{L,R} \begin{pmatrix} d \\ s \\ b \end{pmatrix}_{L,R}. \tag{2.75}$$

Revisiting the charged current, described in Eq. (2.61), a generalization for the three families is made

$$\mathcal{L}_{cc}^q = -\left(\frac{G_F m_W^2}{\sqrt{2}}\right)^{1/2} [\bar{u}'\gamma^\mu(1-\gamma_5)d' + \bar{c}'\gamma^\mu(1-\gamma_5)s' + \bar{t}'\gamma^\mu(1-\gamma_5)b']W_\mu^+ + h.c., \tag{2.76}$$

where the transformations for the quarks are now

$$\overline{\begin{pmatrix} u', & c', & t' \end{pmatrix}}_L \gamma_\mu \begin{pmatrix} d' \\ s' \\ b' \end{pmatrix} = \overline{\begin{pmatrix} u, & c, & t \end{pmatrix}}_L (U_L^\dagger D_L)\gamma_\mu \begin{pmatrix} d \\ s \\ b \end{pmatrix}_L, \tag{2.77}$$

being the product $(U_L^\dagger D_L)$ the CKM matrix, V, i.e.,

$$V \equiv U_L^\dagger D_L. \tag{2.78}$$

As for the neutral current, the representation in matrix form is given in two terms

$$\overline{\begin{pmatrix} u', & c', & t' \end{pmatrix}}_L \gamma_\mu \begin{pmatrix} u' \\ c' \\ t' \end{pmatrix} = \overline{\begin{pmatrix} u, & c, & t \end{pmatrix}}_L (U_L^\dagger U_L) \gamma_\mu \begin{pmatrix} u \\ c \\ t \end{pmatrix}_L , \tag{2.79}$$

$$\overline{\begin{pmatrix} d', & s', & b' \end{pmatrix}}_L \gamma_\mu \begin{pmatrix} d' \\ s' \\ b' \end{pmatrix} = \overline{\begin{pmatrix} d, & s, & b, \end{pmatrix}}_L (D_L^\dagger D_L) \gamma_\mu \begin{pmatrix} d \\ s \\ b \end{pmatrix}_L . \tag{2.80}$$

Since $U_L^\dagger U_L = D^\dagger D_L = I$, there are no flavor changes (mixtures) in the neutral current. This feature is only observed in the neutral current for $-1/2$ isospin quarks. The following definition can be made

$$\begin{pmatrix} d' \\ s' \\ b' \end{pmatrix}_L = U_L^\dagger D_L \begin{pmatrix} d \\ s \\ b \end{pmatrix}_L \equiv V \begin{pmatrix} d \\ s \\ b \end{pmatrix}_L , \tag{2.81}$$

thus, the rotation of the u, c, and t quarks is absorbed, leaving no flavor mixture on the neutral current.

The lagrangian for weak interactions of the SM is now assembled,

$$\mathcal{L} = \mathcal{L}_s + \mathcal{L}_l + \mathcal{L}_q + \mathcal{L}_Y + \mathcal{L}_b, \tag{2.82}$$

where $\mathcal{L}_b$ is the lagrangian describing the kinectics of the gauge bosons

$$\mathcal{L}_b = -\frac{1}{4} W_{\mu\nu} W^{\mu\nu} - \frac{1}{4} B_{\mu\nu} B^{\mu\nu}. \tag{2.83}$$

With the discovery of the Higgs boson, the SM was finally complete, being the best description so far of how elementary particles interact. This model also includes interactions between quarks and gluon, or strong interactions, that are not discussed here.

The SM, however, is unable to address many problems observed in nature, one of them being the mass of the neutrinos, already mentioned above. Others worth mentioning are leptogenesis, baryogenesis, and the dark matter, the focus of this work.

Therefore, to understand more about the nature of dark matter, one has to step beyond the SM and use fundamental knowledge from the cosmological model, a task tackled during the next chapter.

3 The Standard Cosmological Model

A fundamental ingredient to discuss dark matter physics is to understand the evolution of the Universe. Several topics, not only in physics, but in Science as a whole, overlap with each other, this is not different for Particle Physics and Cosmology. So there is no surprise that dark matter is a problem which particle physicists try to solve, but it also reflects in Cosmology. It is then necessary to set the groundwork before diving into the study of dark matter.

One of the pillars of the standard cosmological model is the cosmological principle, the cornerstone to modern cosmology (Peebles, 1993). It states that no matter where or who the observer is, the Universe will look the same. There is absolutely nothing special about the place where the Earth, or any object, occupies in the Universe. This simple albeit powerful statement can be validated at very large scales. Around hundreds of Megaparsecs, the Universe becomes smooth, with the properties of homogeneity and isotropy, and all positions are essentially equivalent. This assumption is not able to answer whether the Universe holds these properties since its origin, or only during some temporary present phase. However, over all its history that can be directly reached with observational data, the Universe has been highly homogeneous and isotropic (Clarkson, 2012; Goodman, 1995; Maartens, 2011; Clarkson; Maartens, 2010; Pandey; Sarkar, 2015).

That said, throughout this chapter the standard cosmological model will be presented, beginning with a sense of an expanding Universe, followed by a brief history of the Early Universe, where some pillars of the Big Bang Theory lie, a few key points of the first stages of the Universe are shown, such as decoupling of elementary particles from the thermal bath that compose the Universe, the Big Bang Nucleosynthesis, which address the formation of light elements, and a glimpse of the Cosmic Microwave Background.

3.1 The Expanding Universe

A very interesting feature of the Universe described by Cosmology is its expansion. While trying to correlate the distance between the galaxies and the Earth with the velocity of recession of such galaxies, Edwin Hubble, during the 1920's (Hubble, 1929), observed a linear pattern, showing that these objects move away from our planet at velocities, $\vec{v}$, proportional to their distances, $\vec{\ell}$, as seen in Figure 2. This relation is called **Hubble Law**, and it can be expressed in mathematical language through the following equation

$$\vec{v} = H_0 \vec{\ell}, \tag{3.1}$$

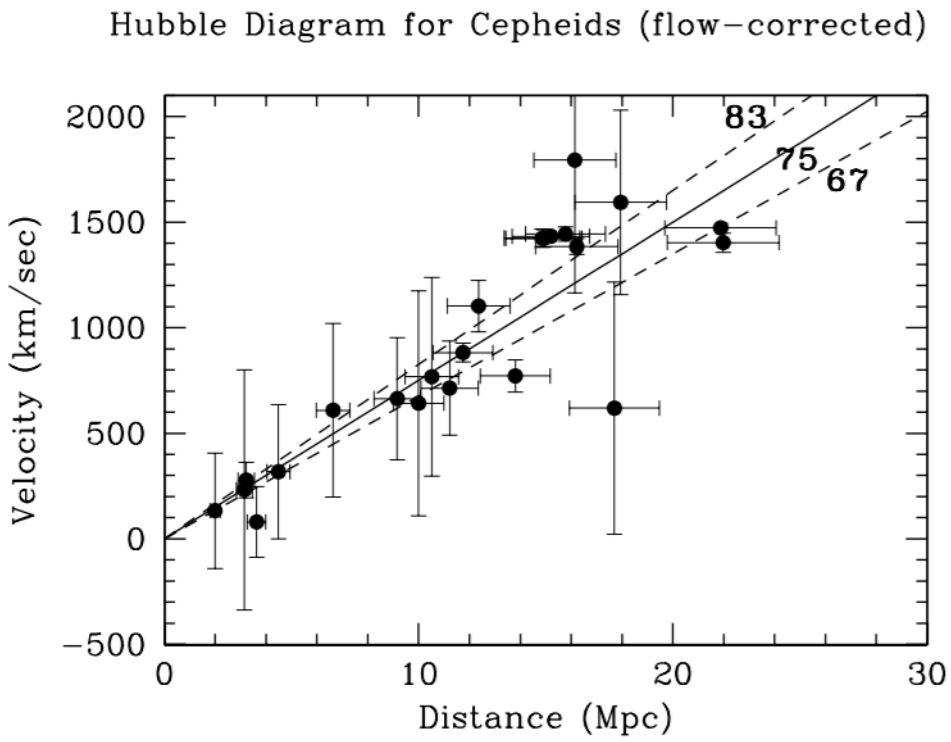

Figure 2 – 2001 version of the Hubble diagram from the Hubble Space Key Telescope Program (Freedman et al., 2001). The distance of each galaxy was obtained using pulsating stars, also known as Cepheid variables.

where the constant of proportionality H_0 is the Hubble's constant, which is the current value of the Hubble parameter, H. The Hubble parameter, in turn, varies with time. The value of H_0 is

$$H_0 = 100 \text{ h km s}^{-1} \text{ Mpc}^{-1}, \tag{3.2}$$

where h is a constant that accounts for the uncertainties on the measurements of the Hubble's constant. There is still no consensus about the accurate value of h (Freedman, 2017), however, this work will use the value measured by the Planck Collaboration (Aghanim et al., 2020b), being $\text{h} = 0.677 \pm 0.004$.

The Hubble parameter is defined in terms of the scale factor a by the expression

$$H(t) \equiv \frac{\dot{a}}{a}. \tag{3.3}$$

The present value of a is set as 1, and going back in time decreases the value of a, as seen in Figure (3). Therefore, the scale factor has the purpose of measuring the universal expasion rate.

Taking into account the expansion of the Universe, it is convenient to change to a coordinate system where the coordinates can carry such effect. These are called comoving

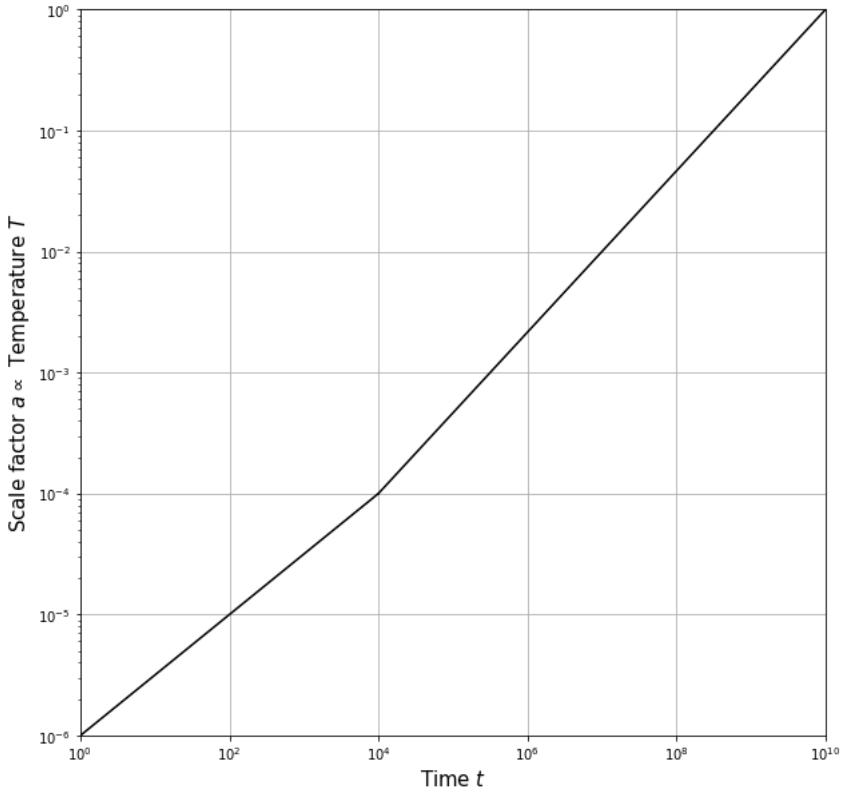

Figure 3 – Scale factor evolution with cosmic time.

coordinates. Therefore, the real distance $\vec{\ell}$ is proportional to the comoving distance, say $\vec{r}$, via the relation

$$\vec{\ell} = a(t)\vec{r}. \tag{3.4}$$

Since the Universe is homogeneous at large scales, the scale factor should be a function of time alone. The comoving distance is always fixed, whereas the real distance, or the physical coordinate, ℓ, evolves with time.

As the Universe expands, all galaxies seem to be moving away from the Milky Way. Due the Hubble Law, the further away these astronomical objects are, the faster is its recession. Each galaxy can be identified by their spectra of electromagnetic absortion and emission lines. Because of the Doppler effect, when a galaxy is approaching the Milky Way, such lines move towards a higher frequency of the visible spectrum, an event known as *blueshift* (Campbell, 1906). Whereas if the galaxy is travelling in the opposite direction, i.e., moving far away, the lines of the spectrum will shift to a lower frequency, causing the *redshift*. This use of the Doppler effect was first made by Vesto Slipher (Slipher, 1913), in the decade of 1910, and Edwin Hubble then applied the same technique (Hubble, 1929).

Since in general the galaxies are receding, the use of the redshift is more standard,

and it can be mathematically described as (Peebles, 1993)

$$z = \frac{\lambda_o - \lambda_e}{\lambda_e}, \tag{3.5}$$

where z is the redshift, λ_o is the observed wavelength of the light observed, and λ_e the wavelength of the light emitted by the moving object. There is another way of writing the formula for redshift considering the equation for the Doppler effect in special relativity,

$$1 + z = \sqrt{\frac{1 + v/c}{1 - v/c}}. \tag{3.6}$$

At lower speeds compared to the speed of light ($v \ll c$), the following equation for redshifts can be used

$$z = \frac{v}{c}. \tag{3.7}$$

From this point, a relationship between the redshift and the scale factor can be traced. Still at the low speed limit, and using the Eqs. (3.5) and (3.7), to obtain

$$\frac{d\lambda}{\lambda} = \frac{dv}{c} = \frac{Hdl}{c} = \frac{da}{dt}\frac{1}{ca}dl = \frac{d\lambda}{\lambda} = \frac{da}{a}, \tag{3.8}$$

meaning that

$$\lambda \propto a, \tag{3.9}$$

and substituting into the Eq. (3.5), the result is

$$1 + z = \frac{a(t_o)}{a(t_e)}. \tag{3.10}$$

Since $a(t_0) = 1$, the redshift can be used to compare the Universe today to the same Universe with a fraction of its actual size, or even to look at the primordial Universe. Therefore, the redshift and the scale factor are tools to trace the Universe and describe it.

3.2 The Friedmann equations

In order to understand how the Universe evolves, a specific metric is needed, and the homogeneity and isotropic properties are used. The metric that follows from this model is named the Friedmann-Lemaître-Roberston-Walker (FLRW) metric, given by (Weinberg, 2008)

$$ds^2 = dt^2 - a^2(t)\left(\frac{dr^2}{1 - kr^2} + r^2 d\theta^2 + r^2 \sin^2\theta d\phi^2\right), \tag{3.11}$$

where k is a curvature factor, t, r, θ, and ϕ are time and spatial comoving coordinates, respectively. In addition, $a(t)$ is the scale factor previously introduced.

Henceforth, not only the scale factor and the expansion are characteristics of the Universe, but also its geometry, which can have a flat, open or close geometry. Each possibility can have an influence in the values of some observable quantities.

Using the FLRW metric in the Einstein's equations, written as (Weinberg, 2008; Weinberg, 1972)

$$R_{\mu\nu}(t) - \tfrac{1}{2}g_{\mu\nu}(t)R(t) + \Lambda(t)g_{\mu\nu}(t) = 8\pi G T_{\mu\nu}, \tag{3.12}$$

where the Ricci scalar has the form $R = g^{\mu\nu}R_{\mu\nu}$, and the Ricci tensor can be described in terms of the scale factor as

$$R_{00} = -\frac{3\ddot{a}}{a} \qquad \text{and} \qquad R_{ij} = \delta_{ij}[2\dot{a}^2 + a\ddot{a}], \tag{3.13}$$

and Λ receives the name of cosmological constant (Einstein, 1917). This equation describes the standard cosmological model, or ΛCDM[1]. Taking into account the period of the Universe considered in this work, the cosmological constant will not contribute much, therefore it is out of the scope to discuss the topic[2], and for the rest of this chapter it can be considered $\Lambda = 0$.

Taking the 00 component of the Einstein's equation, the Friedmann equation is obtained,

$$\frac{\dot{a}^2}{a^2} + \frac{k}{a^2} = \frac{8\pi G}{3}\rho, \tag{3.14}$$

whereas the spatial components of the Einstein's equation yield

$$2\frac{\ddot{a}}{a} + \frac{\dot{a}^2}{a^2} + \frac{k}{a^2} = -8\pi G p, \tag{3.15}$$

where p is the pressure of the system.

Dividing the Friedmann equation by the squared Hubble parameter results in

$$\frac{k}{a^2H^2} = \frac{8\pi G}{3H^2}\rho - 1, \tag{3.16}$$

the right hand side (RHS) of the equation can be written as

$$\Omega - 1 = \frac{k}{a^2H^2}, \tag{3.17}$$

[1] Here, CDM stands for cold dark matter.

[2] For a more detailed analysis on the cosmological constant, see (Peebles, 1993; Dodelson; Schmidt, 2020).

where Ω is defined as

$$\Omega \equiv \frac{\rho}{\rho_c}, \text{ with } \rho_c \equiv \frac{3H^2}{8\pi G}, \tag{3.18}$$

which is called density parameter. Experiments were created to obtain the value of Ω today, Ω_0, such as the WMAP experiment and the Planck Collaboration, with the result very close to one[3] (Aghanim et al., 2020b). The parameter ρ_c is called critical energy density, or the energy density of the Universe considering $k = 0$. The current value for the critical density is (Zyla et al., 2020)

$$\rho_c = 1.88 \text{ h}^2 \times 10^{-26} \text{ kg m}^{-3}. \tag{3.19}$$

Since k is a curvature parameter, with values going from -1 to 1, and as can be noted, H^2a^2 is always positive, the curvature parameter will thus dictate if ρ_c is greater or less than ρ; namely, saying what is the curvature of the Universe. That said, from Eq. (3.17), the density parameter can assume the following values for each possible curvature of the Universe

$$\begin{cases} \Omega > 1, & \text{if } k = +1 \text{ (closed)}, \\ \Omega = 1, & \text{if } k = 0 \text{ (flat)}, \\ \Omega < 1, & \text{if } k = -1 \text{ (open)}. \end{cases} \tag{3.20}$$

Taking the difference between Eqs. (3.14) and (3.15), results in the acceleration equation

$$\frac{\ddot{a}}{a} = -\frac{4\pi G}{3}(\rho + 3p), \tag{3.21}$$

which describes the acceleration of the scale factor. If the material in question has any pressure, the gravitational force will increase, decelerating the expansion.

Another important equation is the fluid equation, which is useful to determine how the energy density depends on the scale factor, and it is based on the principle that the Universe behaves as perfect fluid that expands adiabatically. It is given by

$$\dot{\rho} + 3H(\rho + p) = 0. \tag{3.22}$$

[3] With $\Omega_k = \frac{k}{a^2 H_0^2} = 0.001 \pm 0.002$, from (Aghanim et al., 2020b).

The pressure and energy density can be related with the thermodynamic equation of state (EOS)

$$p = \omega\rho, \tag{3.23}$$

where ω is 0 for non-relativistic matter, since it exerts no pressure, 1/3 for relativistic radiation, and -1 for vacuum energy.

Integrating the fluid equation with time, and combining with the equation of state, the energy density is given by

$$\rho = \rho_0 a^{-3(1+\omega)}, \tag{3.24}$$

where ρ_0 is the present energy density.

Henceforth, an analysis is made for periods in which the Universe is composed by different contents (Weinberg, 2008).

- Matter

In the context adopted here, matter would be non-relativistic matter, or any material that does not exert pressure. The energy density for matter is proportional to

$$\rho_m \propto a^{-3}, \tag{3.25}$$

meaning that the energy density of matter is inversely proportional to the volume of the Universe.

The Friedmann equation informs how the scale factor evolves with time, depending on the geometry and content of the Universe. Considering a flat and matter-dominated Universe, the Eq. (3.14), is now

$$\dot{a}^2 = \frac{8\pi G\rho_0}{3}\frac{1}{a}. \tag{3.26}$$

An attempt to solve this differential equation can be made by guessing that the solution is a power law, i.e., $a \propto t^q$. The only solution possible is $q = 2/3$, and hence the scale factor reads as

$$a(t) = \left(\frac{t}{t_0}\right)^{2/3}, \tag{3.27}$$

whereas for the energy density

$$\rho(t) = \frac{\rho_{m_0} t_0^2}{t^2}, \tag{3.28}$$

and the rate of expansion decreases with time, following

$$H \propto \frac{2}{3t}. \tag{3.29}$$

- Radiation

Radiation can be referred to as particles with velocities large enough that they exert pressure in the Universe, such as neutrinos or photons. Therefore

$$\rho_r \propto a^{-4}. \tag{3.30}$$

In analogy to the previous item, the radiation-dominated scenario has

$$a(t) = \left(\frac{t}{t_0}\right)^{1/2}, \tag{3.31}$$

the energy density evolves as

$$\rho(t) = \frac{\rho_{r_0} t_0^2}{t^2}, \tag{3.32}$$

and the Hubble parameter behaves like

$$H \propto \frac{1}{2t}. \tag{3.33}$$

Compared to the scenario in which the Universe is matter-dominated, now the Universe expands more slowly. Figure (4) shows the evolution of energy density for matter and radiation in the Universe.

If the radiation has the black-body spectrum, the Rayleigh-Jeans-Wien-Planck can be applied (Peebles, 1993), and the energy density also has the form

$$\rho_r c^2 = \alpha T^4, \tag{3.34}$$

where α is the Stefan-Boltzmann constant. Thus, still considering the radiation-dominated Universe, the temperature is a parameter proportional to

$$T \propto a^{-1}. \tag{3.35}$$

As the Universe expands, it also cools down, and looking with a time-reversed frame, the Universe in the past was hotter and denser, a conclusion that is in agreement with the Hot Big Bang Theory.

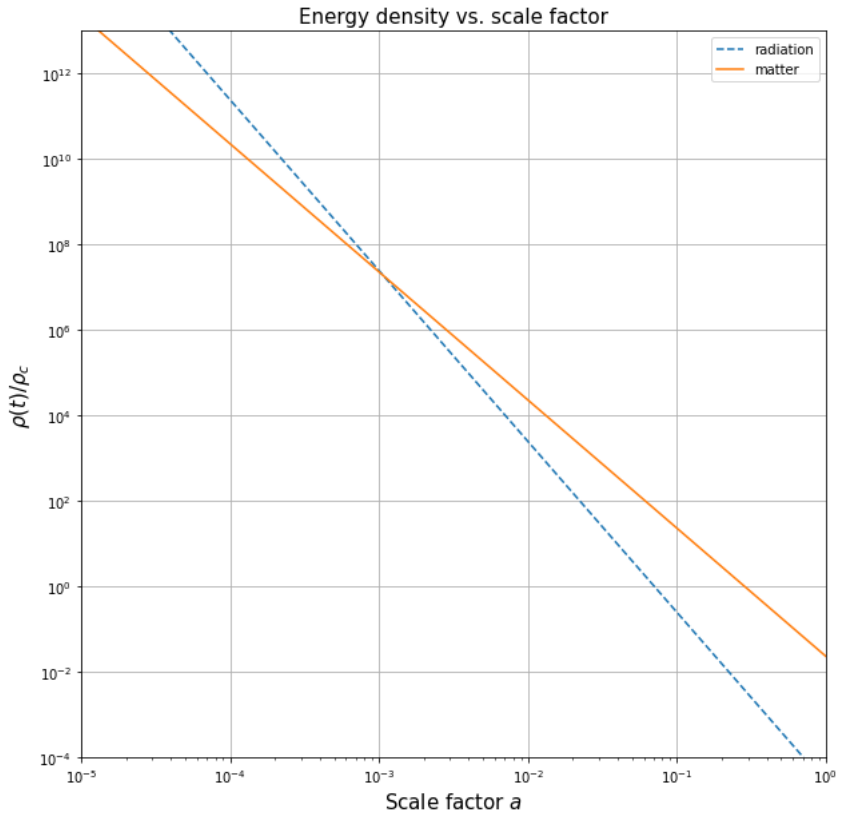

Figure 4 – Plot for energy density vs scale factor for radiation and matter.

3.3 The Early Universe

Throughout the history of the Universe, it can be considered that the scenario has been very close to a state called thermal equilibrium. In the initial stages, all particles species were composing a primordial plasma, or thermal bath. As the Universe expanded and cooled down, these species started to decouple from the plasma. The departures from equilibrium have a large contribution on the formation of light elements during this early stage, on the recombination of electrons and protons to form hydrogen, and as discussed further, possibly on the production of dark matter. That said, to discuss the thermal history of the Universe, it is not only crucial to understand the Equilibrium Thermodynamics, but also the conditions that have led to breaking the equilibrium of particle species with the thermal bath (Kolb; Turner, 1990).

For illustrative purposes of this section, a good rule to guarantee that thermal equilibrium is maintained, is that the interaction rate for processes involving such species must be quicker than the expansion rate of the Universe. Putting it into other words, as long as

$$\Gamma \geq H \tag{3.36}$$

holds, the particle is in thermal equilibrium with the plasma. Here $\Gamma \equiv n\sigma|v|$, being n

the number density, and $\sigma|v|$ the cross section times the averaged relative velocity. This condition is valid because, as the Universe expands, the energy density of the particle decreases, reaching a point where processes involving the production of the species can hardly occur. Therefore, equilibrium will no longer be maintained.

This condition, however, is not sufficient, as only the rate of some reaction that is crucial to conserve equilibrium shall remain lower than H to assert the decoupling. A much more reliable tool to determine the evolution of particles is the Boltzmann equation, used in the next section. For the moment, the case where $\Gamma > H$ will be used to state that a particle is in thermal equilibrium, and if it is decoupled from the thermal bath, the condition $\Gamma < H$ will be required.

Considering the scenario $\Gamma \gg H$, where the process that Γ takes into account involves four different species transforming into one another, i.e., a process of the type

$$1 + 2 \leftrightarrow 3 + 4, \tag{3.37}$$

the particles are then in chemical equilibrium, and therefore

$$\mu_1 + \mu_2 = \mu_3 + \mu_4, \tag{3.38}$$

where μ_i is the chemical potential of each species. If $\Gamma \gg H$ holds for a scatting process, described as

$$1 + 2 \leftrightarrow 1 + 2, \tag{3.39}$$

the particles are in kinetic equilibrium. Having chemical or kinetic equilibrium, or both, is a warranty of thermal equilibrium. There is the possibility where a species no longer stays in chemical equilibrium, but still preserves thermal equilibrium with the cosmic plasma via kinetic equilibrium (Bringmann; Hofmann, 2007).

As a consequence, by falling out of equilibrium with the thermal bath, each component left a signature, displaying features of the Universe at the time of decoupling. Such signatures today are evidence of how the Universe looked like during its earlier moments.

The starting point considered here is around the neutrino decoupling. The processes responsible for maintaining the neutrino in thermal equilibrium are

$$\bar{\nu} + e^- \leftrightarrow \bar{\nu} + e^-, \tag{3.40}$$

$$\nu + \bar{\nu} \leftrightarrow e^+ + e^- \tag{3.41}$$

such weak interaction processes have the cross section approximately given by

$$\sigma \backsimeq G_F^2 T^2, \tag{3.42}$$

where G_F is the Fermi constant. From Eq. (B.6), the number density for a relativistic particle is

$$n = \begin{cases} \frac{\zeta(3)}{\pi^2} g T^3 & \text{(bosons)} \\ \frac{3}{4}\frac{\zeta(3)}{\pi^2} g T^3 & \text{(fermions)}, \end{cases} \tag{B.6}$$

and therefore the interaction rate is

$$\Gamma \backsimeq G_F^2 T^5, \tag{3.43}$$

The ratio of Γ to H is

$$\frac{\Gamma}{H} \backsimeq \frac{G_F^2 T^5 M_{Pl}}{T^2} \backsimeq \left(\frac{T}{1\text{ MeV}}\right)^3. \tag{3.44}$$

Approximately 10^{-2} seconds after the Big Bang, the temperature of the Universe is $T = 10$ MeV, the Universe is composed mostly by radiation, and the relativistic degrees of freedom are 3 neutrino species ($g = 6$), $e^{\pm}$ pairs ($g = 4$), and the photon ($g = 2$), so $g_* = 10.75$, where (Kolb; Turner, 1990)

$$g_* = \sum_{i=bosons} g_i \left(\frac{T_i}{T}\right)^4 + \frac{7}{8} \sum_{i=fermions} g_i \left(\frac{T_i}{T}\right)^4, \tag{B.9}$$

and

$$g_{*s} = \sum_{i=bosons} g_i \left(\frac{T_i}{T}\right)^3 + \frac{7}{8} \sum_{i=fermions} g_i \left(\frac{T_i}{T}\right)^3 \tag{B.15}$$

are the number of effective degrees of freedom of the thermal bath. The quantities g_* and g_{*s} account for species considered relativistic at the given temperature T. As the Universe cools down, the species become non-relativistic, start to annihilate, and therefore the number of effective degrees of freedom decreases. Therefore g_* is a good parameter to describe the thermal evolution of the Universe, as seen in Fig 5.

Going back to the moment where $T = 10$ MeV, the interaction rates are larger than the expansion rate for the reactions (3.40) and (3.41). Therefore, the neutrino is in thermal equilibrium with the thermal bath, hence $T_\nu = T$.

As the temperature drops below $T = 1$ MeV, the neutrinos decouple from the thermal bath, and the neutrino temperature is now proportional to a^{-1}. At this point, the

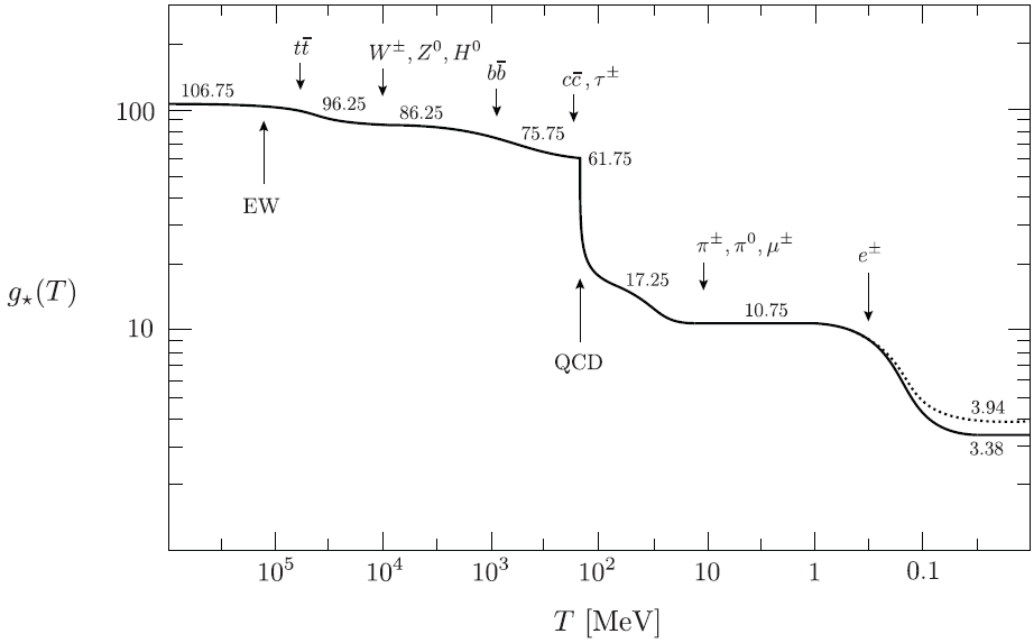

Figure 5 – Evolution of g_* and g_{*s} with the temperature for the SM. The number of degrees of freedom changes as the Universe cools down, and it is noticeable that, for most of the period, g_{*s} (dashed lines) does not differrs much from g_{*s}. Figure from (Baumann, Lecture Notes).

relativistic particle species in thermal equilibrium are the photon, and electron-positron pairs, resulting in $g_* = 11/2$.

The temperature of the plasma continues to decrease, and soon after the neutrino decoupling, the $e^{\pm}$ pairs can no longer be created, since the temperature is below $T_e = 0.511$ MeV. The entropy of the $e^{\pm}$ pair is transferred to the photons. Now, only the photons are relativistic particles in thermal bath, therefore $g_* = 2$. From the conservation of entropy (Baumann, 2018), the difference between the neutrinos temperature and the photons temperature due the entropy injection can be obtained

$$\frac{T_\gamma}{T_\nu} = \left(\frac{11}{4}\right)^{1/3} = 1.40. \tag{3.45}$$

Around the same temperature of the neutrino decoupling, the processes that were maintaining the neutrons and the protons in thermal equilibrium with the cosmic plasma, specified by

$$n + \nu \leftrightarrow p + e^-, \tag{3.46}$$

$$n + e^+ \leftrightarrow p + \bar{\nu}, \text{ and} \tag{3.47}$$

$$n \leftrightarrow p + e^- + \bar{\nu}, \tag{3.48}$$

have the interaction rate to start falling below the expansion rate of the Universe, hence the baryons fall out of equilibrium.

Before that period, while the chemical equilibrium is preserved, the following relation is obtained

$$\mu_n + \mu_\nu = \mu_p + \mu_e, \tag{3.49}$$

and the neutron-to-proton ratio is

$$\frac{n}{p} = \frac{n_n}{n_p} = \frac{X_n}{X_p} = \exp\left[-\frac{Q}{T} + \frac{(\mu_e - \mu_\nu)}{T}\right], \tag{3.50}$$

where $Q \equiv m_n - m_p = 1.3$ MeV. Based on charge neutrality, it can be inferred that $\mu_e/T \ll 1$. Assuming also that the number of leptons is small, hence $|\mu_\nu|/T \ll 1$. The neutron-to-proton ratio at equilibrium is then

$$\left(\frac{n}{p}\right)_{EQ} = \exp\left(-\frac{Q}{T}\right). \tag{3.51}$$

When the chemical equilibrium can no longer hold due the fact that Γ becomes smaller than H, the neutron-to-proton ratio is

$$\left(\frac{n}{p}\right)_f \backsimeq \frac{1}{6}, \tag{3.52}$$

where $T_f = 1$ MeV. After the freeze-out of neutrons and protons, this ratio slowly decreases.

Between 3 and 4 minutes after the Big Bang, light nuclei[4] start to form (Steigman, 2007). That is possible because the blackbody radiation does not have energy enough to separate the deuterium nuclei. However, such photons do have energy to keep such nuclei ionized, preventing them to form atoms.

Several hundred thousand years after the formation of light elements, the photons lose energy and the electrons start bond with nuclei, forming the first atoms. This period receives the name of recombination. Although the binding energy for the electron is 13.6 eV, the recombination period started when the thermal bath had a temperature significantly below this value[5], and the temperature where recombination starts can be obtained using the Saha equation.

Before deriving the Saha equation, some results from the photon decoupling are important to consider. After the atoms are formed, the photons can no longer interact with

[4] Other than hydrogen, which the nuclei is composed by one proton.

[5] This happens because the baryons to photon ratio, as seen forwardly in this chapter, is very low. Also, since the photons follow the blackbody energy spectrum, at $T = 13.6$ eV, there are still photons with enough energy to keep the atoms ionized.

the electrons, since they do not have energy to separate the atoms anymore. The photons then decouple from the thermal bath, traveling freely through the Universe, which now becomes visible. This radiation can be measured today and it is called Cosmic Microwave Background Radiation (CMBR). The current temperature of such photons experimentally measured is

$$T_{\gamma,0} = 2.4 \times 10^{-4} \text{ eV} = 2.73 \text{ K}. \tag{3.53}$$

This result can be also used to obtain the current temperature of the neutrinos that were created during the early Universe, or the relic neutrinos, from Eq. (3.45). Its value corresponds to

$$T_{\nu,0} = 1.7 \times 10^{-4} \text{ eV} \backsimeq 1.95 \text{ K}. \tag{3.54}$$

Since the decoupling, these neutrinos stream freely through the Universe. This cosmic neutrino background radiation (CNB or CνB) has not been detected so far, however. Compared to the cosmic microwave background radiation (CMB or CMBR), discussed in more details in Chapter 4, that describes a Universe 380,000 years old, the CNB corresponds to roughly one minute after the Big Bang, containing information about a much younger Universe. Detecting high energy neutrinos is already a difficult task, therefore it is extremely hard to directly measure the CNB, although strong evidences indicate its existence (Dodelson; Schmidt, 2020).

The number density of relic photons today is

$$n_{\gamma,0} = \frac{2\zeta(3)}{\pi^2} T_{0,\gamma}^3 = 410 \text{ cm}^{-3}. \tag{3.55}$$

Consider n_H, n_p, and n_e the number density for hydrogen, free protons, and free electrons, respectively. Assuming charge neutrality, $n_p = n_e$, and from baryon number conservation, $n_b = n_p + n_H$, recombination takes place when the process

$$p + e \leftrightarrow H + \gamma \tag{3.56}$$

is in chemical equilibrium, therefore

$$\mu_p + \mu_e = \mu_H, \tag{3.57}$$

where, as seen in the end of this chapter, since the photons from this epoch follow the blackbody radiation, its chemical potential is zero (Pathria, 2016).

The number density of hydrogen can then be expressed as

$$n_H = \frac{g_H}{g_p g_e} n_p n_e \left(\frac{m_e T}{2\pi}\right)^{-3/2} \exp\left(B/T\right), \tag{3.58}$$

where $B \equiv m_p + m_e - m_H = 13.6$ eV is the binding energy of hydrogen, $g_p = g_e = 2$. The fractional ionization, or the fraction of free electrons, is given by

$$X_e \equiv \frac{n_e}{n_p + n_H} = \frac{n_p}{n_p + n_H}. \tag{3.59}$$

Using Eq. (3.59) and Eq. (3.58), the Saha equation can be derived

$$\frac{X_e^2}{1 - X_e} = \frac{1}{n_b}\frac{n_e n_p}{n_H} = \frac{1}{n_e + n_H}\left(\frac{m_e T}{2\pi}\right)^{3/2} \exp\left(-B/T\right). \tag{3.60}$$

It is possible to write the Saha equation in the form

$$\frac{X_e^2}{1 - X_e} = \frac{\sqrt{\pi}}{4\sqrt{2}\zeta(3)\eta}\left(\frac{m_e T}{2\pi}\right)^{3/2} \exp\left(-B/T\right), \tag{3.61}$$

where η is the baryon-to-photon ratio

$$\eta \equiv \frac{n_b}{n_\gamma}, \tag{3.62}$$

Since the baryon abundance measured today is $\Omega_b \cong 0.02$ h^{-2} (Zyla et al., 2020), the current baryon number density, using the equations (3.18), and (B.11) is

$$n_{b,0} = \Omega_b \frac{\rho_{cr}}{m_b} \cong 0.2 \times 10^{-6} \text{ cm}^{-3}. \tag{3.63}$$

The baryon-to-photon ratio can then be estimated as $\eta \cong 5.4 \times 10^{-10}$. That is, for each baryon in the Universe there are 10^{10} photons. This ratio remains constant as the Universe expands, since the photon number and the baryon number are conserved.

With these ingredients, for a temperature close to the binding energy for the electron, $T \backsimeq B$ the Saha equation reads

$$\frac{X_e^2}{1 - X_e} \cong 1 \times 10^{15}. \tag{3.64}$$

One way to interpret this result is to see that when the temperature of the Universe reaches the binding energy of the hydrogen, the fraction of free electrons is close to one, meaning that, most if not all of the hydrogen is still ionized. It takes then a longer time so the recombination is able to start. The standard definition of the beginning of the

recombination is when about 90% of the electrons are captured by the protons, i.e., when $X_e = X_{rec} = 0.1$. That being said, the temperature for recombination is equivalent to

$$T_{rec} \cong 3575 \text{ K} = 0.31 \text{ eV}. \tag{3.65}$$

Since $T = T_0(1+z)$, the redshift corresponding to when the recombination begins is

$$1 + z_{rec} \cong 1300. \tag{3.66}$$

After recombination, at some point the temperature reaches the moment where the photons stop interacting with the electrons, decoupling from matter. With the same approach for the decoupling of the neutrino, the CMBR photons will decouple roughly when $\Gamma_\gamma \backsimeq H$, where the interaction rate is expressed in terms of the photon mean free path, L, by

$$L = \frac{1}{n_e \sigma_T} = \frac{1}{X_e n_b \sigma_T} = \frac{1}{\Gamma_\gamma}, \tag{3.67}$$

being σ_T the Thomson cross section, $\sigma_T = 6.65 \times 10^{-25}$ cm^2.

In order to obtain the redshift and temperature for the photons decoupling, the relation $\Gamma_\gamma \backsimeq H$ must be written in terms of z. The equations

$$1 + z = \frac{a(t_o)}{a(t_e)}, \text{ and} \tag{3.10}$$

$$\rho_m \propto a^{-3}, \tag{3.25}$$

are used in the relation for Γ_γ to form

$$\Gamma_\gamma = X_e n_{b,0} (1+z)^3 \sigma_T = 4.39 \times 10^{-21} (1+z)^3 X_e \text{ s}^{-1}. \tag{3.68}$$

Assuming that by the time where the photons decouple the Universe was dominated by matter, and using the equations (3.63), (3.16), and (3.18) the expansion rate is

$$\frac{H^2}{H_0^2} = \frac{\Omega_0}{a^3}, \tag{3.69}$$

where $\Omega \cong 0.28$. Using the equation for redshift, (3.10),

$$H = H_0 \sqrt{\Omega_{m,0}(1+z)^3} = 1.77 \times 10^{-18} \sqrt{(1+z)^3} \text{ h s}^{-1}. \tag{3.70}$$

Now imposing the condition for decoupling,

$$(1 + z_{dec}) = \frac{44.2}{X_e^{2/3}}. \tag{3.71}$$

The redshift value for the photons decoupling is found to be somewhere in the range

$$1 + z_{dec} \cong 1100 \text{ to } 1200, \tag{3.72}$$

suggesting that the fraction of free electron lies between 8×10^{-3} and 7×10^{-3}. The temperature at decoupling for $z_{dec} \cong 1100$ is

$$T_{dec} \cong 3030 \text{ K} = 0.26 \text{ eV}. \tag{3.73}$$

When the photons decouple from matter, the event marks the last scattering surface, making the Universe visible. These photons follow the most perfect blackbody radiation spectrum ever found in nature, measured by WMAP (Bennett et al., 2013), as shown in Figure (6).

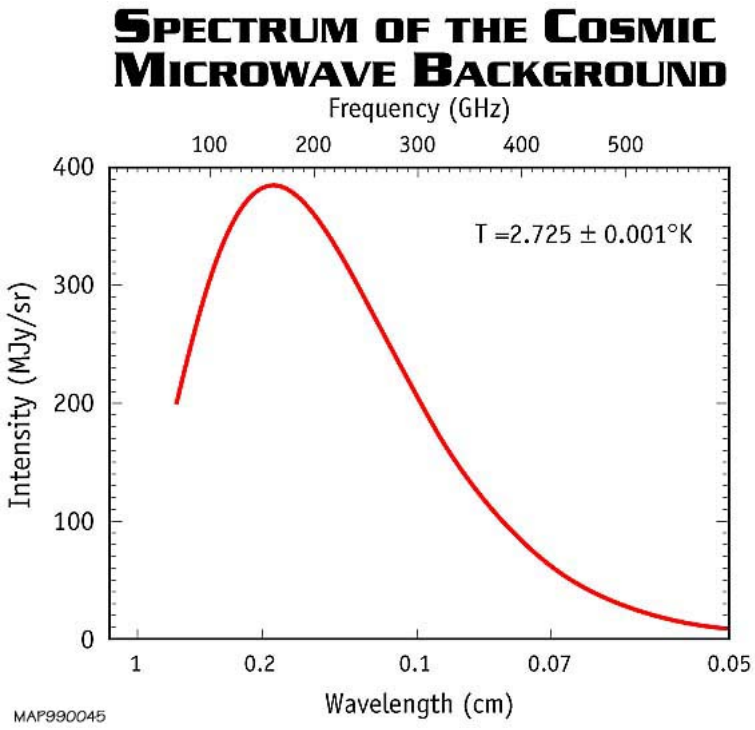

Figure 6 – Spectrum of the CMBR, measured by WMAP. Figure obtained from https://map.gsfc.nasa.gov/Universe/bb_tests_cmb.html.

The CMBR is so far the most powerful probe of the early Universe. These evidences show that, even being homogeneous and isotropic, the Universe had minor perturbations of order 10^{-5} (Smoot et al., 1992; Bennett et al., 2003; Ade et al., 2016), and as a consequence,

the relic photons carried such irregularities that were responsible to form structures some hundred thousands years after decoupling.

As this topic will be revisited further in this work, for now the focus turns back into finding a more precise method to describe how a species evolves in the thermal bath.

3.4 Introducing the Boltzmann Equation

While in thermal equilibrium, the evolution of a species is easily described, being relativistic or not, following either the Fermi-Dirac or the Bose-Einstein distribution. After the decoupling, the behavior of the species is also simple, with the energy density decreasing as a^{-4} if the particle is relativistic, or a^{-3} if it is non-relativistic. However, the decoupling is not instantaneous, and the period around this event is more challenging to describe.

As mentioned previously, the condition $\Gamma \gtrsim H$ implies that the species is coupled to the thermal bath, while if $\Gamma \lesssim H$, then the species is decoupled. Although this method is very useful and sometimes valid, a more appropriate analysis of the decoupling is done using the Boltzmann equation, which describes a thermodynamic system that is not in equilibrium. The Boltzmann equation is initially given by (Kolb; Turner, 1990)

$$\hat{L}(f) = \hat{C}(f), \tag{3.74}$$

where $\hat{L}$ is the Liouville operator and $\hat{C}$ is the collision operator, both depending on the phase space distribution function, $f(p^\mu, x^\mu)$. The relativistic Liouville operator for the FLRW model[6] is

$$\hat{L}[f(E,t)] = E\frac{\partial f}{\partial t} - \frac{\dot{a}}{a}|\mathbf{p}|^2\frac{\partial f}{\partial E}. \tag{3.75}$$

Since the number density is defined as

$$n = \frac{g}{(2\pi)^3}\int d^3p f(E,t), \tag{3.76}$$

performing integration by parts helps to write the Boltzmann equation in the form

$$\frac{dn}{dt} + 3\frac{\dot{a}}{a}n = \frac{g}{(2\pi)^3}\int \frac{d^3p}{E}\hat{C}[f(E,t)]. \tag{3.77}$$

Considering the generalized process $\psi + a + b + \cdots \leftrightarrow i + j + \cdots$[7], the collision term is then

[6] In this case, the phase space density has space homogeneity and isotropy, therefore, $f = f(|\mathbf{p}|, t) = f(E,t)$

[7] For the Boltzmann equation, the abundance in interest is the one of the species ψ.

$$\frac{g}{(2\pi)^3}\int\frac{d^3p}{E}\hat{C}[f(E,t)] = -\int d\Pi_\psi d\Pi_a d\Pi_b\cdots d\Pi_i d\Pi_j\cdots$$
$$\times(2\pi)^4\delta^4(p_\psi+p_a+p_b\cdots-p_i-p_j\cdots)$$
$$\times[|\mathcal{M}|^2_{\psi+a+b+\cdots\to i+j+\cdots}f_af_b\cdots f_\psi(1\pm f_i)(1\pm f_j)\cdots$$
$$-|\mathcal{M}|^2_{i+j+\cdots\to\psi+a+b+\cdots}f_if_j\cdots(1\pm f_a)(1\pm f_b)\cdots(1\pm f_\psi)], \quad (3.78)$$

where f_x are the phase space densities of the particles $i,j,\cdots,a,b,\psi$, and the $+$ signal corresponds to bosons, whereas the $-$ is referred to fermions. The $d\Pi$ factor is a simplified version, given by

$$d\Pi \equiv \frac{g}{(2\pi)^3}\frac{d^3p}{2E}. \quad (3.79)$$

The delta function guarantees energy and momentum conservation, and $\mathcal{M}$ are matrix elements squared for the processes described in Eq. (3.78) as subscript. The different matrix elements can be approximated assuming CP invariance, leading to

$$|\mathcal{M}|^2 \equiv |\mathcal{M}|^2_{i+j+\cdots\to\psi+a+b+\cdots} = |\mathcal{M}|^2_{\psi+a+b+\cdots\to i+j+\cdots}. \quad (3.80)$$

Another approximation that can be done is that since there are no degenerate species, both Fermi-Dirac and Bose-Einstein statistics are replaced by the Maxwell Boltzmann statistics. Therefore, for all species in kinetic equilibrium, the phase space density is

$$f_x = \exp\left[-\frac{(E_x-\mu_x)}{T}\right], \quad (3.81)$$

and also $1\pm f\cong 1$. The Boltzmann equation is now read as

$$\dot{n}_\psi + 3Hn_\psi = -\int d\Pi_\psi d\Pi_a d\Pi_b\cdots d\Pi_i d\Pi_j\cdots(2\pi)^4|\mathcal{M}|^2$$
$$\times\delta^4(p_i+p_j\cdots-p_\psi-p_a-p_b\cdots)[f_af_b\cdots f_\psi - f_if_j\cdots]. \quad (3.82)$$

On the left hand side of Eq.(3.82) there is the evolution of the number density of the species with respect with time, where the $3Hn_\psi$ term refers to the dilution effect that the expansion of the Universe provides. As for the right hand side, it describes the interactions that are able to change the amount of ψ particles. That way, if there are no interactions, $n_\psi \propto a^{-3}$.

It is useful to define the comoving density number,

$$Y \equiv \frac{n}{s}, \quad (3.83)$$

where s is the entropy density. With this definition the effect of expansion is no longer explicit in the Boltzmann equation. The left hand side of Eq. (3.82) is now

$$\dot{n_\psi} + 3Hn_\psi = s\dot{Y}. \tag{3.84}$$

Since the Boltzmann equation is used to study the thermal history of the Universe, another useful quantity to be introduced is the independent variable

$$x \equiv \frac{m}{T}, \tag{3.85}$$

to rewrite Eq. (3.82) in terms of the temperature. Performing the change of variables

$$\frac{dY}{dt} = \frac{dY}{dx}\frac{dx}{dt}, \tag{3.86}$$

where, for x,

$$\dot{x} = \frac{dx}{dt} = -\frac{m}{T^2}\frac{dT}{dt} = -\frac{m}{T^2}\dot{T}. \tag{3.87}$$

Using the equation for the Hubble parameter, Eq. (3.3), and since $a \propto T^{-1}$,

$$H = \frac{\dot{a}}{a} = -\frac{T}{T^2}\dot{T} = -\frac{\dot{T}}{T}, \tag{3.88}$$

therefore

$$\frac{dx}{dt} = xH, \tag{3.89}$$

and also

$$\frac{dY}{dt} = xH\frac{dY}{dx}. \tag{3.90}$$

Now, the Eq. (3.82) is rewritten as

$$\begin{aligned}\frac{dY}{dx} = &-\frac{x}{H(m)s}\int d\Pi_\psi d\Pi_a d\Pi_b \cdots d\Pi_i d\Pi_j \cdots (2\pi)^4 |\mathcal{M}|^2 \\ &\times \delta^4(p_i + p_j \cdots - p_\psi - p_a - p_b \cdots)[f_a f_b \cdots f_\psi - f_i f_j \cdots],\end{aligned} \tag{3.91}$$

where H now explicitly depends on the mass of the particle, since x and t are related by

$$t = 0.3\frac{M_{Pl}}{\sqrt{g_*}T^2} = 0.3\frac{M_{Pl}}{\sqrt{g_*}m^2}x^2 \tag{3.92}$$

during the radiation-dominated period. The Hubble parameter is then, from Eq. (B.19),

$$H(m) = 1.66\frac{\sqrt{g_*}m^2}{M_{Pl}} = H(x)x^2, \tag{3.93}$$

The applications here developed for the Boltzmann equation are described in the next chapter as an attempt to extract possible information about the production of dark matter during the early Universe.

4 Dark Matter

One of the questions that humanity tries to answer regards to what are the contents of the Universe, or more fundamentally, what its building blocks are. This wonderment started so long ago that there are evidences from centuries before Christ, such as the atomic theory by Democritus (400 b.C.) (Bertone; Hooper, 2018). Of course, the approaches used to answer this question at that period were very different from today. Traveling all the way back to the last century, not only the atom was shown to be formed by a nucleus by Rutherford, in 1911, but also a plethora of particles were detected. In the last decade, with the discovery of the Higgs boson, the Standard Model was finally complete, providing an unified description of the electromagnetic and weak forces.

Does it mean that the initial question is answered? No. Although the Standard Model is a very good description of three of the four forces that interact between visible matter, apparently, said matter only accounts for roughly 5% of the total content of the universe, which is called ordinary matter[1]. Approximately 25% of the universe is composed of dark matter, while around 70% is made of dark energy (Caldwell; Kamionkowski, 2009; Weinberg et al., 2013). As the title of the chapter suggests, this work will be, from now on, focused on some aspects of the dark matter.

One of the first to try to measure the quantity of dark matter from a dynamical estimate was Lord Kelvin. He started from the argument that the Milky Way could be described as a gas of particles in which gravity acts upon, and thus formulated a relationship between the size of the system and the velocity dispersion of the stars, reaching the conclusion that there could be around 10^9 stars within the Milky Way, although a great majority would be dark bodies, i.e., either extinct or not bright enough to be seen by an observer on Earth (Kelvin, 1904). Henri Poincaré mentioned Kelvin's work, stating that the amount of dark matter was probably very similar or less than the amount of visible matter (Poincare, 1906). Other astronomers kept on the similar conclusions, such as Ernst Öpik, Jacobus Kapteyn, Jan Oort, and James Jeans[2], and they also thought that dark matter was likely to be made of faint stars. Although another type of matter was not mentioned, a majority of authors agreed that more information should be obtained to achieve further results. Until today, the research around local dark matter density have a great relevance, and these astronomers were the pioneers.

Currently, it is known that dark matter is at least mostly composed by non-baryonic matter, it interacts with other particles through the gravitational force, and also that it

[1] Even for ordinary matter, there are still unsolved problems which the SM does not address, such as baryon on lepton asymmetry, or neutrino masses.

[2] For a deeper discussion about the history of dark matter, see (Bertone; Hooper, 2018).

does not emit light. Although not very much information is concrete about dark matter, its existence is supported by many evidences (Feng, 2010).

4.1 Dark Matter Evidences

4.1.1 Galaxy Clusters

One of the first scientist to point out a big deficit on the total amount of mass was Fritz Zwicky (Zwicky, 1937), during the decade of 1930, via a careful observation of galaxies within the Coma Cluster. Zwicky applied the virial theorem to determine the total mass of the Coma Cluster, a cluster of approximately 1000 galaxies distributed nearly in a spherically symmetrically fashion, and showed that this averaged mass differs notably from the mass expected from the galaxies luminosity.

Zwicky's results shows a very high mass-to-light ratio of $\frac{M}{L} \cong 500$. His work used the Hubble constant with the value $H_0 = 558\text{km/s/Mpc}$, obtained by Hubble and Humason (Hubble; Humason, 1931). Rescaling Zwicky's result by the current value for the Hubble constant[3], he overestimated the mass-to-light ratio by a factor of ~ 8.9 (Bertone; Hooper, 2018).

Even with this correction, the Coma Cluster velocity dispersion still points to a high mass-to-light ratio, suggesting the existence of an invisible amount of matter.

4.1.2 Galactic Rotation Curves

With the discovery of 21-line radio emission (Muller; Oort, 1951) and subsequent rise of the radio astronomy during the decades of 1950 and 1960, astronomers started to compute rotation curves, which correlate the orbital velocity of gas and stars with their distance to the galactic center(Rubin; Ford W. Kent, 1970b; Rubin et al., 1980).

For a galaxy with mass $M(r)$ distributed within a radius r, there should be an equilibrium between the gravitational pull and the centrifugal acceleration so the following relation is carried out (Liddle, 1998)

$$\frac{v^2}{r} = \frac{GM(r)}{r^2}, \tag{4.1}$$

where G is the gravitational constant, and v is the velocity of the object of interest. The Eq. (4.1) can be reorganized as

$$v = \sqrt{\frac{GM(r)}{r}}. \tag{4.2}$$

[3] From the Planck Collab (Aghanim et al., 2020b), $H_0 = 67.70$ km/s/Mpc.

The mass $M(r)$ can be supposed to have a spherically symmetric distribution in the region, therefore it obeys

$$M(r) = \frac{4\pi r^3}{3}\rho, \tag{4.3}$$

ρ being the matter density of the galaxy. Substituting Eq. (4.3) in Eq. (4.2), the velocity is expected to behave like

$$v \propto r, \tag{4.4}$$

for an object inside the galaxy. For an external region, the mass $M(r)$ is approximately constant, therefore

$$v \propto \frac{1}{\sqrt{r}}, \tag{4.5}$$

however, the observed result was that the velocity of the objects outside the galaxy tend to be constant, in other words, the rotation curves of galaxies lean to be 'flat' (Swart; Bertone; Dongen, 2017), as can be seen in Fig. 7.

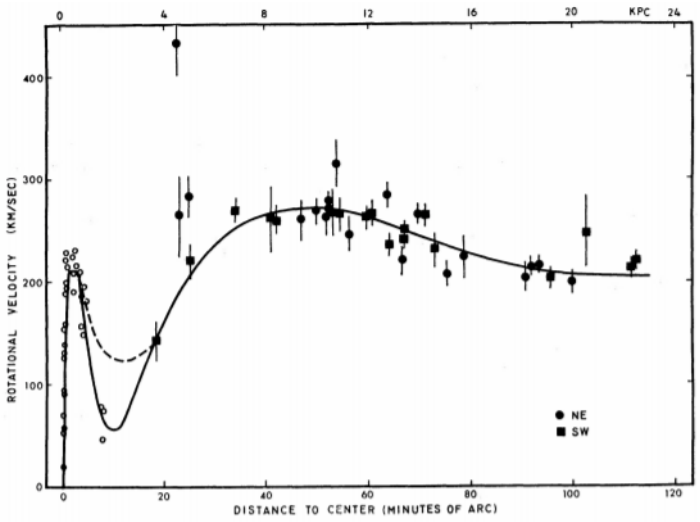

Figure 7 – Rotation curve of ionized hydrogen in M31, by Rubin and Ford. Their observed results are one of the most mentioned in history of dark matter, but others contributed to confirm such results, as can be seen in (Bertone; Hooper, 2018; Swart; Bertone; Dongen, 2017). Figure from (Rubin; Ford W. Kent, 1970a).

This result suggests that there is a great amount of unknown mass forming a halo where the galaxy is embedded in. Fig. 8 shows the rotation curve for the NGC3198 galaxy, which represent the dots with error bars, there are also contributions from the dark matter halo only and visible contributions from the galactic disk only (van Albada et al., 1985).

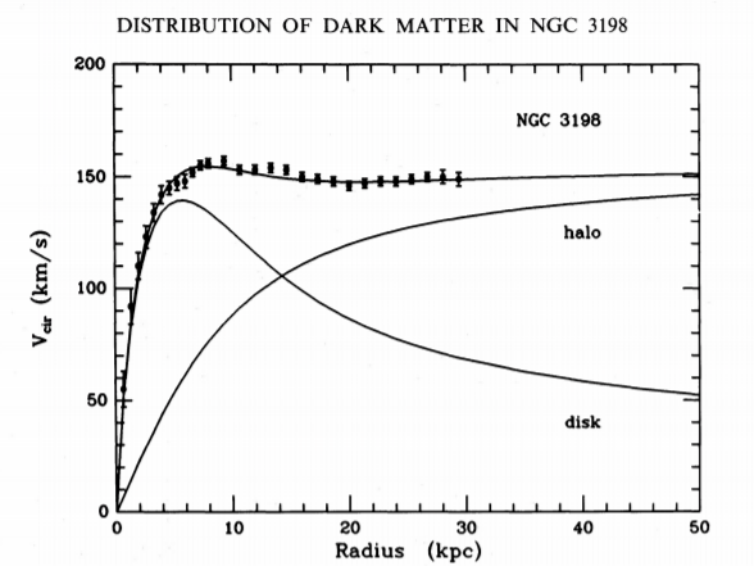

Figure 8 – Galactic rotation curve from NGC3198. Figure from (van Albada et al., 1985).

This is not the only possible explanation for the observed events, since there are propositions for modified newtonian dynamics[4] (MOND) (Milgrom, 1983), for instance. It also does not explains what kind of matter could be composing the dark matter halo, a notable possibility being baryonic matter, i.e., massive objects that do not emit light[5], or non-baryonic matter. However, the study of galactic rotation curves represent another piece of the foundation of the dark matter community.

4.1.3 Gravitational Lensing

Gravitational lensing is an effect predicted by general relativity, where, because of the intense gravitational influence that very massive objects have on space-time, the path made by light bends as it meets such objects while traveling towards an observer. In other words, the massive object generates a gravitational field that deflects the trajectory made by light (emitted by a luminous object), as seen in Fig. 9. The observed result can be amplification, multiplication, or distortion of the image of the object that emits the deviated light. In addition, the mass of the object that provokes the lensing effect can be measured based on how much the light is deflected (Schneider; Ehlers; Falco, 1992).

The gravitational lensing is divided into three classes: strong lensing, weak lensing, and microlensing (Einasto, 2010).

The strong lensing occurs when the source is close and the lens (the object that causes the effect) is significantly massive. The visible result of strong lensing is multiplied images and also the formation of rings, as seen in Fig. 10. Objects responsible for strong

[4] These are theories that modify the newtonian gravitational model for large scales.
[5] It is well known nowadays that MACHOs,massive compact halo objects, do not provide the total abundance of DM.

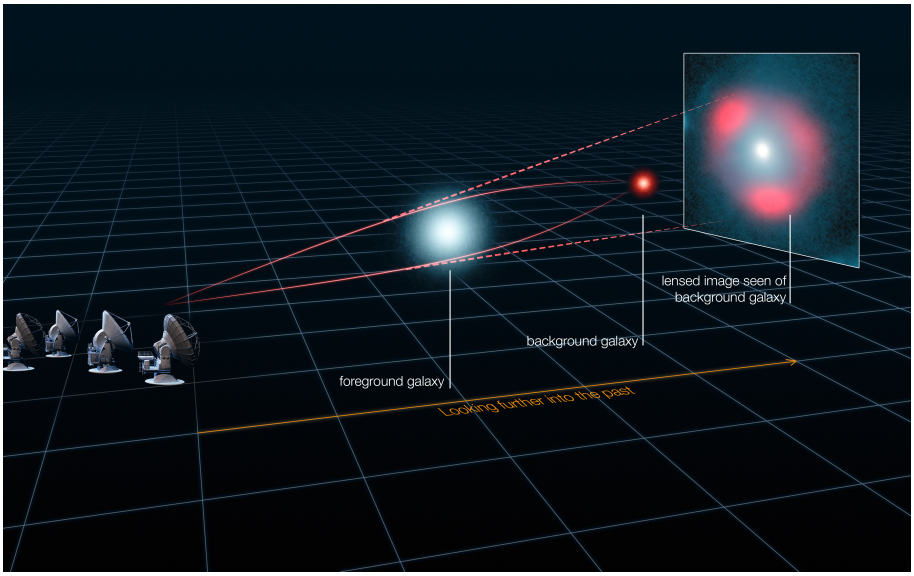

Figure 9 – Schematic illustration of the gravitational lensing effect. Credit: ALMA (ESO/NRAO/NAOJ), L. Calçada (ESO), Y. Hezaveh et al.

lensing are rich clusters or massive galaxies, and their effects allow the measurement of mass distribution in these regions.

Figure 10 – Example of strong lensing. Credits: ESA/Hubble & NASA.

In order to observe weak lensing, it requires a less massive lens compared to the strong lensing, causing only distortions on the background objects and rarely producing rings or multiplication of image, as the strong lensing. This effect can only be detected by analyzing a large number of distorted objects. Weak lens are used to obtain the mass distribution of dark matter in clusters. An example of work with weak lensing is (Clowe et al., 2006).

For the microlensing, no distortion can be observed, but the source at some point appears to be brighter. These events are used to locate massive compact halo objects

(MACHOs), small astronomical bodies that emit a light amount of radiation, being barely visible. MACHOs can be considered planets, dead stars, brown dwarfs, etc.

4.1.4 Bullet Cluster

The collision between a pair of clusters known as "bullet cluster- or 1E0657-588 (Clowe; Gonzalez; Markevitch, 2004; Clowe et al., 2006) - is perhaps the main evidence for DM. The first observation was made in 2004, and in detail in 2006.

The idea behind this evidence is that in the past, there was two ordinary clusters composed by visible and dark matter. Around 150 million years ago, a collision between these clusters happened, making the visible matter in each cluster interact substantially with itself. The dark matter of each system, on the other hand, had a negligible interaction, merely passing through each other.

With weak lensing it is possible to map out the center of mass of the bullet cluster, corresponding to the distribution of total mass. While only the hot gas made of ordinary matter emits X-rays, the visible matter can be localized, therefore the difference between both (total matter and visible matter) can be traced, as shown in Fig. 11.

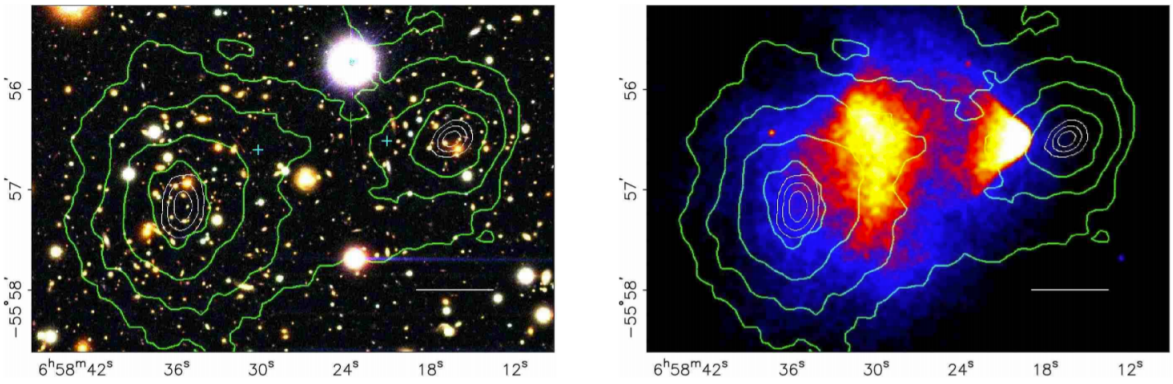

Figure 11 – Color images of the merging cluster 1E0657-588, or bullet cluster. Figure from (Clowe et al., 2006).

In Fig. 11, the green contour on both panels represents the weak lensing reconstruction or the matter distribution after the collision. On the right panel, the colored map represents the observed X-ray emission of the hot baryonic gas obtained by the Chandra space telescope. This result shows that the center of baryonic mass does not coincide with the center of the total mass. In 2015, the observation of 72 similar system was reported, concluding the existence of DM with a 7σ significance (Harvey et al., 2015). This evidence is a problem for MOND theories, since there is no explanation for the discrepancy between the centers of mass. Although being an evidence for DM, the Bullet Cluster can also be a challenge for the ΛCDM model (Lee; Komatsu, 2010).

The reports on collision between clusters also mention a superior bound to the DM self-interaction cross section. Results from 2015 (Harvey et al., 2015) show, with 95% confidence limit, that

$$\frac{\sigma}{m} < 0.47 \quad \frac{\text{cm}^2}{\text{g}}, \tag{4.6}$$

where σ is the self-interaction cross-section, and m is the dark matter mass.

4.1.5 Cosmic Microwave Background Radiation

As mentioned in Chapter 3, the CMB is a very powerful evidence for the early Universe. It is related to the period where the photons decoupled from the thermal bath, after not being able to ionize atoms anymore. This happened shortly after the recombination and since their decoupling, these photons created during the early stages of the Universe travel until today, being detected by observers (Samtleben et al., 2007).

The CMB was proposed by Alpher and Herman (Alpher; Herman, 1948) in 1948 and discovered accidentally in 1965 by Penzias and Wilson[6] (Penzias; Wilson, 1965). The photons that originated the CMB follow a blackbody radiation spectrum for a temperature $T = 2.73$ K with remarkable precision (Aghanim et al., 2020b). A deep analysis of the CMB power spectrum shows slight temperature variations in different directions in space. These anisotropies due to temperature fluctuations, are seen in Fig 12. The CMB anisotropies can be used to establish bounds for the cosmological parameters.

While developing a cosmological model to explain the evolution of the Universe, the first assumption made was that the Universe is homogeneous and isotropic. As the cosmological principle states, this assumption is really observed in large scales. However, how can an universe that hold these properties since its beginning have such large structures as the ones observed today? Following the same reasoning, once the CMB photons carry characteristics of the early Universe, such anisotropies show that, before the photon decoupling, the Universe already had these minor inhomogeneities on its mass distribution (Dodelson; Schmidt, 2020).

The temperature fluctuations resulted in the CMB anisotropy can be expressed as (Coles; Lucchin, 2002; Dodelson; Schmidt, 2020)

$$\frac{\delta T}{T}(\theta, \phi) = \frac{T(\theta, \phi) - T_0}{T_0} \tag{4.7}$$

[6] The astronomers were using a suspersentive antenna to detect faint radio waves and while trying to eliminate all interference they could notice, a residual noise persisted until they reached the conclusion that the noise was originated outside of Milky Way.

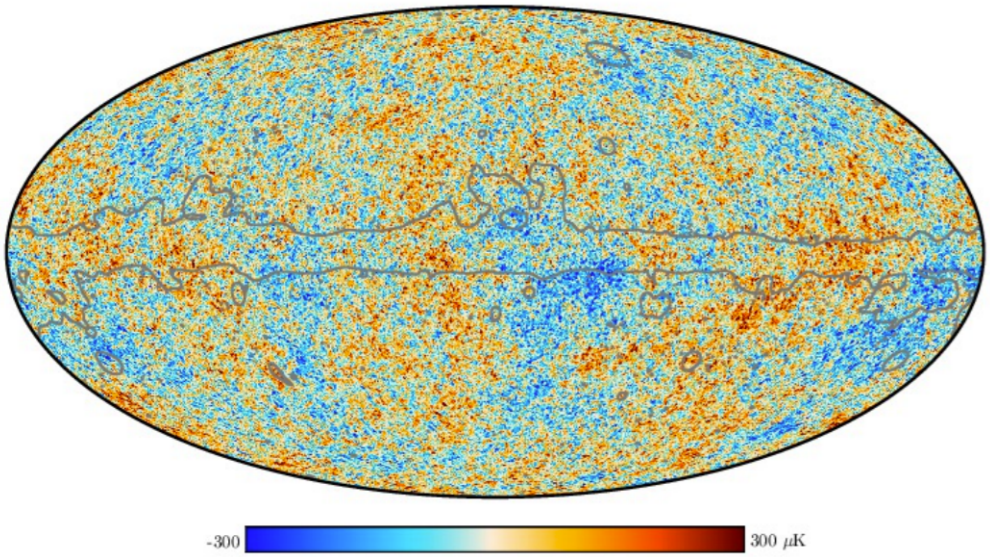

Figure 12 – CMB sky, obtained by Planck Collaboration. The panel shows the spectral matching independent component analysis (SMICA) temperature map. Figure from (Aghanim et al., 2020a).

where θ and ϕ are angles that separate different regions of the sky. The temperature distribution can also be quantified by expanding the distribution of temperature T on the as a sum over spherical harmonics as follows

$$\frac{\delta T(\theta,\phi)}{T} = \sum_{l=0}^{\infty} \sum_{m=-l}^{m=l} a_{lm} Y_{lm}(\theta,\phi), \tag{4.8}$$

the coefficients a_{lm} of the expansion define the variance C_l by

$$C_l \equiv \langle |a_{lm}|^2 \rangle = \frac{1}{2l+1} \sum_{m=-l}^{m=l} |a_{lm}|^2. \tag{4.9}$$

The θ angle is related with the multipole moment l by

$$l \cong \frac{180^o}{\theta}. \tag{4.10}$$

The Fig. 13 shows the CMB power spectrum. The anisotropies observed are related to the cosmological parameters.

The first peak of the power spectrum, for instance, is associated with the curvature of the Universe, whereas acoustic oscillations are connected to dark matter, baryonic, and dark energy abundances (Perkins, 2008). The value of these parameters for the ΛCDM model, can then be obtained by comparison with the experimental data.

From Table 1, it is clear that the amount of non-baryonic matter is much larger than the amount of baryonic matter, implying that, from CMB power spectrum analysis,

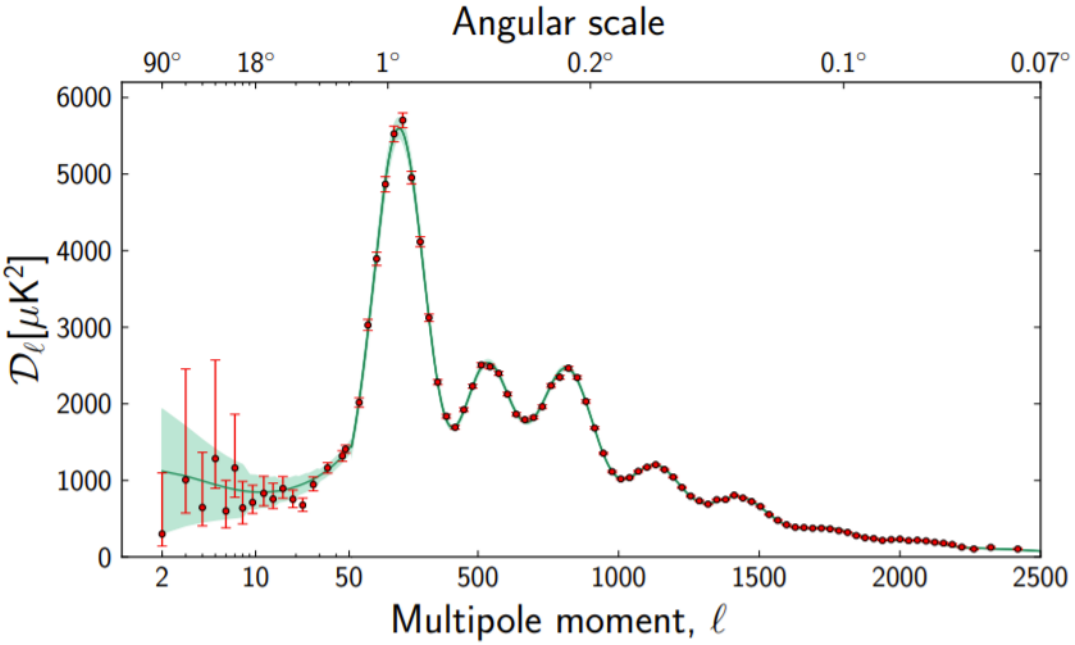

Figure 13 – Angular power spectrum of CMB, obtained by the Planck satellite (Ade et al., 2014).

Name	Symbol	Value
Baryonic Matter Density	$\Omega_b h^2$	0.02242 ± 0.00014
Dark Matter Density	$\Omega_c h^2$	0.11933 ± 0.00091
Dark Energy Density Parameter	Ω_Λ	0.6889 ± 0.0056
Total Mass Density Parameter	Ω_m	0.3111 ± 0.0056
Total Density Parameter	Ω	0.9993 ± 0.0019
Curvature Parameter	Ω_k	0.001 ± 0.002
Hubble Constant	H_0 [km s^{-1}Mpc^{-1}]	67.66 ± 0.42

Table 1 – Cosmological Parameters obtained by the Planck Collaboration (Zyla et al., 2020; Aghanim et al., 2020a).

the Universe is dominated by dark energy and non-baryonic dark matter. It also shows how close to one the total density parameter is, resulting in a flat Universe.

There are other important evidences for the existence of dark matter, such as the structure formation, where dark matter plays a crucial role on the distribution of galaxies and clusters, leading to a homogeneous and isotropic Universe essentially on large scales. The structure formation is important to rule out hot dark matter[7] as a candidate, and to reinforce the fact that largest amount of matter comes from non-baryonic matter. For a more in-dept discuss on this topic, the reference (Einasto, 2010) is a suggestion.

Another evidence that is worth mentioning is the Big Bang Nucleosynthesis (BBN)

[7] The difference between hot, cold, and warm dark matter lies on the speed which each candidate travels, being hot the faster, traveling in ultra-relativistic speeds, and cold the slower. The difference between these candidates also reflects on the early Universe, when considering a thermal production.

(Steigman, 2007). As previously stated, BBN is the process where light nuclei were formed in the early Universe, but atoms were not able to form yet, due the high concentration of very energetic photons. With the BBN, predictions on abundances of these light elements that are synthesized during the first three minutes of the Universe can be made[8], as seen in Fig. 14. The relevance here for BBN is that it provides an estimate for the abundance of baryons, given by (Olive et al., 2014)

$$0.021 \leq \Omega_b h^2 \leq 0.025. \tag{4.11}$$

Since $\Omega_b h^2 \ll 1$, the amount of baryonic matter is not sufficient to account for the total content in the Universe.

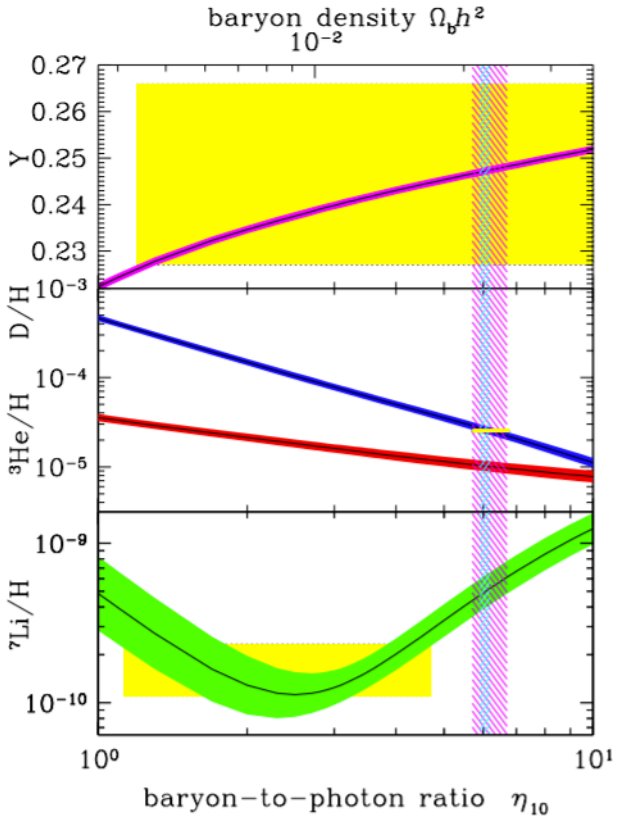

Figure 14 – Abundances for ^{4}He, ^{3}He, D, and ^{7}Li, predicted by the BBN (Olive et al., 2014).

These evidences motivate physicists around the world to gather more and more information about the nature of dark matter, so its detection can be possible. The next section dives into what could be the nature of dark matter, or even to describe its evolution since the early Universe.

[8] A good reference to the subject is (Kolb; Turner, 1990)

4.2 Solving the Boltzmann Equation

The Boltzmann equation is a great tool to describe the evolution of species that eventually fall out of equilibrium with the thermal bath. It is not only used to obtain abundance of dark matter particles that could be produced thermally and start in equilibrium with the cosmic plasma, but also to determine the abundance of light elements produced during the early Universe, or even the abundance of relic photons, neutrinos, etc. Unfortunately, the Boltzmann equation is not so simple to solve, requiring in some cases, approximations, or in some circumstances, it has a semi-analytical solution. Here the goal is to solve the Boltzmann equation for two cases: hot and cold relics. Starting with the Boltzmann equation, from Chapter 3, as described below

$$\frac{dY}{dx} = -\frac{x}{H(m)s}\int d\Pi_\psi d\Pi_a d\Pi_b \cdots d\Pi_i d\Pi_j \cdots (2\pi)^4 |\mathcal{M}|^2 \times \delta^4(p_i + p_j \cdots - p_\psi - p_a - p_b \cdots)[f_a f_b \cdots f_\psi - f_i f_j \cdots], \tag{3.91}$$

where, again,

$$d\Pi \equiv \frac{g}{(2\pi)^3}\frac{d^3p}{2E}, \tag{3.79}$$

and

$$H(m) = 1.67\frac{\sqrt{g_*}m^2}{M_{Pl}} = H(x)x^2, \tag{B.19}$$

remembering that $x = m_\psi/T$.

The first assumption is that the particle in question is stable, or has a life-time comparable to the age of the Universe. Therefore, the only process that can influence on the number density is the one involving annihilation of the species involved in the process, that is

$$\psi + \bar{\psi} \longleftrightarrow X + \bar{X}. \tag{4.12}$$

The second assumption is that there is no asymmetry between the quantities ψ and $\bar{\psi}$. The next hypothesis is that the species X and $\bar{X}$ are in thermal equilibrium during the whole process of ψ's decoupling.

With those statements in mind, the term in squared brackets on the RHS of Eq. (3.91) is now

$$[f_a f_b \cdots f_\psi - f_i f_j \cdots] = [f_\psi f_{\bar{\psi}} - f_X f_{\bar{X}}], \tag{4.13}$$

using Eq. (3.81), with $\mu_{X,\bar{X}} = 0$[9],

$$f_X = \exp\left(-\frac{E_X}{T}\right) \tag{4.14}$$

$$f_{\bar{X}} = \exp\left(-\frac{E_{\bar{X}}}{T}\right). \tag{4.15}$$

The δ-function on Eq. (3.91) guarantees that

$$E_\psi + E_{\bar{\psi}} = E_X + E_{\bar{X}}, \tag{4.16}$$

hence

$$f_X f_{\bar{X}} = \exp\left[-\frac{(E_X + E_{\bar{X}})}{T}\right] = \exp\left[-\frac{(E_\psi + E_{\bar{\psi}})}{T}\right] = f_{\psi_{eq}} f_{\bar{\psi}_{eq}}. \tag{4.17}$$

The interaction term, or RHS, of the Boltzmann equation is then expressed as

$$\frac{dn_\psi}{dt} + 3Hn_\psi = -\langle\sigma_{\psi\psi\to\bar{X}\bar{X}}|v|\rangle(n_\psi^2 - n_{\psi_{eq}}^2), \tag{4.18}$$

where the thermally averaged annihilation cross section times velocity is given by

$$\begin{aligned}\langle\sigma_{\psi\psi\to\bar{X}\bar{X}}|v|\rangle =& n_{\psi_{eq}}^{-2}\int d\Pi_\psi d\Pi_{\bar{\psi}} d\Pi_X d\Pi_{\bar{X}}(2\pi)^4 \\ &\times |\mathcal{M}|^2\delta^4(p_\psi + p_{\bar{\psi}} - p_X - p_{\bar{X}})exp\left(-\frac{E_\psi}{T}\right)exp\left(-\frac{E_{\bar{\psi}}}{T}\right).\end{aligned} \tag{4.19}$$

Another way of describing the Boltzmann equation is using the variables defined in Chapter 3,

$$x \equiv \frac{m_\psi}{T}, \quad \text{and} \quad Y \equiv \frac{n_\psi}{s},$$

The equation now reads

$$\frac{dY}{dx} = -\frac{x\langle\sigma_{\psi\psi\to\bar{X}\bar{X}}|v|\rangle s}{H(m)}(Y^2 - Y_{eq}^2). \tag{4.20}$$

The scenario can be generalized to any process of the type $\psi + \bar{\psi} \to F$, being F not necessarily a two-body state. In that sense, the thermally averaged cross section can be substituted by the total annihilation cross section $\langle\sigma_A|v|\rangle$, involving all channels, yielding the two forms of the Boltzmann equation

[9] This relation is considered by simplicity, once X and $\bar{X}$ are in thermal equilibrium.

$$\frac{dn_\psi}{dt} + 3Hn_\psi = -\langle\sigma_A|v|\rangle(n_\psi^2 - n_{\psi_{eq}}^2), \tag{4.21}$$

$$\frac{dY}{dx} = -\frac{x\langle\sigma_A|v|\rangle s}{H(m)}(Y^2 - Y_{eq}^2). \tag{4.22}$$

It is possible to realize from Eq. (4.21) that the species are in equilibrium when $n = n_{eq}$, or if the annihilation is balanced by the creation process. The Boltzmann equation is divided in the relativistic and the non-relativistic regimes. For each, the comoving number density in equilibrium is

$$Y_{eq}(x) = \begin{cases} \frac{45}{2\pi^4}\left(\frac{\pi}{8}\right)^{1/2}\frac{g_{eff}}{g_{*S}(x)}x^{3/2}e^{-x}, & \text{non-relativistic } (x \gg 3), \\ \frac{45\zeta(3)}{2\pi^4}\frac{g_{eff}}{g_{*S}(x)}, & \text{relativistic } (x \ll 3), \end{cases} \tag{4.23}$$

where g_{eff} for bosons and $g_{eff} = \frac{3}{4}g$ for fermions. From Eq. (B.19), $H = x^{-2}H(m)$, allowing Eq. (4.22) to be rewritten as

$$\frac{dY}{dx} = -\frac{x\langle\sigma_A|v|\rangle s}{H(m)}(Y^2 - Y_{eq}^2) = -\frac{x\langle\sigma_A|v|\rangle n_{eq}}{x^2H(m)Y_{eq}}Y_{eq}^2\left(\frac{Y^2}{Y_{eq}^2} - 1\right), \tag{4.24}$$

since the interaction rate is $\Gamma_A \equiv n_{eq}\langle\sigma_A|v|\rangle$, Eq. (4.24) reads

$$\frac{x}{Y_{eq}}\frac{dY}{dx} = -\frac{\Gamma_A}{H}\left(\frac{Y^2}{Y_{eq}^2} - 1\right). \tag{4.25}$$

This version of the Boltzmann equation is interesting because it can be related to the analysis made in Chapter 3, about the rule for the Γ/H fraction, and a qualitative discussion can be made before actually solving the equation.

The familiar term appears multiplied by a deviation factor. When $\Gamma_A > H$, the comoving number density decreases. Since $\Gamma = n_{eq}\langle\sigma|v|\rangle$, Γ_A is proportional to a power of x, because[10] $n_{eq} \propto x^{-3}$. Considering that the species starts in chemical equilibrium, hence for $x < 1$, Y tracks Y_{eq}, thus $Y = Y_{eq}$. As x approaches to 1, $\Gamma_A < H$, the particles fall out of equilibrium, and Γ_A decreases exponentially, once n has a Boltzmann suppression. At some point, the annihilations are no longer effective enough to overcome the expansion of the Universe. The relative change in Y becomes small, the annihilation rate freezes-out, and the comoving number density "freezes-in", in other words, the abundance remains the same after the decoupling. After decoupling, the number density of the particles is proportional to T^3 as the Universe cools down.

[10] Before falling out of equilibrium, the species is considered relativistic.

4.2.1 Hot Relics

Hot relics refer to species that are relativistic when they decouple from the thermal bath. In this case, consider $x_f \lesssim 3$. The value of Y is the value of Y_{eq} at freeze-out, once a comoving number density out of equilibrium behaves as a relativistic species in thermal equilibrium due to the expansion of the Universe. Therefore, the quantity Y today, Y_∞ is

$$Y_\infty = Y_{eq}(x_f) = \frac{45\zeta(3)}{2\pi^4}\frac{g_{eff}}{g_{*S}(x_f)} = 0.278\frac{g_{eff}}{g_{*S}(x_f)}. \tag{4.26}$$

Considering that, after the freeze-out, the expansion remains isentropic, that is, sa^3 =constant, the current number density for a hot relic is

$$n_{\psi,0} = s_0 Y_\infty = 2970\, Y_\infty = 826\frac{g_{eff}}{g_{*S}(x_f)}\ \text{cm}^{-3}, \tag{4.27}$$

whereas the relic mass density is

$$\rho_{\psi,0} = s_0 Y_\infty m_\psi = 826\,\frac{g_{eff}}{g_{*S}(x_f)}\frac{m_\psi}{\text{eV}}\ \text{cm}^{-3}, \tag{4.28}$$

and the relic abundance is

$$\Omega_\psi \text{h}^2 \cong 7.8\times 10^{-2}\frac{g_{eff}}{g_{*S}(x_f)}\frac{m_\psi}{\text{eV}}. \tag{4.29}$$

Knowing that $\Omega_0 h^2$ is close to unit, a cosmological bound can be imposed upon the mass of the species

$$m_\psi < 14\,\frac{g_{*s}(x_f)}{g_{eff}}\ \text{eV}. \tag{4.30}$$

An example of hot relic are light neutrinos, those have mass below MeV scales and decouple when the temperature is around a few MeV, hence, for a neutrino with one helicity, $g_\nu = 1$,

$$g_{*s} = g_\gamma + \frac{7}{8}(g_e + g_{e^+} + 3g_\nu + 3g_{\bar{\nu}}) = 10.75 \tag{4.31}$$

and

$$g_{eff} = \frac{3}{4}\times 2 = 1.5. \tag{4.32}$$

Therefore,

$$m_\nu < 93\ \text{eV}. \tag{4.33}$$

This bound on neutrinos masses is referred to as the Cowsik-McClelland bound (Cowsik; McClelland, 1972). Note that the bound is upon the sum of the neutrino masses, ν_e, ν_μ, and ν_τ. It is important to stress that more stringent limits over neutrino masses comes from oscillation data, such as the KATRIN Collaboration (Aker et al., 2019), where $\Sigma m_\nu < 1.1$ eV.

4.2.2 Cold Relics

The cold relics are species that decouple while non-relativistic, or at $x_f \gtrsim 3$. In this case, Y_{eq} is decreasing exponentially after falling out of equilibrium, therefore the solution is a rather less simple than the last one. Bringing back the Boltzmann equation,

$$\frac{dY_\psi}{dx} = -\frac{x\langle\sigma_A|v|\rangle s}{H(m)}(Y^2 - Y_{eq}^2), \tag{4.22}$$

since $H(m) = Hx^2$, then

$$\frac{dY_\psi}{dx} = -\frac{\langle\sigma_A|v|\rangle s}{Hx}(Y^2 - Y_{eq}^2). \tag{4.34}$$

The first approach is to suggest for the cross section that $\sigma|v| \propto v^p$, being p a power factor. From the Boltzmann distribution equation,

$$\langle v\rangle = \left(\frac{8T}{\pi m}\right)^{1/2} \propto T^{1/2}, \tag{4.35}$$

therefore, $\sigma|v| \propto T^n$, for $n = \frac{p}{2}$. It is useful to parametrize the thermally averaged cross section as

$$\langle\sigma|v|\rangle = \sigma_0\left(\frac{m}{T}\right)^{-n} = \sigma_0 x^{-n}, \tag{4.36}$$

where σ_0 does not depends on x. The factor n then stands[11] for s-wave if $n = 0$, and for p-wave if $n = 2$.

The Boltzmann equation can be more simplified by remembering that

$$H = 1.66\frac{m^2}{M_{Pl}x^2}, \quad \text{and} \quad s = \frac{2\pi^2}{45}g_{*s}\frac{m^3}{x^3}, \tag{4.37}$$

thus

$$\frac{dY}{dx} = -x^{-n-2}\lambda(Y^2 - Y_{eq}^2), \tag{4.38}$$

[11] These denominations come from the partially-spherical parametrization of scattered particles on quantum mechanics.

where

$$\lambda \equiv \left[\frac{\langle\sigma|v|\rangle s}{Hx}\right]_{x=1} = 0.264\frac{g_{*s}}{\sqrt{g_*}}M_{Pl}\, m\, \sigma_0, \tag{4.39}$$

and the equilibrium comoving number density is

$$Y_{eq} = \frac{n_{eq}}{s} = 0.145\frac{g}{g_{*s}}x^{3/2}e^{-x} = ax^{3/2}e^{-x}. \tag{4.40}$$

To solve the equation, the difference between the comoving number density and the equilibrium comoving number density, $\Delta \equiv Y - Y_{eq}$, is substituted in the Boltzmann equation. Then, the following regimes are considered: before the freeze out, where $x \ll x_f$, a long time after the freeze-out, or $x \gg x_f$, in order to obtained Y_∞, and another for $x \cong x_f$, to achieve a more detailed description of the behavior of Y around the freeze-out. The differential equation for Δ is

$$\Delta' = \frac{d\Delta}{dx} = \frac{dY}{dx} - \frac{dY_{eq}}{dx} = -\lambda x^{-n-2}(Y^2 - Y_{eq}^2) - \frac{dY_{eq}}{dx} \tag{4.41}$$

$$\Delta' = -Y'_{eq} - \lambda x^{-n-2}(Y^2 - Y_{eq}^2), \tag{4.42}$$

however,

$$Y^2 - Y_{eq}^2 = \Delta(2Y_{eq} + \Delta), \tag{4.43}$$

and hence

$$\Delta' = -Y'_{eq} - \lambda x^{-n-2}\Delta(2Y_{eq} + \Delta). \tag{4.44}$$

In the region $1 \ll x \ll x_f$, Y tracks Y_{eq} very closely, so that Δ and Δ' are very small quantities, hence an approximate solution is achieved considering $\Delta' = 0$, resulting in

$$\Delta \cong -\frac{x^{n+2}Y'_{eq}}{\lambda(2Y_{eq} + \Delta)} \cong \frac{x^{n+2}}{\lambda}, \tag{4.45}$$

where, in the last step, the following approximation was made

$$\frac{Y'_{eq}}{Y_{eq}} = \frac{3}{2x} - 1 \cong -1 \tag{4.46}$$

Whereas for $x \gg x_f$, Y_{eq} is exponentially small compared to Δ. Since Y tracks Y_{eq} very poorly, $\Delta \cong Y \gg Y_{eq}$, making terms involving Y_{eq} negligible and

$$\Delta' = -\frac{\lambda}{x^{n+2}}\Delta^2. \tag{4.47}$$

At this point, the creation of particles has practically ceased, while the annihilations are somewhat important. Integrating Eq. (4.47) from $x = x_f$ to $x \to \infty$ leads to

$$-\frac{1}{\Delta_\infty} - \frac{1}{\Delta_f} = -\frac{1}{Y_\infty} - \frac{1}{\Delta_f} = \lambda \left(\frac{x^{-n-1}}{n+1} \right)_{x_f}^{\infty} = -\frac{\lambda}{n+1}\frac{1}{x_f^{n+1}}. \tag{4.48}$$

To simplify Eq. (4.48), consider the scenario around the freeze-out temperature, Y stops tracking Y_{eq}, and Δ becomes of order Y_{eq}. The change is abrupt, as Y goes from decreasing exponentially to leveling out to a constant. The freeze-out can be defined by the condition

$$Y_f = (1 + c)Y_{eq}(x_f), \tag{4.49}$$

where c is of order unity and determined empirically. Then, at the vicinity of x_f, Δ is given by

$$\Delta_f = Y_f - Y_{eq}(x_f) = cY_{eq}(x_f). \tag{4.50}$$

Back to the period after the freeze-out, Y is considerably small compared to Y_{eq} around the freeze-out, hence this can be extended to $Y_\infty \ll \Delta_f$. Using Eq. (4.48),

$$-\frac{1}{Y_\infty} - \frac{1}{\Delta_f} \cong -\frac{1}{Y_\infty}, \tag{4.51}$$

and

$$Y_\infty = \frac{n+1}{\lambda}x_f^{n+1}. \tag{4.52}$$

The Eq. (4.52) can be used on the relation for the cold dark matter relic abundance to obtain some information about the cross-section, for example. However, before doing so, an attempt to describe x_f can be made. Going back to the freeze-out period to use Eq. (4.40), and to derive Δ_f with respect to x leads to

$$\begin{aligned}\left[\frac{d\Delta}{dx}\right]_{x_f} &= -\left[\frac{dY_{eq}}{dx}\right]_{x_f} - \frac{\lambda\Delta_f(2Y_{eq}(x_f)+\Delta_f)}{x_f^{n+2}}, \qquad (4.53)\\ &= -a\left(\frac{3}{2}-x_f\right)x_f^{1/2}e^{-x_f} - \frac{\lambda\Delta_f(2Y_{eq}(x_f)+\Delta_f)}{x_f^{n+2}},\\ &= a\left(x_f-\frac{3}{2}\right)x_f^{1/2}e^{-x_f} - \frac{\lambda cY_{eq}(x_f)(2Y_{eq}(x_f)+cY_{eq}(x_f))}{x_f^{n+2}},\\ \frac{d\Delta_f}{dx} &= a\left(x_f-\frac{3}{2}\right)x_f^{1/2}e^{-x_f} - \frac{\lambda cY_{eq}^2(x_f)(2+c)}{x_f^{n+2}}, \qquad (4.54)\end{aligned}$$

where $a = 0.145\frac{g}{g_{*s}}$. Now, using the approximations $\frac{d\Delta}{dx} \ll 1$ and $x_f \gg \frac{3}{2}$, the equation for x_f is

$$ax_f^{3/2}e^{-x_f} = \frac{\lambda cY_{eq}^2(x_f)(2+c)}{x_f^{n+2}}, \qquad (4.55)$$

$$Y_{eq}(x_f) = \frac{\lambda cY_{eq}^2(x_f)(2+c)}{x_f^{n+2}}, \qquad (4.56)$$

$$e^{x_f} = \frac{a\lambda c(2+c)}{x_f^{n+1/2}}, \qquad (4.57)$$

which is approximately

$$x_f \cong \ln\left[(2+c)a\lambda c\right] - \left(n+\frac{1}{2}\right)\ln\left\{\ln\left[(2+c)a\lambda c\right]\right\}. \qquad (4.58)$$

The best fit to numerical values is $c(2+c) = n+1$ (Kolb; Turner, 1990).

Back to the comoving number density for today, substituting in the equation for number density yields

$$n_{\psi,0} = s_0Y_\infty = 2970Y_\infty \text{ cm}^{-3}, \qquad (4.59)$$

$$n_{\psi,0} = 1.13\times10^4\frac{(n+1)\sqrt{g_*}x_f^{n+1}}{g_{*s}mM_{Pl}\sigma_0} \text{ cm}^{-3}, \qquad (4.60)$$

and then the energy density is

$$\rho_{\psi,0} = 1.13\times10^4\frac{(n+1)\sqrt{g_*}x_f^{n+1}}{g_{*s}M_{Pl}\sigma_0} \text{ cm}^{-3}, \qquad (4.61)$$

finally leading to the relic abundance

$$\Omega_\psi h^2 = 1.04\times10^9 \text{ GeV}^{-1}\frac{(n+1)\sqrt{g_*}x_f^{n+1}}{g_{*s}M_{Pl}\sigma_0}. \qquad (4.62)$$

The relic abundance can be rewritten in terms of the cross section, so its value can be estimated. Remembering that $\langle\sigma_A|v|\rangle = \sigma_0 x^{-n}$, and for s-wave annihilations, $n = 0$,

$$\Omega_\psi h^2 = 1.04 \times 10^9 \text{ GeV}^{-1} \frac{\sqrt{g_*} x_f}{g_{*s} M_{Pl} \langle\sigma_A|v|\rangle}. \tag{4.63}$$

Assuming $\Omega_c h^2 \cong 0.11$ and $M_{Pl} = 1.22 \times 10^{19}$ GeV,

$$\langle\sigma_A|v|\rangle \lesssim 7.75 \times 10^{-10} \text{ GeV}^{-2} x_f \frac{\sqrt{g_*}}{g_{*s}}. \tag{4.64}$$

Typical values of Weakly Interactive Massive Particles (WIMPs) are $x_f \cong 20$, $g_* \cong g_{*s} = 106.75$, and $m \propto 10^2$ GeV. For these candidates, the annihilation cross section would be around

$$\langle\sigma_A|v|\rangle \lesssim 3 \times 10^{-26} \text{ cm}^3\text{s}^{-1}. \tag{4.65}$$

Fig. 15 shows the behavior of this species around the freeze-out epoch. It is important to notice that as the annihilation cross section increases, the species takes longer to decouple, decreasing its abundance.

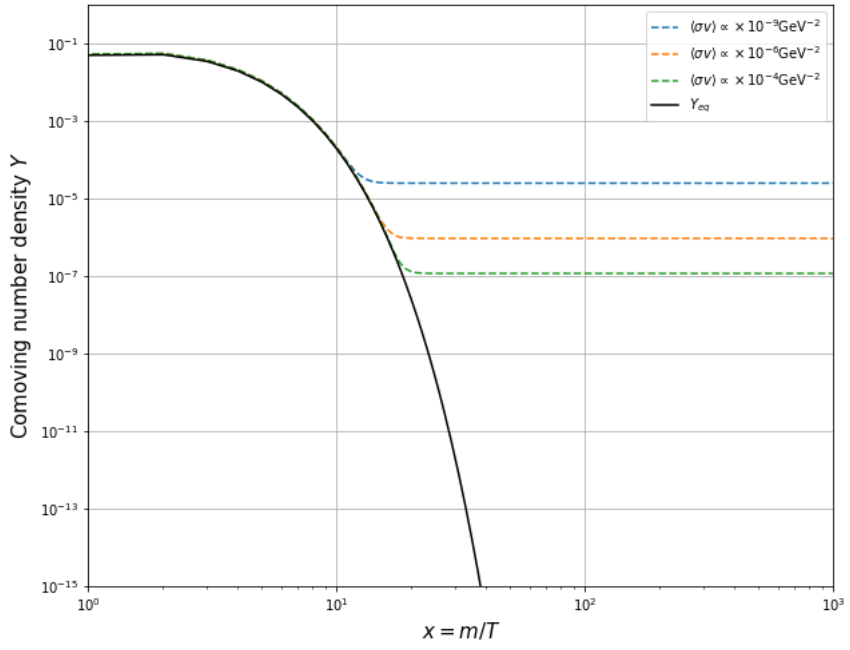

Figure 15 – Freeze-out for massive species. The solid black line represents the comoving number density in equilibrium with the thermal bath, while the dashed lines represent the abundance for different annihilation cross sections.

The result from Eq. (4.65) is very interesting and frequently referred to as "WIMP miracle" due the fact that the value lies in the same region of cross sections for electroweak interactions. This dark matter candidate is assumed to interact weakly with standard model particles, making it difficult to detect, however "strongly" enough to keep in thermal

equilibrium until its eventual freeze-out, since WIMP's are supposed to be heavier the SM particles, the latter would no longer be able to produce DM particles once the Universe reaches temperatures of order of the WIMP's mass, leading to the suppression on the comoving number density, and eventually on the decoupling of DM and the relic abundance observed today. The WIMP miracle could point to models of new physics at weak scales to solve this and other problems of the standard model. This is a possibility that motivates the detection of DM particles, setting efforts on searches at colliders, satellites, telescopes, and underground detectors.

4.3 Detection Methods

As demonstrated in the previous section, in order to produce CDM thermally in the early Universe the WIMPs must interact with the SM particles via processes mediated by interactions interactions with the cross section of order $\langle \sigma v \rangle$ 10^{-9} GeV^{-2} 10^{-26} cm^3 s^{-1}. This lower bound guarantees that DM is no overproduced. It also provides interactions that, ideally, can be measured today. That said, it is interesting to briefly analyze, before discussing the detection methods, what would be a good range of mass for WIMP candidates.

The first bound that can be imposed is the unitarity bound on the annihilation cross section (Griest; Kamionkowski, 1990). As result, the DM mass cannot be higher than PeV scales. Also, the DM mass cannot be too low, for a mass of order keV or below could impact on structure formation processes due to the free streaming length (Viel et al., 2013). Moreover, thermal relics with mass below MeV can affect BBN and CMB (Sabti et al., 2020). Finally, assuming the thermal WIMPs with s-wave annihilation with visible final states, the mass window is given by (Leane et al., 2018)

$$10 \text{ GeV} \lesssim m_{WIMP} \lesssim 100 \text{ TeV}. \tag{4.66}$$

as shown in Fig. 16.

The experiments that search for WIMPs are built with this mass window in mind. From now on, an overview of the current detection methods will be presented. The three search strategies can be described in essence by the following diagram from Figure 17, where the arrows represent the DM interactions of each possible way to search for a DM particle.

Therefore, the DM detection methods are called indirect, direct, and collider searches. This section presents an overview on the first two detection methods mentioned. For a review on collider searches, see (Boveia; Doglioni, 2018).

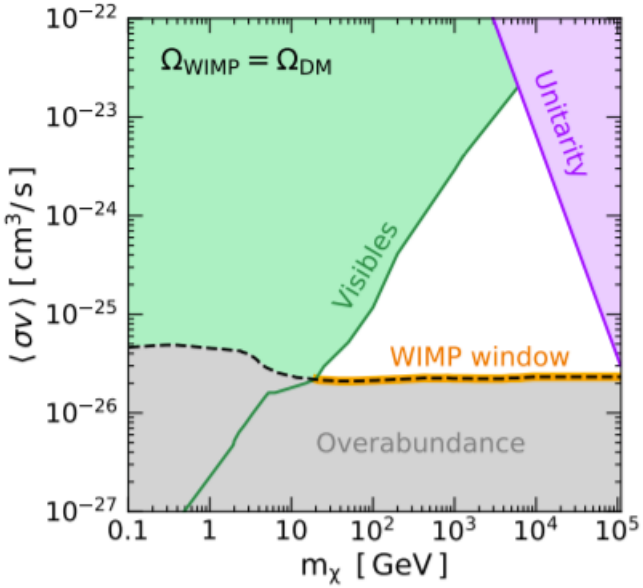

Figure 16 – Bounds on thermal WIMP for a *s*-wave annihilation, considering that all DM is composed by WIMP. Figure from (Leane et al., 2018).

4.3.1 Indirect Detection

Indirect detection refers to searches of WIMP annihilation processes where the final state is composed by SM particles. This method is explored using telescopes to observe regions that have high DM particles density, where such aforementioned processes occur. Good targets are the center of the Milky Way and nearby dwarf galaxies.

For non-relativistic DM, annihilations and decays can produce all SM particles, this first process is called primary production. However, the final product observed on Earth is composed of stable particles[12] (Figure 18), this is the secondary process, given by the decay of unstable particles or the hadronization process. The mostly discussed scenario here is the gamma rays, whose energy scale is set by the DM mass. For a WIMP candidate, the DM particle moves slowly compared to the speed of light, thus both annihilation and decay processes are approximately equivalent in terms of kinematics, since the DM initial state is considered at rest.

When searching for photons as the final product, the indirect detection has the advantage that photons carry direction and energy information, for they propagate without much further interaction after their production. In contrast to the charged particles, for example, that interact with magnetic fields, accelerating and changing the direction in a way that it turns to be challenging to reconstruct their propagation path, and localize their source. On the other hand, many astrophysical processes also produce photons, being the gamma rays production via DM annihilation usually subdominant. Therefore, it is difficult to discriminate the astrophysical background from the process of interest. Fig. 19

[12] Such as electrons, positrons, neutrinos, protons, anti-protons, and gamma rays.

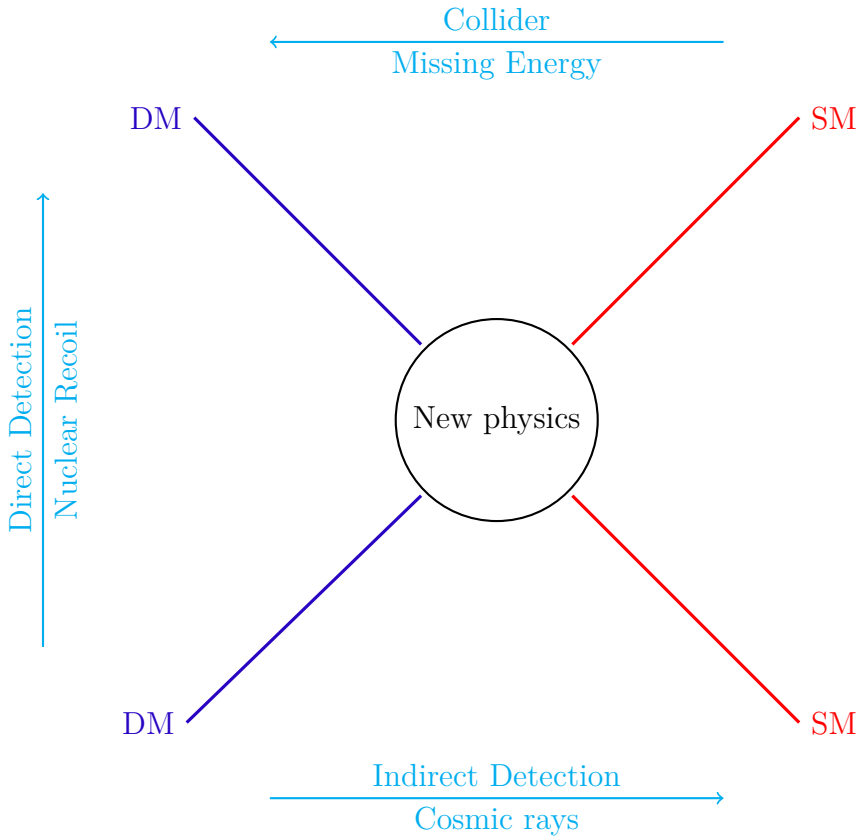

Figure 17 – Detection methods for Dark Matter.

shows the gamma-rays spectra for DM annihilations, where the gray band that is accounts for secondary particles are very difficult to distinguish.

The flux of gamma rays provenient from DM annihilations can be obtained by the number of photons per unit energy[13]

$$\frac{dN_\gamma}{dE_\gamma} = \frac{1}{4\pi r^2} \times \frac{dn_\gamma(m_\chi)}{dE_\gamma} \times \frac{1}{2} n_\chi^2 \langle \sigma v \rangle \times \Delta V \times \Delta A \Delta t, \tag{4.67}$$

where r is the distance between the observer and the signal, $\frac{dn_\gamma}{dE_\gamma}$ is the amount of photons produced per unit energy given the DM mass. The $1/2$ factor avoids the double counting of DM particles, ΔV is the observed volume where the photons are produced, ΔA is the area of the telescope, and Δt is the exposition time. The equation (4.67) can be rewritten as

$$\frac{dN_\gamma}{dE_\gamma} = (\Delta A \Delta t) \times \left(\frac{\langle \sigma v \rangle}{m_\chi^2} \right) \times \left(\frac{dn_\gamma(m_\chi)}{dE_\gamma} \right) \times \left(\frac{1}{8\pi} \int \rho_\chi^2 dr d\Omega \right). \tag{4.68}$$

Considering the RHS of Equation (4.68), the first term depends only on the detector, the second and third terms address only particle physics properties, and the last one is related

[13] For more detail, the lecture from (Slatyer, 2017) is a suggestion.

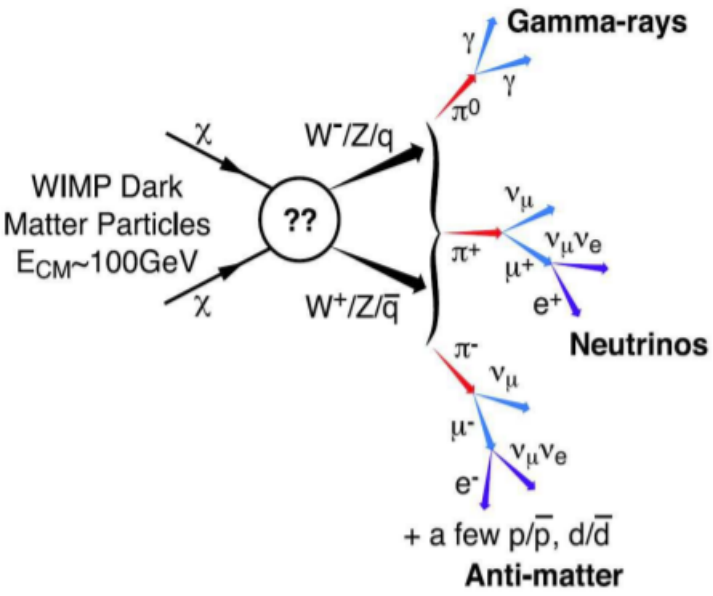

Figure 18 – Possible final states for DM annihilation. Figure from (Vitale; Morselli, 2009).

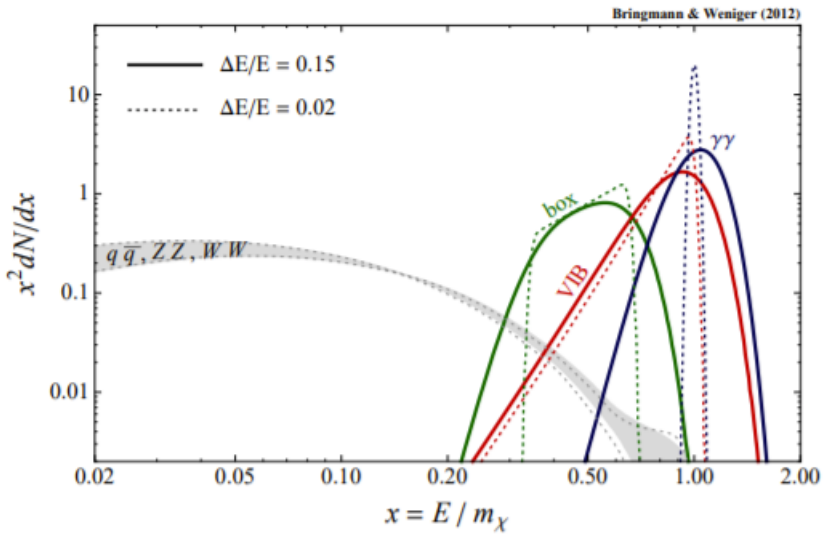

Figure 19 – Gamma ray spectra for different energies, where x is the photon energy, normalize in a way that for $x = 1$, $E = m_\chi$, being χ the DM particle. Figure from (Bringmann; Weniger, 2012).

to astrophysics. The observed quantity is usually the differential flux per unit energy per unit solid angle, given by

$$\frac{d\Phi_\gamma}{dE_\gamma d\Omega} = \frac{\langle \sigma v \rangle}{m_\chi^2} \frac{dn_\gamma(m_\chi)}{dE_\gamma} J, \tag{4.69}$$

where the astrophysical properties are parameterized by the J-factor

$$J_{ann} \equiv \frac{1}{8\pi} \int_{l.o.s} d\ell \rho_\chi^2, \tag{4.70}$$

which is an integration along the line of sight. For DM decay the J-factor will change to

$$J_{decay} \equiv \frac{1}{8\pi} \int_{l.o.s} d\ell \rho_{\chi}. \tag{4.71}$$

Considering the thermal annihilation cross section obtained in the last section,

$$\langle \sigma v \rangle \cong 3 \times 10^{-26} \text{ cm}^3 \text{ s}^{-1}, \tag{4.72}$$

cold relics lighter than 100 GeV are excluded by the Fermi-LAT observations, as shown in figure 20. Another main experiments that search for gamma rays are H.E.S.S., Veritas, and the Cherenkov Telescope Array (CTA), the latter currently under construction and planned to probe higher masses for the WIMP candidates.

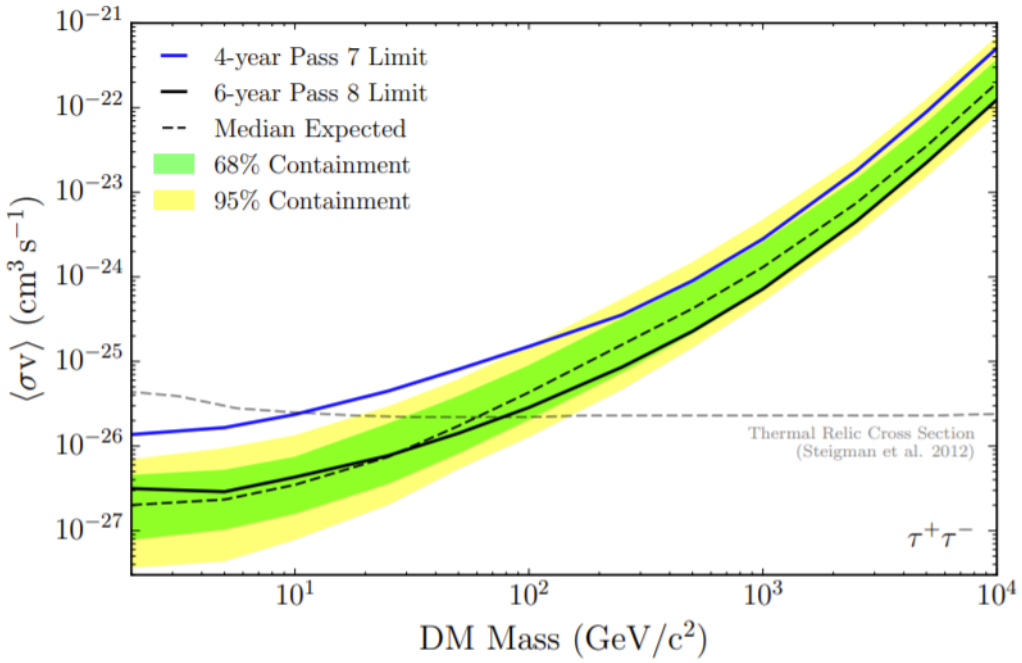

Figure 20 – Constrains on DM annihilations for the $\tau^+\tau^-$ channel. The dashed gray line represents the thermal relic cross section. Figure from (Ackermann; Albert et al., 2015).

4.3.2 Direct Detection

The second method, first discussed by Goodmann and Witten (Goodman; Witten, 1985), refers to the elastic scattering between a WIMP particle and a DM nuclei target inside a detector. The reasoning behind this type of experiment is that, since the Milky

Way is surrounded by a DM halo, there is a flux of DM particles that depends on it mass. For instance, considering $m_\chi = 100$ GeV, the flux is estimated to be

$$\Phi_\chi = \frac{\rho_\chi}{m_\chi}\langle v\rangle \cong 10^4 \left(\frac{\text{GeV}}{m_\chi}\right) \text{cm}^{-2}\ \text{s}^{-1}, \tag{4.73}$$

where $\rho_\chi = 0.3$ GeV cm^{-3} the local DM density, and $\langle v\rangle = 220$ km s^{-1} the averaged velocity of WIMP particles on Earth.

As WIMPs are weakly interacting, it is very difficult to detect such particles. The experiments built for direct searches have a nuclear target shielded and located underground in order to avoid the interaction of other cosmic particles with the experiment. Suppose that the incoming flux of invisible particles is reaching the underground detector. Therefore, at some point, the targeted nuclei, initially at rest, starts to move for no apparent reason, namely, an interaction between the DM particle and the nuclei provokes a nuclei recoil. If no signal is observed, a bound on the scattering cross section is imposed over the DM parameter space.

The kinematics of the elastic scattering in this case is a relatively simple one, since the non-relativistic limit can be taken into account. Considering the scattering process

$$\chi N \to \chi N, \tag{4.74}$$

where N is the SM nucleon. The transferred momentum q can be obtained using the Mandelstam variable t,

$$|q|^2 = -t = -(p_1^\mu - p_3^\mu)^2 = 2\mu^2 v^2(1-\cos\theta), \tag{4.75}$$

being

$$\mu = \frac{m_\chi m_N}{m_\chi + m_N} \tag{4.76}$$

the reduced mass, and θ the scattering angle for a center-of-mass frame. Hence, the recoil energy of the nucleon is

$$E_R = \frac{|q|^2}{2m_N} = \frac{\mu^2 v^2(1-\cos\theta)}{m_N}. \tag{4.77}$$

The maximum recoil energy is achieved when $\theta = 180^\text{o}$, where there is practically no scattering between the WIMP particle and the nucleon. Related to the maximum recoil energy there is a minimum value for the velocity,

$$v_{min} = \sqrt{\frac{m_N E_R}{2\mu^2}}, \tag{4.78}$$

where the limits can be considered

$$v_{min} = \begin{cases} \sqrt{\frac{m_N E_R}{2m_\chi^2}}, & \text{for } m_\chi \ll m_N, \text{ and} \\ \sqrt{\frac{E_R}{2m_N}}, & \text{for } m_N \ll m_\chi. \end{cases} \tag{4.79}$$

Therefore, for a WIMP mass much lower than the nucleon mass, the minimum velocity increases as m_χ decreases. The importance is that, if the DM mass is too small, the velocity is greater than the escape velocity[14] of the galaxy. There should be then a maximum velocity in the halo. This means that the experiment can only probe a part of the WIMP velocity distribution function, for a given DM mass, since the experiments are sensitive to interaction above certain energy threshold, E_T.

The expected rate of scattering between WIMPs and the nucleus is given by (Schumann, 2019)

$$\frac{dR}{dE_R} = \frac{\rho_0 M}{m_N m_\chi} \int_{v_{min}}^{v_{esc}} v f(v) \frac{d\sigma}{dE_R} dv, \tag{4.80}$$

where M is the target mass of the detector, $f(v)$ is the WIMP velocity distribution, and $\rho_0 = 0.3$ GeV cm^{-3} is the local DM density. Integration of Eq. (4.80) over the energy yields the observed number of events for a running time T

$$N = T \int_{E_T}^{E_{max}} dE_R \epsilon(E_R) \frac{dR}{dE_R}, \tag{4.81}$$

where

$$E_{max} = \frac{2\mu^2 v_{esc}^2}{m_N} \tag{4.82}$$

is the maximum recoil energy, and $\epsilon(E_R)$ is the detector efficiency, usually energy-dependent. Figure 21 shows the expected rate for different values of recoil energy (Schumann, 2019).

The WIMP-nucleon cross section appears in Eq. (4.80) and accounts for interactions between the WIMP particles and the quarks. It depends on the model considered, since the interaction of WIMPs with baryonic matter is unknown. In general, the scattering cross section is given by

$$\frac{d\sigma}{dE_R} = \left(\frac{d\sigma}{dE_R}\right)_{SI} + \left(\frac{d\sigma}{dE_R}\right)_{SD} = \frac{m_N}{2v^2\mu^2}(\sigma_{SI} F_{SI}^2(E_R) + \sigma_{SD} F_{SD}^2(E_R)), \tag{4.83}$$

which consists of the sum of spin-independent (SI) and spin-dependent (SD) components. F_{SI} and F_{SD} are form factors, relevant for heavy targets, as Xe, I or W, due the loss of

[14] The scape velocity of the Milky Way is 544 km/s (Smith; Ruchti et al., 2007).

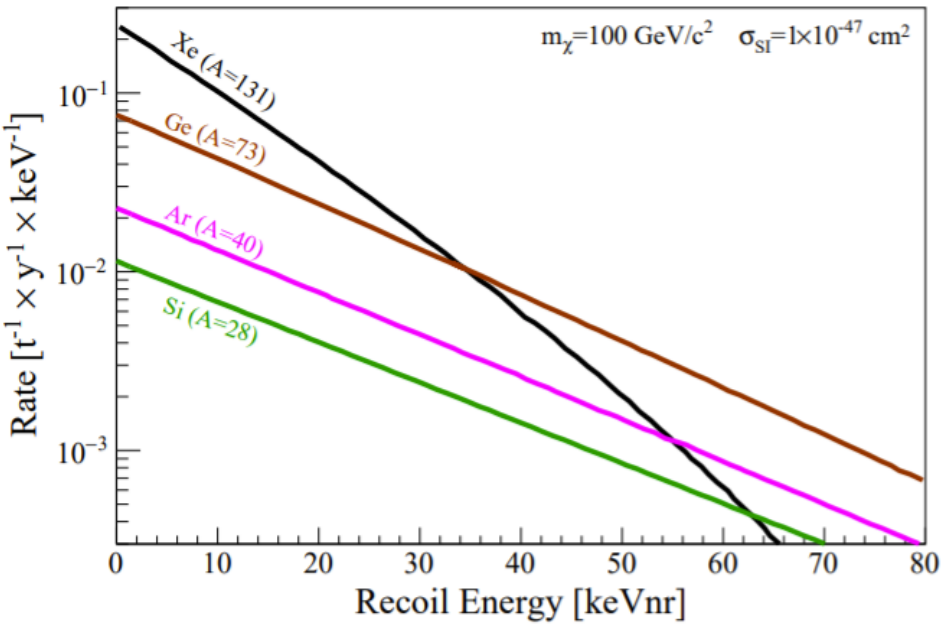

Figure 21 – Spectra for nuclear recoil, considering different target materials. The assumed mass of the DM particle is 100 GeV. The WIMP-nucleon cross section is spin-independent. Figure from (Schumann, 2019).

coherence during the scattering. The SI contributions are related to scalar and vector couplings in the Lagrangian, described by (Bertone, 2010)

$$\mathcal{L} \supset \alpha_q^s(\bar{\chi}\chi)(\bar{q}q) + \alpha_q^v(\bar{\chi}\gamma_\mu\chi)(\bar{q}\gamma^\mu q), \tag{4.84}$$

being α_q^s and α_q^v scalar and vector couplings, respectively. The differential cross section in this case is

$$\left(\frac{d\sigma}{dE_R}\right)_{SI} = \frac{2m_N}{\pi v^2}\left\{[Zf^p + (A-Z)f^n]^2 + \frac{B_N}{256}\right\}F_{SI}^2(E_R), \tag{4.85}$$

where Z is the atomic number, A the mass number, f^p and f^n the WIMP-proton and WIMP-neutron couplings, respectively, and B_N is defined by[15]

$$B_N \equiv \alpha_u^v(A+Z) + \alpha_d^v(2A-Z), \tag{4.86}$$

where α_u^v and α_d^v are vector couplings for the up and down quarks. The WIMP coupling to neutrons and protons is generally similar, leading to the good approximation for the SI contribution

$$\left(\frac{d\sigma}{dE_R}\right)_{SI} = \frac{2m_N A^2(f^p)^2)}{\pi v^2}F^2(E_R). \tag{4.87}$$

[15] For more details, see (Bertone, 2010).

The SD contributions, on the other hand, can be described by an axial-vector coupling in the Lagrangian,

$$\mathcal{L} \supset \alpha_q^A(\bar{\chi}\gamma^\mu\gamma_5\chi)(\bar{q}\gamma_\mu\gamma_5 q). \tag{4.88}$$

The differential cross section is

$$\left(\frac{d\sigma}{dE_R}\right)_{SD} = \frac{16 m_N}{\pi v^2}\Lambda^2 G_F^2 J(J+1) F_{SD}(E_R), \tag{4.89}$$

where Λ accounts for expectation values of the spin content for the nucleus, determined by nuclear models, G_F is the Fermi constant, and J is the total angular momentum of the nucleus.

Although both contributions are taken into account, the fact that the SI one is proportional to A^2, this factor is dominant over the SD contribution[16]. For this reason, the detectors are usually more sensitive to the SI WIMP coupling.

Figure 22 shows current upper limits from several direct detection experiments over the scattering cross section versus DM mass. The experiments include CDEX (Liu et al., 2019), CDMSLite (Agnese et al., 2019), COSINE-100 (Adhikari et al., 2018), CRESST (Angloher et al., 2017; Abdelhameed et al., 2019), DAMA (Bernabei et al., 2008), DAMIC (Aguilar-Arevalo et al., 2020), DarkSide (Agnes et al., 2018a; Agnes et al., 2018b), EDELWEISS (Armengaud et al., 2019; Hehn et al., 2016), LUX (Akerib et al., 2017; Akerib et al., 2019), NEWS-G (Arnaud et al., 2018), PANDA (Cui et al., 2017), and XENON (Aprile et al., 2016; Aprile et al., 2018; Aprile et al., 2019; Aprile et al., 2021) collaborations. The most restrictive limits come from XENON1T. Moreover figure 23 shows projections from different experiments, described in (Billard et al., 2021).

So far, WIMPs are the main candidates for DM. The intense activity and impressive progress on experimental searches lead to no conclusive or undisputed signals of DM, but several bounds for WIMPs interactions were imposed. Even though DM has not been yet observed, the WIMP framework is still motivating, and future experiments are expected to probe the surviving scenarios.

It is worth pointing out once more that WIMPs are not the only existing candidates for DM. Different alternatives are also explored, such as the feebly interacting massive particles (FIMPs) (Hall et al., 2010), axions[17] or axion-like particles (ALPs), and sterile neutrinos. An important alternative for particle DM are the primordial black holes (PBH) (Carr; Kühnel; Sandstad, 2016). Since candidates aside WIMPs are not discussed here,

[16] Most of the experiments use heavy nuclei, then, in general $A > 20$.

[17] Axions are particles proposed to solve the strong CP problem in quantum chromodynamics (QCD) (Peccei; Quinn, 1977).

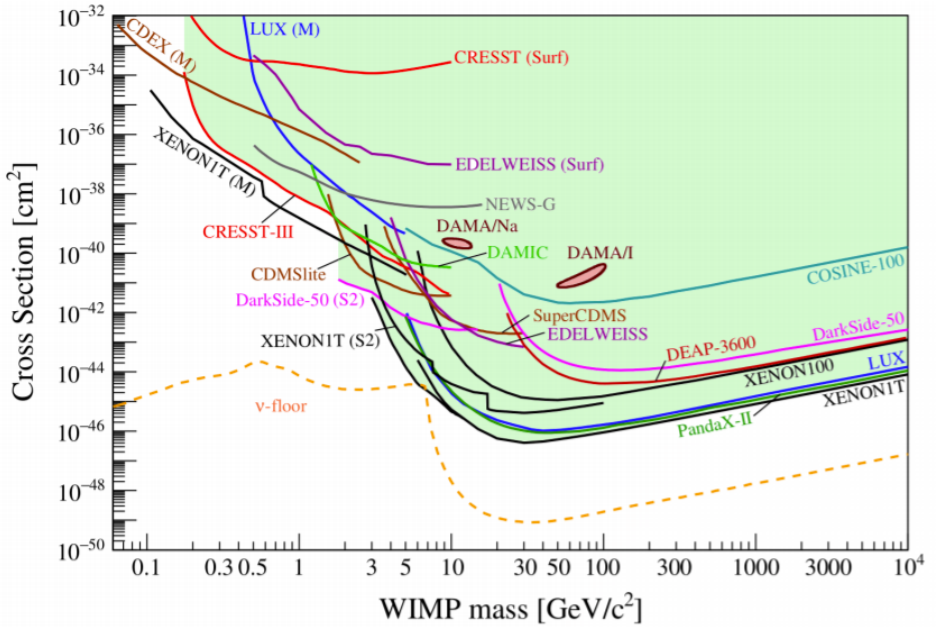

Figure 22 – Current scenario for searches for SI elastic WIMP-nucleus scattering. The dashed line limits the parameter space from below and represents the “neutrino floor", a irreducible background due coherent neutrino interactions with target nuclei (Billard; Figueroa-Feliciano; Strigari, 2014). Figure from (Billard et al., 2021).

reviews on particle DM candidates can be found in (Zyla et al., 2020), and (Profumo; Giani; Piattella, 2019).

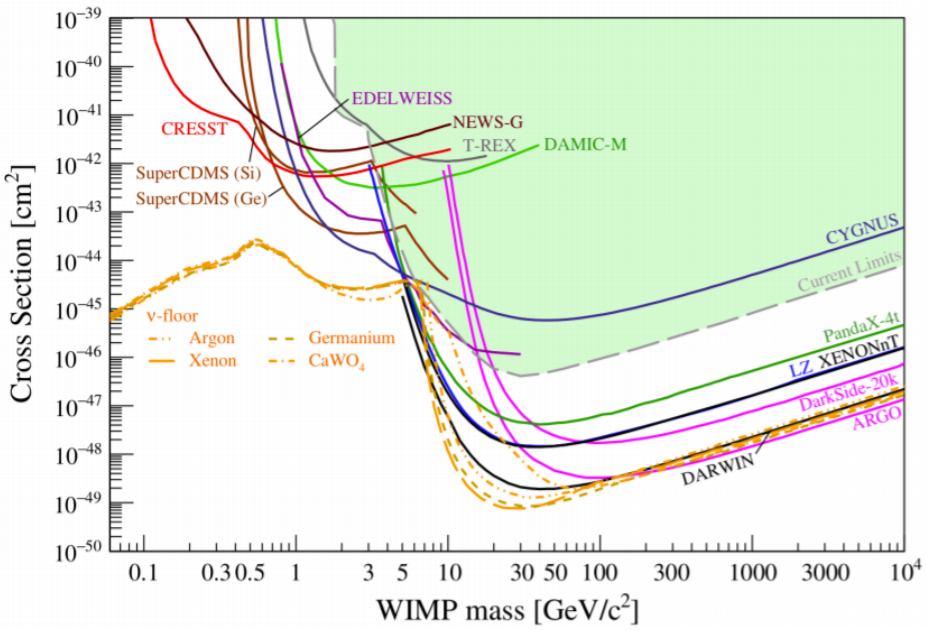

Figure 23 – Projections for direct detection experiments considering standard parameters for WIMPs. Figure from (Billard et al., 2021).

5 Conclusions

This dissertation started with a summary of the SM of particle physics, specifically the electroweak sector, presented on Chapter 2 as a motivation for the DM problem, for it fails to describe all of the contents of the Universe. Nevertheless, it is necessary to acknowledge that the SM led to a plethora of successful predictions, and is so far the best description of elementary particles, and the electroweak and strong interactions. In order to properly introduce the DM problem, the standard cosmology was discussed on Chapter 3, describing how the Universe evolves with time, essentially based on the cosmological principle. Important cosmological parameters were presented along with the thermal history of the Universe. The analysis from the third chapter was also important to understand in the Chapter that not only the CMBR shows a fairly homogeneous and isotropic early Universe, with minor perturbations, but also that it is a very convincing evidence for the existence of non-baryonic DM. During Chapter 4, other important evidences were shown, with their historical relevance. The evidences give a clue of what DM can or cannot be. After establishing the need of DM from cosmological and astrophysical observations, the thermal production of DM was explored, and through the Boltzmann equation, abundances for hot and cold relics were obtained. This is where the core of this work lies, since the cold relic for DM particles, in specific the WIMP candidate, leads to a annihilation cross section that lies in a range compatible to the scale electroweak of interactions. This result is what motivates the searches for such candidates, and different methods of detection where proposed in order to probe DM properties.

This work accomplished its main goal of presenting the usual WIMP scenario as a possible description of particle DM. The topics here discussed are fundamental to understand more about the nature of DM, especially those candidates that are supposed to be produced thermally during the early Universe. The insights provided are necessary for different studies over DM, such as the three types of searches, or some beyond SM models that incorporate DM candidates.

References

Abbott, B. et al. Observation of gravitational waves from a binary black hole merger. *Physical Review Letters*, American Physical Society (APS), v. 116, n. 6, Feb 2016. ISSN 1079-7114. Available on: <http://dx.doi.org/10.1103/PhysRevLett.116.061102>.

Abdelhameed, A. et al. First results from the cresst-iii low-mass dark matter program. *Physical Review D*, American Physical Society (APS), v. 100, n. 10, Nov 2019. ISSN 2470-0029. Available on: <http://dx.doi.org/10.1103/PhysRevD.100.102002>.

Ackermann, M.; Albert, A. et al. Searching for dark matter annihilation from milky way dwarf spheroidal galaxies with six years of fermi large area telescope data. *Physical Review Letters*, American Physical Society (APS), v. 115, n. 23, Nov 2015. ISSN 1079-7114. Available on: <http://dx.doi.org/10.1103/PhysRevLett.115.231301>.

Ade, P. A. R. et al. Planck2013 results. xvi. cosmological parameters. *Astronomy & Astrophysics*, EDP Sciences, v. 571, p. A16, Oct 2014. ISSN 1432-0746. Available on: <http://dx.doi.org/10.1051/0004-6361/201321591>.

Ade, P. A. R. et al. Planck2015 results. *Astronomy & Astrophysics*, EDP Sciences, v. 594, p. A13, Sep 2016. ISSN 1432-0746. Available on: <http://dx.doi.org/10.1051/0004-6361/201525830>.

Adhikari, G. et al. An experiment to search for dark-matter interactions using sodium iodide detectors. *Nature*, Springer Science and Business Media LLC, v. 564, n. 7734, p. 83–86, Dec 2018. ISSN 1476-4687. Available on: <http://dx.doi.org/10.1038/s41586-018-0739-1>.

Aghanim, N. et al. Planck 2018 results. *Astronomy & Astrophysics*, EDP Sciences, v. 641, p. A1, Sep 2020. ISSN 1432-0746. Available on: <http://dx.doi.org/10.1051/0004-6361/201833880>.

Aghanim, N. et al. Planck 2018 results. VI. Cosmological parameters. *Astron. Astrophys.*, v. 641, p. A6, 2020.

Agnes, P. et al. Darkside-50 532-day dark matter search with low-radioactivity argon. *Physical Review D*, American Physical Society (APS), v. 98, n. 10, Nov 2018. ISSN 2470-0029. Available on: <http://dx.doi.org/10.1103/PhysRevD.98.102006>.

Agnes, P. et al. Low-mass dark matter search with the darkside-50 experiment. *Physical Review Letters*, American Physical Society (APS), v. 121, n. 8, Aug 2018. ISSN 1079-7114. Available on: <http://dx.doi.org/10.1103/PhysRevLett.121.081307>.

Agnese, R. et al. Search for low-mass dark matter with cdmslite using a profile likelihood fit. *Physical Review D*, American Physical Society (APS), v. 99, n. 6, Mar 2019. ISSN 2470-0029. Available on: <http://dx.doi.org/10.1103/PhysRevD.99.062001>.

Aguilar-Arevalo, A. et al. Results on low-mass weakly interacting massive particles from an 11 kgd target exposure of damic at snolab. *Physical Review Letters*, American Physical Society (APS), v. 125, n. 24, Dec 2020. ISSN 1079-7114. Available on: <http://dx.doi.org/10.1103/PhysRevLett.125.241803>.

Aker, M. et al. Improved upper limit on the neutrino mass from a direct kinematic method by katrin. *Physical Review Letters*, American Physical Society (APS), v. 123, n. 22, Nov 2019. ISSN 1079-7114. Available on: <http://dx.doi.org/10.1103/PhysRevLett.123.221802>.

Akerib, D. et al. Results from a search for dark matter in the complete lux exposure. *Physical Review Letters*, American Physical Society (APS), v. 118, n. 2, Jan 2017. ISSN 1079-7114. Available on: <http://dx.doi.org/10.1103/PhysRevLett.118.021303>.

Akerib, D. et al. Results of a search for sub-gev dark matter using 2013 lux data. *Physical Review Letters*, American Physical Society (APS), v. 122, n. 13, Apr 2019. ISSN 1079-7114. Available on: <http://dx.doi.org/10.1103/PhysRevLett.122.131301>.

Akiyama, K. et al. First M87 Event Horizon Telescope Results. I. The Shadow of the Supermassive Black Hole. *Astrophys. J. Lett.*, v. 875, p. L1, 2019.

Alpher, R. A.; Herman, R. C. On the relative abundance of the elements. *Phys. Rev.*, American Physical Society, v. 74, p. 1737–1742, Dec 1948. Available on: <https://link.aps.org/doi/10.1103/PhysRev.74.1737>.

Angloher, G. et al. Results on mev-scale dark matter from a gram-scale cryogenic calorimeter operated above ground. *The European Physical Journal C*, Springer Science and Business Media LLC, v. 77, n. 9, Sep 2017. ISSN 1434-6052. Available on: <http://dx.doi.org/10.1140/epjc/s10052-017-5223-9>.

Aprile, E. et al. Xenon100 dark matter results from a combination of 477 live days. *Physical Review D*, American Physical Society (APS), v. 94, n. 12, Dec 2016. ISSN 2470-0029. Available on: <http://dx.doi.org/10.1103/PhysRevD.94.122001>.

Aprile, E. et al. Dark matter search results from a one ton-year exposure of xenon1t. *Physical Review Letters*, American Physical Society (APS), v. 121, n. 11, Sep 2018. ISSN 1079-7114. Available on: <http://dx.doi.org/10.1103/PhysRevLett.121.111302>.

Aprile, E. et al. Search for light dark matter interactions enhanced by the migdal effect or bremsstrahlung in xenon1t. *Physical Review Letters*, American Physical Society (APS), v. 123, n. 24, Dec 2019. ISSN 1079-7114. Available on: <http://dx.doi.org/10.1103/PhysRevLett.123.241803>.

Aprile, E. et al. Search for coherent elastic scattering of solar b8 neutrinos in the xenon1t dark matter experiment. *Physical Review Letters*, American Physical Society (APS), v. 126, n. 9, Mar 2021. ISSN 1079-7114. Available on: <http://dx.doi.org/10.1103/PhysRevLett.126.091301>.

Armengaud, E. et al. Searching for low-mass dark matter particles with a massive ge bolometer operated above ground. *Physical Review D*, American Physical Society (APS), v. 99, n. 8, Apr 2019. ISSN 2470-0029. Available on: <http://dx.doi.org/10.1103/PhysRevD.99.082003>.

Arnaud, Q. et al. First results from the news-g direct dark matter search experiment at the lsm. *Astroparticle Physics*, Elsevier BV, v. 97, p. 54–62, Jan 2018. ISSN 0927-6505. Available on: <http://dx.doi.org/10.1016/j.astropartphys.2017.10.009>.

ATLAS, C. Observation of a new particle in the search for the standard model higgs boson with the atlas detector at the lhc. *Physics Letters B*, v. 716, n. 1, p. 1–29, 2012. ISSN 0370-2693. Available on: <https://www.sciencedirect.com/science/article/pii/S037026931200857X>.

Baumann, D. Primordial Cosmology. *PoS*, TASI2017, p. 009, 2018.

Baumann, D. Cosmology: Part III Mathematica Tripos. Lecture Notes. Lecture Notes. Available on: <http://cosmology.amsterdam/education/cosmology/>.

Bennett, C. L. et al. First-year wilkinson microwave anisotropy probe (wmap) observations: Preliminary maps and basic results. *The Astrophysical Journal Supplement Series*, American Astronomical Society, v. 148, n. 1, p. 1–27, Sep 2003. ISSN 1538-4365. Available on: <http://dx.doi.org/10.1086/377253>.

Bennett, C. L. et al. Nine-year wilkinson microwave anisotropy probe (wmap) observations: Final maps and results. *The Astrophysical Journal Supplement Series*, American Astronomical Society, v. 208, n. 2, p. 20, Sep 2013. ISSN 1538-4365. Available on: <http://dx.doi.org/10.1088/0067-0049/208/2/20>.

Bernabei, R. et al. First results from dama/libra and the combined results with dama/nai. *The European Physical Journal C*, Springer Science and Business Media LLC, v. 56, n. 3, p. 333–355, Aug 2008. ISSN 1434-6052. Available on: <http://dx.doi.org/10.1140/epjc/s10052-008-0662-y>.

Bertone, G. *Particle Dark Matter: Observations, Models and Searches.* : Cambridge University Press, 2010.

Bertone, G.; Hooper, D. History of dark matter. *Reviews of Modern Physics*, American Physical Society (APS), v. 90, n. 4, Oct 2018. ISSN 1539-0756. Available on: <http://dx.doi.org/10.1103/RevModPhys.90.045002>.

Billard, J. et al. *Direct Detection of Dark Matter – APPEC Committee Report.* 2021.

Billard, J.; Figueroa-Feliciano, E.; Strigari, L. Implication of neutrino backgrounds on the reach of next generation dark matter direct detection experiments. *Physical Review D*, American Physical Society (APS), v. 89, n. 2, Jan 2014. ISSN 1550-2368. Available on: <http://dx.doi.org/10.1103/PhysRevD.89.023524>.

Bludman, S. A. On the universal Fermi interaction. *Nuovo Cim.*, v. 9, p. 433–445, 1958.

Boveia, A.; Doglioni, C. Dark matter searches at colliders. *Annual Review of Nuclear and Particle Science*, Annual Reviews, v. 68, n. 1, p. 429–459, Oct 2018. ISSN 1545-4134. Available on: <http://dx.doi.org/10.1146/annurev-nucl-101917-021008>.

Bringmann, T.; Hofmann, S. Thermal decoupling of WIMPs from first principles. *JCAP*, v. 04, p. 016, 2007. [Erratum: JCAP 03, E02 (2016)].

Bringmann, T.; Weniger, C. Gamma ray signals from dark matter: Concepts, status and prospects. *Physics of the Dark Universe*, Elsevier BV, v. 1, n. 1-2, p. 194–217, Nov 2012. ISSN 2212-6864. Available on: <http://dx.doi.org/10.1016/j.dark.2012.10.005>.

Cabibbo, N. Unitary symmetry and leptonic decays. *Phys. Rev. Lett.*, American Physical Society, v. 10, p. 531–533, Jun 1963. Available on: <https://link.aps.org/doi/10.1103/PhysRevLett.10.531>.

Caldwell, R. R.; Kamionkowski, M. The physics of cosmic acceleration. *Annual Review of Nuclear and Particle Science*, Annual Reviews, v. 59, n. 1, p. 397–429, Nov 2009. ISSN 1545-4134. Available on: <http://dx.doi.org/10.1146/annurev-nucl-010709-151330>.

Campbell, W. W. The radial motions of polaris. *Publications of the Astronomical Society of the Pacific*, IOP Publishing, v. 18, p. 307, dec 1906. Available on: <https://doi.org/10.1086/121704>.

Carr, B.; Kühnel, F.; Sandstad, M. Primordial black holes as dark matter. *Physical Review D*, American Physical Society (APS), v. 94, n. 8, Oct 2016. ISSN 2470-0029. Available on: <http://dx.doi.org/10.1103/PhysRevD.94.083504>.

Clarkson, C. Establishing homogeneity of the universe in the shadow of dark energy. *Comptes Rendus Physique*, v. 13, n. 6, p. 682–718, 2012. ISSN 1631-0705. Available on: <https://www.sciencedirect.com/science/article/pii/S1631070512000461>.

Clarkson, C.; Maartens, R. Inhomogeneity and the foundations of concordance cosmology. *Classical and Quantum Gravity*, IOP Publishing, v. 27, n. 12, p. 124008, may 2010. Available on: <https://doi.org/10.1088/0264-9381/27/12/124008>.

Clowe, D. et al. A direct empirical proof of the existence of dark matter. *The Astrophysical Journal*, American Astronomical Society, v. 648, n. 2, p. L109–L113, Aug 2006. ISSN 1538-4357. Available on: <http://dx.doi.org/10.1086/508162>.

Clowe, D.; Gonzalez, A.; Markevitch, M. Weak-lensing mass reconstruction of the interacting cluster 1e0657-558: Direct evidence for the existence of dark matter. *The Astrophysical Journal*, American Astronomical Society, v. 604, n. 2, p. 596–603, Apr 2004. ISSN 1538-4357. Available on: <http://dx.doi.org/10.1086/381970>.

Clowe, D. et al. Weak lensing mass reconstructions of the eso distant cluster survey. *Astronomy & Astrophysics*, EDP Sciences, v. 451, n. 2, p. 395–408, May 2006. ISSN 1432-0746. Available on: <http://dx.doi.org/10.1051/0004-6361:20041787>.

CMS, C. Observation of a new boson at a mass of 125 gev with the cms experiment at the lhc. *Physics Letters B*, v. 716, n. 1, p. 30–61, 2012. ISSN 0370-2693. Available on: <https://www.sciencedirect.com/science/article/pii/S0370269312008581>.

Coles, P.; Lucchin, F. *Cosmology: The Origin and Evolution of Cosmic Structure, Second Edition*. 2002.

Cowsik, R.; McClelland, J. An upper limit on the neutrino rest mass. *Phys. Rev. Lett.*, American Physical Society, v. 29, p. 669–670, Sep 1972. Available on: <https://link.aps.org/doi/10.1103/PhysRevLett.29.669>.

Cui, X. et al. Dark matter results from 54-ton-day exposure of pandax-ii experiment. *Physical Review Letters*, American Physical Society (APS), v. 119, n. 18, Oct 2017. ISSN 1079-7114. Available on: <http://dx.doi.org/10.1103/PhysRevLett.119.181302>.

Dodelson, S.; Schmidt, F. *Modern Cosmology*. : Academic Press, 2020. ISBN 978-0-12-815948-4.

Einasto, J. *Dark Matter*. 2010.

Einstein, A. Cosmological Considerations in the General Theory of Relativity. *Sitzungsber. Preuss. Akad. Wiss. Berlin (Math. Phys.)*, v. 1917, p. 142–152, 1917.

Englert, F.; Brout, R. Broken symmetry and the mass of gauge vector mesons. *Phys. Rev. Lett.*, American Physical Society, v. 13, p. 321–323, Aug 1964. Available on: <https://link.aps.org/doi/10.1103/PhysRevLett.13.321>.

Feng, J. L. Dark matter candidates from particle physics and methods of detection. *Annual Review of Astronomy and Astrophysics*, Annual Reviews, v. 48, n. 1, p. 495–545, Aug 2010. ISSN 1545-4282. Available on: <http://dx.doi.org/10.1146/annurev-astro-082708-101659>.

Fermi, E. An attempt of a theory of beta radiation. 1. *Z. Phys.*, v. 88, p. 161–177, 1934.

Feynman, R. P.; Gell-Mann, M. Theory of the fermi interaction. *Phys. Rev.*, American Physical Society, v. 109, p. 193–198, Jan 1958. Available on: <https://link.aps.org/doi/10.1103/PhysRev.109.193>.

Freedman, W. L. Cosmology at a crossroads. *Nature Astronomy*, v. 1, p. 0121, maio 2017.

Freedman, W. L. et al. Final Results from the Hubble Space Telescope Key Project to Measure the Hubble Constant. *APJ*, v. 553, n. 1, p. 47–72, maio 2001.

Glashow, S. L. Partial Symmetries of Weak Interactions. *Nucl. Phys.*, v. 22, p. 579–588, 1961.

Glashow, S. L.; Iliopoulos, J.; Maiani, L. Weak interactions with lepton-hadron symmetry. *Phys. Rev. D*, American Physical Society, v. 2, p. 1285–1292, Oct 1970. Available on: <https://link.aps.org/doi/10.1103/PhysRevD.2.1285>.

Gonzalez-Garcia, M.; Maltoni, M. Phenomenology with massive neutrinos. *Physics Reports*, Elsevier BV, v. 460, n. 1-3, p. 1–129, Apr 2008. ISSN 0370-1573. Available on: <http://dx.doi.org/10.1016/j.physrep.2007.12.004>.

Goodman, J. Geocentrism reexamined. *Phys. Rev. D*, v. 52, p. 1821–1827, 1995.

Goodman, M. W.; Witten, E. Detectability of certain dark-matter candidates. *Phys. Rev. D*, American Physical Society, v. 31, p. 3059–3063, Jun 1985. Available on: <https://link.aps.org/doi/10.1103/PhysRevD.31.3059>.

Griest, K.; Kamionkowski, M. Unitarity limits on the mass and radius of dark-matter particles. *Phys. Rev. Lett.*, American Physical Society, v. 64, p. 615–618, Feb 1990. Available on: <https://link.aps.org/doi/10.1103/PhysRevLett.64.615>.

Guralnik, G. S.; Hagen, C. R.; Kibble, T. W. B. Global conservation laws and massless particles. *Phys. Rev. Lett.*, American Physical Society, v. 13, p. 585–587, Nov 1964. Available on: <https://link.aps.org/doi/10.1103/PhysRevLett.13.585>.

Hall, L. J. et al. Freeze-in production of fimp dark matter. *Journal of High Energy Physics*, Springer Science and Business Media LLC, v. 2010, n. 3, Mar 2010. ISSN 1029-8479. Available on: <http://dx.doi.org/10.1007/JHEP03(2010)080>.

Harvey, D.; Massey, R.; Kitching, T.; Taylor, A.; Tittley, E. The nongravitational interactions of dark matter in colliding galaxy clusters. *Science*, American Association for the Advancement of Science (AAAS), v. 347, n. 6229, p. 1462–1465, Mar 2015. ISSN 1095-9203. Available on: <http://dx.doi.org/10.1126/science.1261381>.

Hehn, L. et al. Improved edelweiss-iii sensitivity for low-mass wimps using a profile likelihood approach. *The European Physical Journal C*, Springer Science and Business Media LLC, v. 76, n. 10, Oct 2016. ISSN 1434-6052. Available on: <http://dx.doi.org/10.1140/epjc/s10052-016-4388-y>.

Hubble, E. A relation between distance and radial velocity among extra-galactic nebulae. *Proc. Nat. Acad. Sci.*, v. 15, p. 168–173, 1929.

Hubble, E.; Humason, M. L. The Velocity-Distance Relation among Extra-Galactic Nebulae. *APJ*, v. 74, p. 43, jul. 1931.

Kelvin, B. W. *Baltimore lectures on molecular dynamics and the wave theory of light*. C. J. Clay and sons, 1904. Available on: <https://archive.org/details/baltimorelecture00kelviala>.

Kobayashi, M.; Maskawa, T. CP Violation in the Renormalizable Theory of Weak Interaction. *Prog. Theor. Phys.*, v. 49, p. 652–657, 1973.

Kolb, E.; Turner, M. *The Early Universe*. : Westview Press, 1990. ISBN 0-201-11603-0.

Leane, R. K.; Slatyer, T. R.; Beacom, J. F.; Ng, K. C. Gev-scale thermal wimps: Not even slightly ruled out. *Physical Review D*, American Physical Society (APS), v. 98, n. 2, Jul 2018. ISSN 2470-0029. Available on: <http://dx.doi.org/10.1103/PhysRevD.98.023016>.

Lee, J.; Komatsu, E. Bullet cluster: A challenge to lcdm cosmology. *The Astrophysical Journal*, American Astronomical Society, v. 718, n. 1, p. 60–65, Jun 2010. ISSN 1538-4357. Available on: <http://dx.doi.org/10.1088/0004-637X/718/1/60>.

Lee, T. D.; Yang, C. N. Implications of the intermediate boson basis of the weak interactions: Existence of a quartet of intermediate bosons and their dual isotopic spin transformation properties. *Phys. Rev.*, American Physical Society, v. 119, p. 1410–1419, Aug 1960. Available on: <https://link.aps.org/doi/10.1103/PhysRev.119.1410>.

Liddle, A. R. *An introduction to modern cosmology*. 1998.

Liu, Z. et al. Constraints on spin-independent nucleus scattering with sub-gev weakly interacting massive particle dark matter from the cdex-1b experiment at the china jinping underground laboratory. *Physical Review Letters*, American Physical Society (APS), v. 123, n. 16, Oct 2019. ISSN 1079-7114. Available on: <http://dx.doi.org/10.1103/PhysRevLett.123.161301>.

Lopes, J. L. A model of the universal fermi interaction. *Nucl. Phys.*, v. 8, p. 234–236, 1958.

Maartens, R. Is the universe homogeneous? *Philosophical Transactions of the Royal Society A: Mathematical, Physical and Engineering Sciences*, Royal Society of London, v. 369, n. 1957, p. 5115–5137, 2011. ISSN 1364-503X.

Milgrom, M. A modification of the Newtonian dynamics as a possible alternative to the hidden mass hypothesis. *APJ*, v. 270, p. 365–370, jul. 1983.

Muller, C. A.; Oort, J. H. Observation of a Line in the Galactic Radio Spectrum: The Interstellar Hydrogen Line at 1,420 Mc./sec., and an Estimate of Galactic Rotation. *Nature*, v. 168, n. 4270, p. 357–358, set. 1951.

Olive, K. A. et al. Review of Particle Physics, 2014-2015. Review of Particle Properties. *Chin. Phys. C*, v. 38, p. 090001, 2014. All tables, listings, and reviews (and errata) are also available on the Particle Data Group website: http://pdg.lbl.gov. Available on: <http://cds.cern.ch/record/1753419>.

Pandey, B.; Sarkar, S. Testing homogeneity in the Sloan Digital Sky Survey Data Release Twelve with Shannon entropy. *Monthly Notices of the Royal Astronomical Society*, v. 454, n. 3, p. 2647–2656, 10 2015. ISSN 0035-8711. Available on: <https://doi.org/10.1093/mnras/stv2166>.

Pathria, R. *Statistical Mechanics*. Elsevier Science, 2016. ISBN 9781483104973. Available on: <https://books.google.com.br/books?id=pR6TDAAAQBAJ>.

Pauli, W. Pauli letter collection: letter to Lise Meitner. Typed copy. 1930. Available on: <https://cds.cern.ch/record/83282>.

Peccei, R. D.; Quinn, H. R. CP conservation in the presence of pseudoparticles. *Phys. Rev. Lett.*, American Physical Society, v. 38, p. 1440–1443, Jun 1977. Available on: <https://link.aps.org/doi/10.1103/PhysRevLett.38.1440>.

Peebles, P. *Principles of Physical Cosmology*. Princeton University Press, 1993. (Princeton Series in Physics). ISBN 9780691019338. Available on: <https://books.google.com.br/books?id=AmlEt6TJ6jAC>.

Penzias, A. A.; Wilson, R. W. A Measurement of Excess Antenna Temperature at 4080 Mc/s. *APJ*, v. 142, p. 419–421, jul. 1965.

Perkins, D. *Particle Astrophysics, Second Edition*. OUP Oxford, 2008. (EBSCO ebook academic collection). ISBN 9780199545452. Available on: <https://books.google.com.br/books?id=-QoUDAAAQBAJ>.

Poincare, H. The Milky Way and the Theory of Gases. *Popular Astronomy*, v. 14, p. 475–488, out. 1906.

Profumo, S.; Giani, L.; Piattella, O. F. *An Introduction to Particle Dark Matter*. 2019.

Quigg, C. *GAUGE THEORIES OF THE STRONG, WEAK AND ELECTROMAGNETIC INTERACTIONS*. 1983. v. 56. ISBN 978-0-8053-6020-2.

Rubin, V. C.; Ford W. Kent, J. Rotation of the Andromeda Nebula from a Spectroscopic Survey of Emission Regions. *APJ*, v. 159, p. 379, fev. 1970.

Rubin, V. C.; Ford W. Kent, J. Rotation of the Andromeda Nebula from a Spectroscopic Survey of Emission Regions. *APJ*, v. 159, p. 379, fev. 1970.

Rubin, V. C. et al. Rotational properties of 21 SC galaxies with a large range of luminosities and radii, from NGC 4605 (R=4kpc) to UGC 2885 (R=122kpc). *APJ*, v. 238, p. 471–487, jun. 1980.

Rutherford, E. Collision of α particles with light atoms. IV. An anomalous effect in nitrogen. *Phil. Mag. Ser. 6*, v. 37, p. 581–587, 1919.

Sabti, N.; Alvey, J.; Escudero, M.; Fairbairn, M.; Blas, D. Refined bounds on mev-scale thermal dark sectors from bbn and the cmb. *Journal of Cosmology and Astroparticle Physics*, IOP Publishing, v. 2020, n. 01, p. 004–004, Jan 2020. ISSN 1475-7516. Available on: <http://dx.doi.org/10.1088/1475-7516/2020/01/004>.

Sakurai, J. J. MASS REVERSAL AND WEAK INTERACTIONS. *Nuovo Cim.*, v. 7, p. 649–660, 1958.

Salam, A. Weak and Electromagnetic Interactions. *Conf. Proc. C*, v. 680519, p. 367–377, 1968.

Samtleben, D. et al. The cosmic microwave background for pedestrians: A review for particle and nuclear physicists. *Annual Review of Nuclear and Particle Science*, v. 57, n. 1, p. 245–283, 2007. Available on: <https://doi.org/10.1146/annurev.nucl.54.070103.181232>.

Schneider, P.; Ehlers, J.; Falco, E. E. *Gravitational Lenses*. 1992.

Schumann, M. Direct detection of wimp dark matter: concepts and status. *Journal of Physics G: Nuclear and Particle Physics*, IOP Publishing, v. 46, n. 10, p. 103003, Aug 2019. ISSN 1361-6471. Available on: <http://dx.doi.org/10.1088/1361-6471/ab2ea5>.

Sirunyan, A. M. et al. Measurement of the weak mixing angle using the forward–backward asymmetry of drell–yan events in pp collisions at 8 tev. *The European Physical Journal C*, Springer Science and Business Media LLC, v. 78, n. 9, Sep 2018. ISSN 1434-6052. Available on: <http://dx.doi.org/10.1140/epjc/s10052-018-6148-7>.

Slatyer, T. R. *TASI Lectures on Indirect Detection of Dark Matter*. 2017.

Slipher, V. M. The radial velocity of the Andromeda Nebula. *Lowell Observatory Bulletin*, v. 1, p. 56–57, jan. 1913.

Smith, M. C.; Ruchti et al. The rave survey: constraining the local galactic escape speed. *Monthly Notices of the Royal Astronomical Society*, Oxford University Press (OUP), v. 379, n. 2, p. 755–772, Aug 2007. ISSN 1365-2966. Available on: <http://dx.doi.org/10.1111/j.1365-2966.2007.11964.x>.

Smoot, G. F. et al. Structure in the COBE Differential Microwave Radiometer First-Year Maps. *APJ*, v. 396, p. L1, set. 1992.

Steigman, G. Primordial nucleosynthesis in the precision cosmology era. *Annual Review of Nuclear and Particle Science*, v. 57, n. 1, p. 463–491, 2007. Available on: <https://doi.org/10.1146/annurev.nucl.56.080805.140437>.

Sudarshan, E. C. G.; Marshak, R. e. Chirality invariance and the universal Fermi interaction. *Phys. Rev.*, v. 109, p. 1860–1860, 1958.

Swart, J. G. de; Bertone, G.; Dongen, J. van. How dark matter came to matter. *Nature Astronomy*, Springer Science and Business Media LLC, v. 1, n. 3, Mar 2017. ISSN 2397-3366. Available on: <http://dx.doi.org/10.1038/s41550-017-0059>.

Thomson, J. J. Xl. cathode rays. , *Philosophical Magazine*, Series 5, p. 293 – 316, 1897. Available on: <http://dx.doi.org/10.1080/14786449708621070>.

van Albada, T. S.; Bahcall, J. N.; Begeman, K.; Sancisi, R. Distribution of dark matter in the spiral galaxy NGC 3198. *APJ*, v. 295, p. 305–313, ago. 1985.

Viel, M.; Becker, G. D.; Bolton, J. S.; Haehnelt, M. G. Warm dark matter as a solution to the small scale crisis: New constraints from high redshift lyman-α forest data. *Physical Review D*, American Physical Society (APS), v. 88, n. 4, Aug 2013. ISSN 1550-2368. Available on: <http://dx.doi.org/10.1103/PhysRevD.88.043502>.

Vitale, V.; Morselli, A. *Indirect Search for Dark Matter from the center of the Milky Way with the Fermi-Large Area Telescope*. 2009.

Weinberg, D. H. et al. Observational probes of cosmic acceleration. *Phys. Rep.*, v. 530, n. 2, p. 87–255, set. 2013.

Weinberg, S. A Model of Leptons. *Phys. Rev. Lett.*, v. 19, p. 1264–1266, 1967.

Weinberg, S. *Gravitation and Cosmology: Principles and Applications of the General Theory of Relativity*. New York: John Wiley and Sons, 1972. ISBN 978-0-471-92567-5, 978-0-471-92567-5.

Weinberg, S. The making of the standard model. *The European Physical Journal C*, Springer Science and Business Media LLC, v. 34, n. 1, p. 5–13, May 2004. ISSN 1434-6052. Available on: <http://dx.doi.org/10.1140/epjc/s2004-01761-1>.

Weinberg, S. *Cosmology*. OUP Oxford, 2008. (Cosmology). ISBN 9780191523601. Available on: <https://books.google.com.br/books?id=nqQZdg020fsC>.

Zwicky, F. On the Masses of Nebulae and of Clusters of Nebulae. *APJ*, v. 86, p. 217, out. 1937.

Zyla, P. et al. Review of Particle Physics. *PTEP*, v. 2020, n. 8, p. 083C01, 2020.

APPENDIX A – Relevant Physical Quantities

The references used to build this table are (Dodelson; Schmidt, 2020) and (Olive et al., 2014).

Name	Symbol	Value
Speed of light	c	$2.99792458 \times 10^{10}$ cm s^{-1}
Reduced Planck's constant	$\hbar$	$6.58211899 \times 10^{-16}$ eV s
		$1.973269602 \times 10^{-5}$ eV cm c^{-1}
Newtonian gravitational constant	G	6.673×10^{-8} cm^3 g^{-1} s^{-2}
		$\hbar c/M_{Pl}^2$
Planck mass	M_{Pl}	$\sqrt{\hbar c/G}$
		1.221×10^{19} GeV/c^2
Boltzmann constant	k_B	8.617342×10^{-5} eV K^{-1}
Fine structure constant	α	$1/137.03599976$
Electron mass	m_e	0.510998902 MeV/c^2
Neutron mass	m_n	939.565330 MeV/c^2
Proton mass	m_p	938.271998 MeV/c^2
Neutro-proton mass difference	Q	1.2933 MeV/c^2
Fermi constant	G_F	1.16639×10^{-5} GeV^{-2} $(\hbar c)^3$
Thomson cross section	σ_T	$8\pi\alpha^2\hbar^2/(3m_e c^2)$
		$0.665245854 \times 10^{-24}$ cm^2
CMB photon energy density	ρ_γ	$\pi^2 k_B^4 T^4/[15(\hbar c)^3]$
		$2.474 \times 10^{-5} h^{-2}(T/T_0)^4 \rho_{cr}$
CMB Temperature today	T_0	2.726 K
		2.349×10^{-4} eV/k_B
Critical density	ρ_{cr}	$1.879h^2 \times 10^{-29}$ g cm^{-3}
		$8.098h^2 \times 10^{11}$ eV^4/$(\hbar c)^3$
Universe entropy today	s_0	2970 cm^3
Parsec	pc	3.0856×10^{18} cm
Baryonic Matter Density	$\Omega_b h^2$	0.02242 ± 0.00014
Dark Matter Density	$\Omega_c h^2$	0.11933 ± 0.00091
Dark Energy Density Parameter	Ω_Λ	0.6889 ± 0.0056
Total Mass Density Parameter	Ω_m	0.3111 ± 0.0056
Total Density Parameter	Ω	0.9993 ± 0.0019
Curvature Parameter	Ω_k	0.001 ± 0.002
Dimensionless Hubble parameter	h	0.677 ± 0.004
Age of the Universe	t_0	$13.784^{+0.040}_{-0.037}$ Gyr
Hubble Constant	H_0 [km s^{-1}Mpc^{-1}]	67.66 ± 0.42

Table 2 – Relevant physical constants and other parameters.

APPENDIX B – Equilibrium Thermodynamics

The equations here defined can be found in (Pathria, 2016).

Probability distribution functions (PDFs) for Fermi-Dirac distribution (+), i.e., fermions, and for Bose-Einstein distribution (−), or bosons:

$$f(\mathbf{p}) = \frac{1}{\exp\left[\frac{E(\mathbf{p})-\mu}{T}\right] \pm 1} \tag{B.1}$$

Particle number density:

$$n = \frac{g}{(2\pi)^3}\int_0^\infty d^3p f(\mathbf{p}), \tag{B.2}$$

Energy density:

$$\rho = \frac{g}{(2\pi)^3}\int_0^\infty d^3p E(\mathbf{p}) f(\mathbf{p}) \tag{B.3}$$

Pressure:

$$P = \frac{g}{(6\pi)^3}\int_0^\infty d^3p \frac{|\mathbf{p}|^2}{3E(\mathbf{p})} f(\mathbf{p}) \tag{B.4}$$

Relativistic limit, where $T \ll m$,

$$\rho = \begin{cases} \frac{\pi^2}{30} g T^4 & \text{(bosons)} \\ \frac{7}{8}\frac{\pi^2}{30} g T^4 & \text{(fermions)}, \end{cases} \tag{B.5}$$

$$n = \begin{cases} \frac{\zeta(3)}{\pi^2} g T^3 & \text{(bosons)} \\ \frac{3}{4}\frac{\zeta(3)}{\pi^2} g T^3 & \text{(fermions)}, \end{cases} \tag{B.6}$$

$$P = \frac{\rho}{3}. \tag{B.7}$$

The energy density can be simplified as

$$\rho = g_* \frac{\pi^2}{30} T^4, \tag{B.8}$$

where

$$g_* = \sum_{i=bosons} g_i \left(\frac{T_i}{T}\right)^4 + \frac{7}{8} \sum_{i=fermions} g_i \left(\frac{T_i}{T}\right)^4 \tag{B.9}$$

accounts for the degrees of freedom of the relativistic particle as function of the temperature.

Non-relativistic case, where $m \ll T$:

$$n = g \left(\frac{mT}{2\pi}\right)^{3/2} \exp\left(-\frac{m-\mu}{T}\right), \tag{B.10}$$

$$\rho = mn, \tag{B.11}$$

$$P = nT \tag{B.12}$$

The entropy is given by

$$s = \frac{p+\rho}{T} \tag{B.13}$$

therefore, for each case:

$$s = \begin{cases} \frac{2\pi^2}{45} g_{*S} T^3 & \text{relativistic} \\ \frac{mn}{T} & \text{non-relativistic,} \end{cases} \tag{B.14}$$

where

$$g_{*s} = \sum_{i=bosons} g_i \left(\frac{T_i}{T}\right)^3 + \frac{7}{8} \sum_{i=fermions} g_i \left(\frac{T_i}{T}\right)^3 \tag{B.15}$$

Mean speed of non-relativistic particles

$$\langle v \rangle = \int dv f(v) v = 4\pi \left(\frac{m}{2\pi T}\right)^{3/2} \int_0^\infty dv \exp\left(-\frac{mv^2}{2T}\right) v^3, \tag{B.16}$$

where

$$f(v) = 4\pi v^2 \left(\frac{m}{2\pi T}\right)^{3/2} \exp\left(-\frac{mv^2}{2T}\right) dv. \tag{B.17}$$

Therefore

$$\langle v \rangle = \left(\frac{8T}{\pi m}\right)^{1/2}. \tag{B.18}$$

Hubble parameter for a radiation-dominated Universe

$$H^2(t) = \frac{8\pi\rho_r}{3M_{Pl}^2} = \frac{8\pi}{3M_{Pl}^2}\frac{\pi^2}{30}g*(T)T^4 = \left(\frac{\sqrt{8\pi^3}}{\sqrt{90}}\frac{T^2}{M_{Pl}}\right)^2 \cong \left(1.66\frac{T^2}{M_{Pl}}\right)^2, \tag{B.19}$$

where $M_{Pl} = \frac{1}{\sqrt{G}}$.